These

Présentée à

L'Université des Sciences et Technologies de Lille

Pour obtenir le titre de

DOCTEUR EN CHIMIE

Spécialité : Science de la matière, du rayonnement et de l'environnement

par

Benjamin KATRYNIOK

NOUVELLE VOIE DE SYNTHESE D'ACROLEINE A PARTIR DE BIOMASSE

Soutenance le 09 novembre 2010 devant la commission d'examen:

Président du Jury:
Mme. Elisabeth Bordes-Richard, Professeur, Université Lille 1 (France)
Rapporteurs:
M. Jean-Marc Millet, Professeur, Université Lyon 1 (France)
M. Wolfgang Hölderich, Professeur, Université d'Aix-la-Chapelle (Allemagne)
Examinateurs:
Mme. Virginie Bellière-Baca, Docteur, RHODIA (France)
M. Patrick Rey, Docteur, ADISSEO SAS (France)
M. Mickael Capron, Maître de Conférences, Université Lille 1 (France)
Directeur:
M. Franck Dumeignil, Professeur, Université Lille 1 (France)
Co-Directeur:
M. Sebastién Paul, Maître de Conférences, Ecole Centrale de Lille (France)

© 2011 Tous droits réservés.

Acknowledgement

This work was carried out from october 2007 to september 2010 in the *Unité de Catalyse et Chimie du Solide, UMR 8181*, at the *Université des Sciences et Technologies de Lille*.

I want to thank M. Franck Dumeignil for kindly providing the interesting and challenging research topic, for his critical advice and inspiration.

Furthermore I wish to thank M. Sébastien Paul and M. Mickaël Capron for their help, their advice and their guidance.

I am also grateful to ADISSEO Company for financial support and especially M. Patrick Rey for the helpful discussions. Also thanks to Mme. Virginie Bellière-Baca from RHODIA Company for the discussion of the technical and analytical aspects.

Finally thanks to M. Sébastien Royer for his help during my stay in Poitiers which offered me the possibility for becoming familiar with the synthesis of mesostructured silica. Here I also want to thank Mme. Christine Lancelot for the characterization of the supports by electron microscopy and the discussion and interpretation of the scientific results.

Even though a thesis is synonym for an individual project, this task would not have been possible with the help of the whole team of UCCS. Therefore I would like to thank all the technicians for their help – especially M. Olivier Gradoll and M. Gerard Cambien.

Moreover I want to thank M. Wolfgang Hölderich and M. Jean-Marc Millet for accepting their role as referee for this thesis and – of course – thanks to Mme. Elisabeth Bordes-Richard for accepting the presidency of the examination committee.

© 2011 Tous droits réservés.
http://doc.univ-lille1.fr

Abstract

Driven by the issue of the climate change, carbon dioxide emissions have to be drastically reduced within the next decades. Therefore, biomass-derived fuels have been developed, namely, *e.g.*, bio-ethanol and biodiesel, which can be used as substitutes or blenders for gasoline and diesel, respectively. Biodiesel uses vegetable oils and fats as raw materials, which are upgraded in the transesterification process, in which glycerol is formed as a by-product of a low value. Among the numerous possibilities of valorization of this molecule, the reaction of dehydration of glycerol to acrolein is, from an economical point of view, one of the most promising options. Indeed, acrolein as an important intermediate for superabsorbent polymers and cattle feeding additives. This reaction is favored over acid catalysts such as zeolites, mixed metal-oxides and heteropoly acids. The latter offer the possibility for tuning their chemical properties by changing their composition. Therefore, Keggin-type heteropoly acids were chosen as active phases, which were supported on meso-structured silica. The studied catalysts exhibited high performances, but with the tendency of a rapid deactivation, which was ascribed to poisoning by coke deposition. This phenomenon is widely observed for strong acid catalysts. Therefore, the fine-tuning of the acid strength was successfully attempted by modification of the silica support with zirconia. This led to *(i)* an increase in the long-term performances and *(ii)* an increase in the thermal stability of the active phase. The long-term performances of silicotungstic acid supported on zirconia-grafted SBA-15 were significantly increased, compared to that observed over the catalyst supported on the non-modified silica, with a yield to acrolein of 69 % after 24 h on stream (*vs.*24 %). The zirconia supported heteropoly acids showed larger resistance to thermal decomposition and remained intact up to 500 °C (*vs.*350 °C for the zirconia-free solids). This further feature was interesting when considering the possibility of regeneration of the spent catalyst.

© 2011 Tous droits réservés.

Abstract

Du fait du réchauffement climatique, les émissions de dioxyde de carbone doivent être drastiquement réduites dans les prochaines décennies. La synthèse de biodiesel, qui utilise des huiles et graisses végétales transestérifiées, pallie partiellement ce problème avec un bilan CO_2 nettement plus favorable que celui associé aux carburants diesels issus des ressources fossiles. Néanmoins, durant le processus de transestérification, le glycérol est formé à hauteur de 10 % en poids. Parmi les possibilités de valorisation, la déshydratation du glycérol en acroléine est économiquement l'une des réactions les plus intéressantes. Cette réaction est favorisée sur des catalyseurs acides tels que les zéolites, les oxydes mixtes de métaux, et les hétéropolyacides. Ces derniers possèdent l'avantage de propriétés chimiques – et donc de propriétés catalytiques – aisément ajustables grâces aux nombreuses possibilités de variation de composition. Par conséquent, dans ces travaux, des hétéropolyacides de type Keggin ont été choisis comme phase active supportée sur silice. Les catalyseurs étudiés possèdent d'excellentes performances, mais ont tendance à se désactiver beaucoup trop rapidement. Ceci est attribué au dépôt de coke, un phénomène largement observé sur catalyseurs acides, notamment lorsque les propriétés acides ne sont pas optimisées. Par conséquent, l'ajustement de l'acidité par modification du support silice à l'aide de zircone a été entrepris avec succès, ce qui a conduit à *(i)* une augmentation très significative des performances à long terme et *(ii)* une augmentation de la stabilité thermique de la phase active. Les performances à long terme du catalyseur contenant l'acide silicotungstique supporté sur SBA-15 greffée par de la zircone se sont avérées bien plus élevées par rapport au même catalyseur à base de silice cette fois non-modifiée, avec un rendement en acroléine de 69 % après 24 h de réaction contre 24 %.

© 2011 Tous droits réservés.
http://doc.univ-lille1.fr

Index

1 Introduction 1
2 Anterior Art 9
2.1 Glycerol Dehydration 9
2.1.1 Acidity of the catalyst 10
2.1.2 Supported heteropoly acids 14
2.1.3 Zeolites 18
2.1.4 Mixed metal oxides, phosphates and pyrophosphates 21
2.1.5 Reaction mechanism 24
2.2 Keggin-type heteropoly compounds 34
2.2.1 Structure 35
2.2.2 Stability 38
2.2.3 Chemical properties 39
2.3 Mesostructured silica 40
2.3.1 MCM-41 and MCM-48 42
2.3.2 SBA-15 43
2.3.3 KIT-6 44
3 Synthesis procedures and characterization methods 48
3.1 Preparation of the catalysts 48
3.1.1 Preparation of the heteropoly acids 48
3.1.2 Silica supports 52
3.1.3 Zirconia grafting 55
3.1.4 Impregnation procedure 55
3.2 Characterization Techniques 56
3.2.1 Textural parameters 56
3.2.2 X-Ray Diffraction 56

© 2011 Tous droits réservés.
http://doc.univ-lille1.fr

3.2.3 Transmission Electron Microscopy 57
3.2.4 Fourier transform Infrared spectroscopy 57
3.2.5 Nuclear magnetic resonance 58
3.2.6 Inductively Coupled Plasma Mass spectroscopy 58
3.2.7 Temperature programmed desorption of ammonia 58
3.3 Description of the catalytic test 59
4 Characterization results 62
4.1 Bare silica supports 62
4.1.1 Textural parameters 62
4.1.1 Test of the hydrothermal stability of the silica supports 64
4.2 Zirconia-grafted silica 65
4.2.1 SBA-15 loaded with zirconia 66
4.2.2 Evolution of the silica surface coverage with zirconia loading 66
4.2.3 Influence of the thermal treatment temperature 68
4.2.4 Effect of the zirconia loading 72
4.2.5 Influence of the pore size of the silica host support 76
4.2.6 Acid properties of the zirconia-grafted samples 78
4.3 Characterization of the catalysts and comparison between catalysts based on bare silica and zirconia-grafted silica 80
4.3.1 Quantity of active phase 80
4.3.2 Dispersion of the active phase 81
4.3.3 Structural integrity of the active phase upon impregnation 84
4.3.4 Acidity of the catalysts 85
4.3.5 Thermal stability of the catalysts 87
5 Catalytic performance tests 90
5.1 Preliminary tests 90
5.1.1 Test on mass transfer limitations 90

© 2011 Tous droits réservés.
http://doc.univ-lille1.fr

5.2 Performance tests of non-zirconia-grafted catalysts 91
5.2.1 Variation of the active phase 91
5.2.2 Influenceof the reaction temperature 95
5.2.3 Variation of the silica support 97
5.3 Performance tests of zirconia-grafted catalysts 100
5.3.1 Influenceof the zirconia amount 100
5.3.2 Influence of the amount of active phase 103
5.3.3 Influence of the calcination temperature of the support 105
5.3.4 Influence of the silica support 107
5.4 Regeneration of the catalysts 112
5.4.1 Regeneration of non-grafted catalyst 112
5.4.2 Regeneration of zirconia-grafted catalyst 114
6 Synopsis 117
6.1 General discussion of the results 117
6.2 Conclusion 120
6.3 Perspectives 121
7 Annex 123
7.1 Introduction (French) 123
7.2 Conclusion (French) 131
7.3 Curriculum Vitae 133
7.4 Publications 134

© 2011 Tous droits réservés.
http://doc.univ-lille1.fr

© 2011 Tous droits réservés.
http://doc.univ-lille1.fr

1 Introduction

Parts of this chapter are published in:

B. Katryniok, S. Paul, M. Capron, F. Dumeignil *ChemSusChem* **2009**, *2*, 719-730.

B. Katryniok, S. Paul, V. Bellière-Baca, P. Rey, F. Dumeignil, *GreenChem.* **2010** ref. C0GC00194E accepted manuscript

The finiteness of the fossil petrol feedstock has led to an intensive research activity for yielding substitutes for engine fuels like bio-diesel, bio-ethanol or bio-kerosene. In contrast to fossil resources, these fuels offer the advantage of a CO_2 neutral carbon footprint due to their renewable biomass origin. From an economic point of view, none of the bio-fuels can competitively be produced yet, but in order to fulfill the CO_2 reduction objectives imposed by the Kyoto climate protocol, political decisions have pushed the production of fuels from bio resources. For example, the European Union has planned to progressively increase the proportion of bio-ethanol in gasoline to 10 % and of biodiesel as an additive in diesel to 7 %, by 2015.[1]

The alternative gasoline production using vegetable oils and fats has attracted the attention of many academic and industrial researchers. The raw materials for biodiesel production are vegetable oils and fats – from canola, soy, corn… – and a mono-alcohol (usually methanol), which is used to cleave the fatty acids from their glycerol-backbone to finally yield the fatty acid-esters (**Scheme 1-1**). These acid-esters can be directly used as biodiesels, but are more generally blended with fossil fuels-derived diesels.

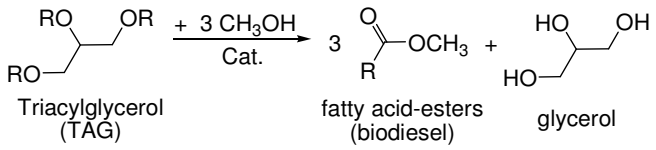

Scheme 1-1: Transesterification reaction of vegetable oils to yield the biodiesel

The capacity of biodiesel production is in continuous expansion all-over the world. For example, in 2008 the USA produced 2.1 million tons and the EU 7.6 million tons of biodiesel (**Figure 1-1**) and these quantities are expected to double by 2012.[2,3] This growth is accompanied with a significant increase in the glycerol production, as

© 2011 Tous droits réservés.
http://doc.univ-lille1.fr

this compound is co-produced with biodiesel (**Scheme 1-1**) in large proportions (~ 10 wt.%). A projection on the global production forecasts a quantity of 1.54 million tons of glycerol generated in the world in 2015,[4] which will have to be processed to achieve a sustainable business.

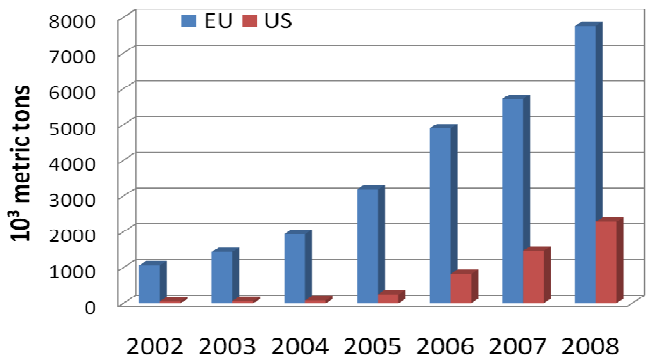

Figure 1-1: European and US-biodiesel production trends[2-3]

According to the applied process for the cleavage of the fatty acids from the glycerol backbone, the quality of the crude glycerol can vary in its purity. The crude glycerol obtained from most of the biodiesel processes contains 80 wt.% of glycerol but, as a drawback, it also comprises water, methanol, traces of fatty acids as well as various inorganic and organic compounds (called MONG, standing for Matter Organic Non Glycerol) in various quantities (Table 1-1).

Table 1-1: Examples of qualities of glycerol derived from biodiesel production[5]

Company/ Production site		Robbe/Diester Compiègne (France)	Saipol/Diester Rouen (France)	Diester/Bioenergy Marl (Germany)
concentration [wt.%]	Glycerol	65	93	85
	Water	31	4	10
	MONG	1	1	0.5
	Salts	3 (Na_2SO_4)	2.5 (NaCl)	4.5 (NaCl)
	Methanol	0.3	0.2	<0.01

As a consequence, in most of the cases, crude glycerol must be purified by an expensive distillation step prior to further use. The proportion of glycerol that is actually refined is steadily decreasing due to the high cost of the distillation step accompanied with a too rapid growth of the quantity of produced crude glycerol, mostly because of the absence of any market able to absorb the overproduction

© 2011 Tous droits réservés. http://doc.univ-lille1.fr

(Figure 1-2). In contrast, a model based on the production and sales of crude glycerol predicts an inverse linear relationship between the neat production cost of biodiesel and the price of glycerol.[6] New economical ways of using glycerol must therefore be developed in order to significantly increase the demand and the price of crude glycerol and therefore to ensure the sustainability of the biodiesel sector.[7]

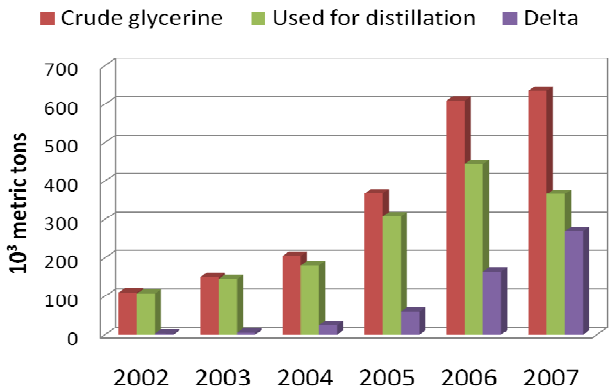

Figure 1-2: Global crude glycerol production and distillation ('Delta' corresponds to the quantity of glycerol that is not upgraded and usually burnt).[8]

More than 1500 direct applications of glycerol are already known, especially in cosmetics, pharmaceuticals and food industries.[9] The large versatility of glycerol use is based on both its chemical and physical properties (**Figure 1-3**). Due to the presence of three hydroxyl groups, glycerol is completely soluble in water and alcohols whereas it is completely insoluble in hydrocarbons. It is a very hydrophilic species and is employed as such where the amount of water has to be controlled – namely in glue or other adhesives. Further, the presence of hydroxyl groups leads to the formation of intra- and inter-molecular hydrogen networks, which explain its high boiling point (290 °C at atmospheric pressure) and its high viscosity. This latter rheological property leads to the use of glycerol as a softener in resins and plastics but also as a lubricant, for instance in pharmaceutical applications. In addition, glycerol is non-toxic and has a sweet taste. It can be incorporated in food, medicines and cosmetics but, as aforementioned, the crude glycerol issued from biodiesel process contains impurities and is thus not suitable for such applications without a preliminary purification stage. Further, as already said, the size of the existing market is not sufficient to absorb the huge amount of glycerol currently produced and the

© 2011 Tous droits réservés.
http://doc.univ-lille1.fr

gap between the absorption capacity of the market and the glycerol production will steadily increase in the near future.

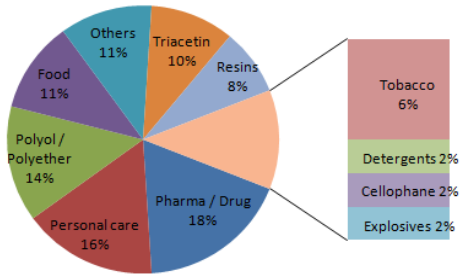

Figure 1-3: Glycerol market segmentation[7]

Today, the crude glycerol that is not refined is generally burned (Figure 1-2),which must be considered as a dramatic waste of a potentially very interesting organic raw material. Actually, glycerol is a molecule with a large functionalization potential that offers many opportunities of chemical or biochemical conversions to produce value-added chemicals. A selection of these possibilities is shown in **Scheme 1-2**.

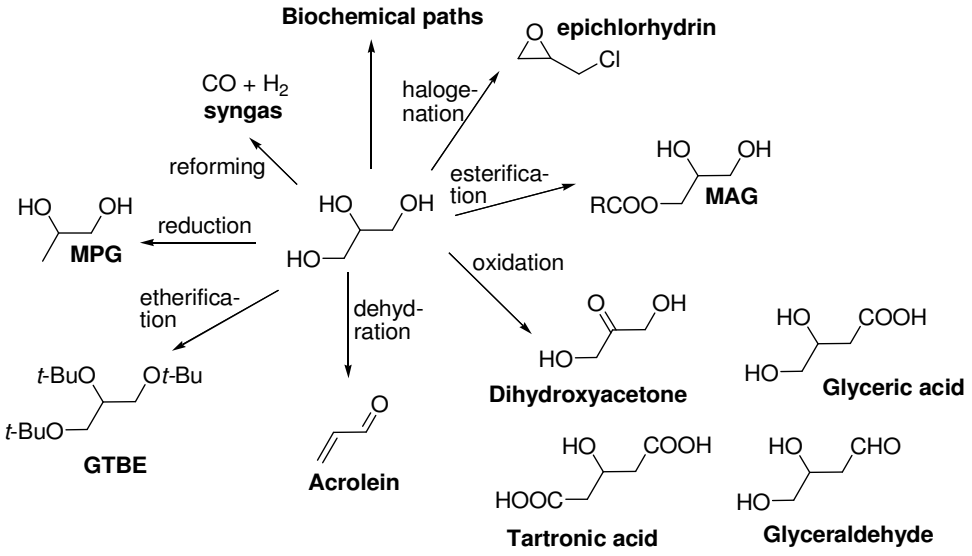

Scheme 1-2: Selection of some glycerol valorization pathways

The reforming of glycerol on Pt-Rh catalysts to yield syngas, which can either be used in the Fischer-Tropsch process for the synthesis of alkanes or for the synthesis of methanol, has been recently reported.[10, 11] A potential application derived from this technology is the production of hydrogen by the water-gas-shift process. Another interesting possibility to valorize glycerol is its selective reduction, which leads either to propylene glycol (MPG) or to 1,3-propanediol (PD) that are used in the polymer

© 2011 Tous droits réservés.
http://doc.univ-lille1.fr

industry. It is also possible to halogenate glycerol to epichlorhydrin, which is an important intermediate for epoxy resins, using hydrochloric acid in the presence of organic acids (caprylic acid – Solvay / acetic acid – Dow)[12] as catalysts working in the gaseous phase at 180-220 °C under 1 ~ 5 bars.[13] This technology is now quite mature, as Solvay has commercialized this process since 2007 in France, using an existing production facility, where glycerol was formerly produced from epichlorhydrin.

Another way of valorization of glycerol is the etherification to glycerol-tert-butylether (GTBE), which is an excellent additive for diesel blending. Further, esterification of glycerol to mono-acylglycerol (MAG) or di-acylglycerol (DAG) used as emulsifiers for example in food (margarines and sauces) or in cosmetics is also a possible option. This latter process can either be catalyzed by a conventional alkaline catalyst or by enzymes (lipase-type).[14] Glycerol partial oxidation leads to a rich chemistry with many possible products such as glyceric, tartronic and ketomalonic (or mesoxalic) acids, glyceraldehyde or dihydroxyacetone (DHA). The challenge is to find catalysts selective to the target molecule among many possible products. For example, Bi/Pt catalysts were proved to be efficient for DHA production with a 37 % yield at a 70 % glycerol conversion.[15] Oxidation can also be performed using modified bacteria.[16] Recently, anodic oxidation of glycerol gave a DHA yield of 25 %, which is comparable to that obtained with the aforementioned biotechnological process.[17]

However, one of the most promising ways of glycerol valorization lies in its catalytic dehydration to acrolein, which is an important intermediate for the chemical and agro-industries. The synthesis of acrolein is currently based on the selective oxidation of propene over complex multicomponents BiMoOx-based catalysts (Scheme 1-3). The selectivity obtained in this process is close to 85 % at 95 % of conversion.[18] New approaches with propane as a starting material are currently explored at the laboratory scale but they still suffer from insufficient yields, which are incompatible with commercialization expectations.[19] Considering the petrochemical feedstock depletion issues, the sustainable resources will become more and more competitive, not to mention the positive effect in terms of impact on the climate. Within this context, massively yielding bio-resourced acrolein is an important challenge. An economical study has shown that a competitive production of acrolein

© 2011 Tous droits réservés. http://doc.univ-lille1.fr

from glycerol would be possible provided a glycerol price lower than *ca.* 300 US$/ton is reached.[20] In January 2010 refined glycerol still costed 500 ~ 550 US$/ton but crude glycerin price was around 200 US$/ton, which already made this latter as a potentially very competitive raw material for sustainable acrolein production.[21]

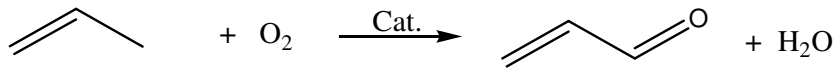

Scheme 1-3: Catalyzed selective oxidation of propene

Due to its toxicity, acrolein is usually directly converted to derivatives such as acrylic acid for instance. The most important consumer of acrolein is the synthesis of acrylic acid, which is used as a starting material for sodium polyacrylate synthesis (Scheme 1-4). According to its physical properties, this polymer, classified as a superabsorbent, finds uses in hygiene products, such as baby diapers. The annual worldwide market for this superabsorbent polymer (SAP) is estimated at 1.9 million tons in 2010.[22]

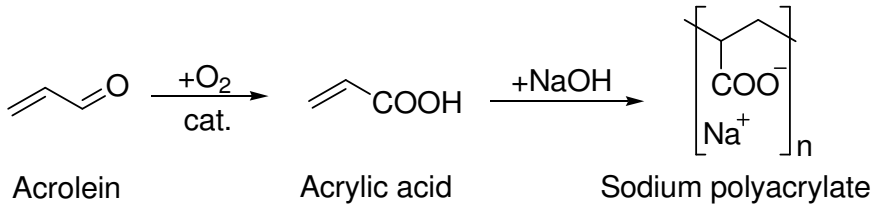

Scheme 1-4: Synthesis of sodium polyacrylate(superabsorbent polymer)

The second largest consumer of acrolein is represented by the synthesis of DL-methionine via 3-methylthiopropionaldehyde as an intermediate (Scheme 1-5).[23] DL-methionine is an essential amino-acid, which cannot be synthesized by the living organisms. It is widely used in meat production to accelerate animal growth. The annual worldwide production capacity of DL-methionine is about 500.000 tons.[24] As the natural methionine sources, like plants and microorganisms, offer too low concentrations, it has to be synthesized at a wide industrial scale to satisfy the needs. It is estimated that the global demand will increase by 3 to 7 % in the near future depending on the regions.[25]

© 2011 Tous droits réservés.
http://doc.univ-lille1.fr

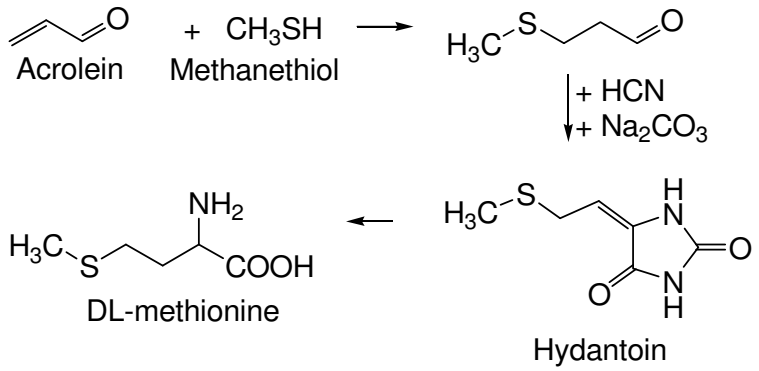

Scheme 1-5: Chemical pathways for the industrial manufacturing of DL-methionine

In the following chapter we will present the state-of-the-art on the sustainable production of acrolein by gas-phase dehydration of glycerol. The general properties needed for yielding high catalytic performances as well as the corresponding three most common catalystic systems will be discussed in detail. Due to the outstanding performances of supported inorganic acids, this catalytic system will be described in details, with a special focus on heteropoly acids as active phases and meso-structured silica as supports. Furthermore, the fundamentals of the reaction are discussed in a specific section devoted to the description of the reaction mechanism.

[1] Directive 2003/30/EC of the European Parliament and of the council of 05/08/2003 on the promotion of the use of biofuels or other renewable fuels for transport.
[2] Eurostat European Commission, http://epp.eurostat.ec.europa.eu.
[3] U.S. National Biodiesel Board, http://www.biodiesel.org.
[4] Global Industry Analysts, http://www.strategyr.com/Glycerin_Market_Report.asp.
[5] J.L. Dubois, G.S. Patience (Arkema) WO2009044051, **2009**.
[6] M. J. Haas, A. J. Mc Aloon, W. C. Yee, T. A. Foglia, *Biores. Tech.*, **2006**, *97*, 671-678.
[7] M. Pagliaro, M. Rossi, in The Future of Glycerol: New Uses of a Versatile Raw Material, RSC Green Chemistry Book Series, **2008**.
[8] Data sources: European Biodiesel Board and HBI.
[9] C. S. Callam, S. J. Singer, T. L. Lowary, C. M. Hadad., *J. Am. Chem. Soc.* **2001**, *123*, 11743.
[10] D. A. Simonetti, J. Ross-Hansen, E. L. Kunkes, R. R. Soares, J. A. Dumesic, *Green Chem.* **2007**, *9*, 1073.
[11] R. R. Soares, D. A. Simonetti, J. A. Dumesic, *Angew. Chem. Int. Ed.* **2006**, *45*, 3982.
[12] D. Siano, E. Santacesaria, V. Fiandra, R. Tesser, G. Di Nuzzi, M. Di Serio, M. Nastasi (ASER), WO 2006111810, **2006**.
[13] D. Schreck, W. Kruper, F. Varjian, M. Jones, R. Campbell, K. Kearns, B. Hook, J. Briggs, J. Hippler (DOW Chemicals), WO 2006020234, **2006**.
[14] N. O. V. Sonntag, *J. Am. Oil. Chem. Soc.* **1992**, *75*, 795.
[15] H. Kimura, Appl. Catal. A: Gen., 1993, 105, 147-158; H. Kimura, K. Tsuto, T. Wakisaka, Y. Kazumi, Y. Inaya, *Appl. Catal. A: Gen.* **1993**, *96*, 217-228.
[16] K. Nabe, N. Izuo, S. Yamada, I. Chibata, *Appl. Environ. Microbiol.* **1979**, *38*, 1056.

© 2011 Tous droits réservés.
http://doc.univ-lille1.fr

[17] R. Ciriminna, G. Palmisano, C. Della Pina, M. Rossi, M. Pagliaro, *Tetrahedron Lett.* **2006**, *47*, 6993.
[18] G.W. Keulks, L.D. Krenzke, T.M. Notermann, *Adv. Catal.*, **1978**, *27*, 183.
[19] M.M. Lin, *Appl. Catal. A: Gen.*, **2001**, *207*, 1.
[20] A. Corma, G.W. Huber, L. Sauvanaud, P. O'Connor, *J. Catal.* **2008**, *257*, 163-171.
[21] ICIS Market-reporter – January 06 **2010** – www.icis.com.
[22] Global Industry Analysts, http://www.strategyr.com/Super_Absorbent_Polymers_Market_Report.asp.
[23] A. Yamamoto, Encyclopaedia of Chemical Technology, 3rd ed. **1978**, Vol. 2, 403.
[24] M. P. Malveda, H. Janshekar, K. Yokose, CEH Marketing Research Report – SRI Consulting, Major Amino Acids, June **2006**.
[25] M. P. Malveda, H. Janshekar, K. Yokose, Chemical Economics Handbook-SRI Consulting, June **2006**, 502.5000 B.

© 2011 Tous droits réservés.
http://doc.univ-lille1.fr

2 Anterior Art

Parts of this chapter are published in:

B. Katryniok, S. Paul, M. Capron, F. Dumeignil *ChemSusChem* **2009**, *2*, 719-730.

B. Katryniok, S. Paul, V. Bellière-Baca, P. Rey, F. Dumeignil, *GreenChem*. **2010** ref. C0GC00194E submitted

2.1 Glycerol Dehydration

It is well known for a long time that heating glycerol induces its decomposition to acrolein and water, with the production of by-products. However, an acid catalyst is needed to get a better control of the reaction and to obtain a significant yield in the unsaturated aldehyde at a moderate temperature. The first patent on the subject was published in 1930 in France.[1] The reaction was carried out in the gas phase over a supported lithium phosphate catalyst, which already provided an acrolein yield close to 75 %. Further, Groll and Hearne claimed a patent for the Shell Company in 1934 for the dehydration of an aqueous glycerol solution in the presence of sulfuric acid at 190 °C, which was supposedly the boiling point of the solution.[2] The resulting acrolein stream was a condensed vapor with a yield of nearly 50 %. Seventeen years later, Hoyt and Manninen patented the dehydration of glycerol using supported phosphorous acid.[3] This heterogeneous catalyst was prepared by impregnation of a clay with 25 wt.% of acid. The authors chose petroleum oil with a boiling point higher than 300 °C as a reaction medium, which enabled the use of higher reaction temperatures compared to those used by Groll and Hearne[2] who worked in the aqueous phase. Even when the glycerol was used at a larger concentration (95 wt.%) a high yield in acrolein (72.3 %) could be reached. However, these early works – in both the gaseous and the liquid phases – remained unfollowed till the end of the 20th century and the upcoming of the massive production of cheap glycerol issued from the biodiesel production process.

The research on the dehydration of glycerol was abandoned until the 90's when the increasing production of bio-diesel led to a glut of cheap glycerol. Neher *et al.* published two patents[4,5] as a following of the old work of Schering-Kahlbaum.[1] They reproduced the tests over the lithium phosphate catalyst and compared its

© 2011 Tous droits réservés. http://doc.univ-lille1.fr

performance to those of a set of acid catalysts with well-defined Hammet acidities (HA) ranged from +3 to -8.2. The authors claimed that aqueous solutions from 10 to 40 wt.% of glycerol could be converted at 300 °C over alumina-supported phosphorous acid to yield acrolein with a selectivity of up to 75 % at full glycerol conversion. The main by-product was hydroxyacetone (selectivity close to 10 %). Neher *et al.* also pursued the research on alumina-supported phosphorous acid but in a view of producing 1,2- and 1,3-propanediol.[6] The yield in the intermediately formed acrolein was however a bit lower (*i.e.*, 70.5 %).

2.1.1 Acidity of the catalyst

Obviously, the acidity of the active phase is a crucial parameter that influences the catalytic performance and stability. The first quantitative studies of this effect were published by Dubois *et al.* in 2006.[7,8] They carried out several tests with Zeolites, Nafion®, heteropoly acids and also with different types of acid-impregnated metal oxides. All these catalysts have a well defined Hammet acidity (HA) ranged between -9 and -18. The selectivity to acrolein depended on the catalyst: For Nafion® catalysts (HA = -12) and for tungsten oxide on zirconium oxide (HA = -14.5), the selectivity to acrolein was close to 70 % at full glycerol conversion, while the selectivity over zeolitic catalysts (HA < 2) did not exceed 60 %. The authors concluded that the catalysts with a HA within the range of -10 to -16 are the best candidates for the selective dehydration yielding acrolein.

Inspired by these rough values, a second research group focused its activities on the influence of the catalyst's acidity. In 2007, Chai *et al.* published two papers on sustainable production of acrolein from glycerol. Whereas the first paper focuses on niobium oxide as a catalyst,[9] the second compares the catalytic performances of different types of acid catalysts.[10] As the acidity of niobium oxide is inversely correlated to the calcination temperature (the higher the calcination temperature of the hydrous niobium oxide precursor, the lower the acidity, as previously described by Chen *et al.*[11] and Lizuka *et al.*[12], this compound is particularly suitable as a model catalyst for studying the influence of the acidity on a given reaction. The best results were obviously obtained for catalysts calcined at low temperatures (250-300 °C). In addition to their high acidity, these catalysts are also advantageous as they show higher specific surface areas than those of the same catalysts calcined at higher temperatures. Nevertheless, the selectivity to acrolein barely exceeded

© 2011 Tous droits réservés. http://doc.univ-lille1.fr

50 % at 90 % of glycerol conversion. In addition, the catalysts calcined at low temperatures showed high carbon deposition and therefore quick deactivation. Thereby, one can already see that the strength of the acid sites must be carefully kept in a narrow window, as too weak acid sites give low selectivity, but too strong acid sites result in accelerated deactivation.

Therefore, Chai's team screened two dozens of catalysts, which they systematically classified into four different groups according to their acidity.[10] Group 1 represents basic catalysts with a HA higher than 7 like magnesium oxide. These catalysts show no selectivity to acrolein at all. Group 2 contains catalysts with a Hammet acidity (HA) ranged between -3 and 7 like zirconium oxide. According to the work of Neher[4], these catalysts should give high acrolein selectivities but, in practice, the selectivity did not exceed 30 % although the performances remained quite stable for 10 h on stream. Group 3, which was more promising, represents catalysts with a HA between -8 and -3. In this group, alumina-supported phosphorous acid can be found next to alumina-supported heteropoly acids, niobium oxide (calcined at 400-500 °C), but this group also contains HZSM zeolites or pure alumina. In good agreement with previous results[7,8], the selectivity is generally higher than that observed for Group 2 catalysts with the exception of pure alumina and niobium oxide calcined at 500 °C. Interesting results were also observed over the alumina-supported phosphotungstic heteropoly acid and a mixed phase of tungsten oxide/zirconium oxide with approximately 70 % of selectivity at a 70 % conversion in both cases after 2 hours on stream. Unfortunately, these catalysts showed poor stability, and their performance significantly decreased during time on stream. Actually, for both catalysts, the glycerol conversion dropped from 68-69 % to 23-25 % between 1 and 10 h under reactant flow, the selectivity being rather unchanged at roughly 66-70 %. The other catalysts were globally less efficient, and gave selectivities between 35 % and 55 % at conversions between 55 % and 100 % after 10 h on stream. In Group 4, one can find catalysts with a HA less than -8, like Hβ-Zeolite, niobium oxide calcined at 350 °C and also alumina-silicate as well as sulfonated zirconium oxide. These catalysts were less selective to acrolein than those of Group 3 but they showed superior performance with time on stream. As an example, the glycerol conversion on an alumina-silicate dropped from 94 to 75 % between 1 to 10 h under reactant flow, the selectivity being rather unchanged at

© 2011 Tous droits réservés.
http://doc.univ-lille1.fr

roughly 43-46 %. Nevertheless, like niobium oxide, Group 4 catalysts were also subjected to a detrimental coking, with a carbon deposit that represented between 100 mg and 400 mg of carbon per gram of catalyst after ten hours on stream.

Additionally to the acidity strength of the catalysts, the type of acid sites has also an important influence on the catalytic performances. When Chai *et al.* classified the catalysts according to their acidity strength[10], they mixed up Brønsted and Lewis acid catalysts without any differentiation. Whereas Brønsted acids are defined as molecules or ions that can donate a proton, like the aforementioned silicotungstic acid, protonated zeolites or phosphorous acid, Lewis acids are described as acceptors for electron pairs, like niobium oxide or pure alumina. From the catalytic results found by Chai *et al.* for these two different types of acids, one can already conclude that they do not follow the same reaction pathway as these authors obtained rather low selectivities to acrolein over Lewis acids.[10]A more detailed study on the different catalytic behaviors of Brønsted and Lewis acids was performed by Alhanash *et al.*[13]who compared a pure Brønsted acid catalyst (cesium salts of phosphotungstic acid) to a pure Lewis acid catalyst (stannous-chromium mixed oxide). Thereby, they could show that:

- Lewis acid catalysts need higher reaction temperatures according to the required higher activation energies compared to Brønsted acid catalysts;
- Lewis acid catalysts give increased selectivity to acetol, the major by-product of the reaction of glycerol dehydration.

These results were confirmed by Kim *et al.*, who used HZSM-5 alumino-silicates with different ratios of alumina and silica.[14]

According to Alhanash *et al.*[13],the reaction on Brønsted acid catalysts starts with the protonation of the secondary hydroxyl-group of the glycerol by a proton from a Brønsted site, like postulated by Bühler for homogenous reaction media (**Scheme 2-3**).[15]The resulting intermediate reacts by cleavage of an hydronium-ion (H_3O^+), and a subsequent keto-enol rearrangement gives 3-hydroxypropion-aldehyde. Acrolein is finally formed after a second dehydration step. The reacted Brønsted acid site is re-protonated by the aforementioned cleaved hydronium-ion. On the other hand, the reaction on Lewis acid sites is completely different as glycerol interacts *via* a concerted transfer of a terminal hydroxyl-group on one of the metal centers, and a

© 2011 Tous droits réservés. http://doc.univ-lille1.fr

migration of the secondary proton to the other metal center. Consequently, 1,2-dihydroxypropene and a pseudo-Brønsted site are formed. The enol will tautomerize to acetol, whereas the pseudo-Brønsted site can either catalyze the dehydration like the aforementioned Brønsted sites or regenerate the initial Lewis site by thermal dehydration. Thereby, one can explain why Lewis acid catalysts generally show higher selectivities in acetol than Brønsted acid catalysts.

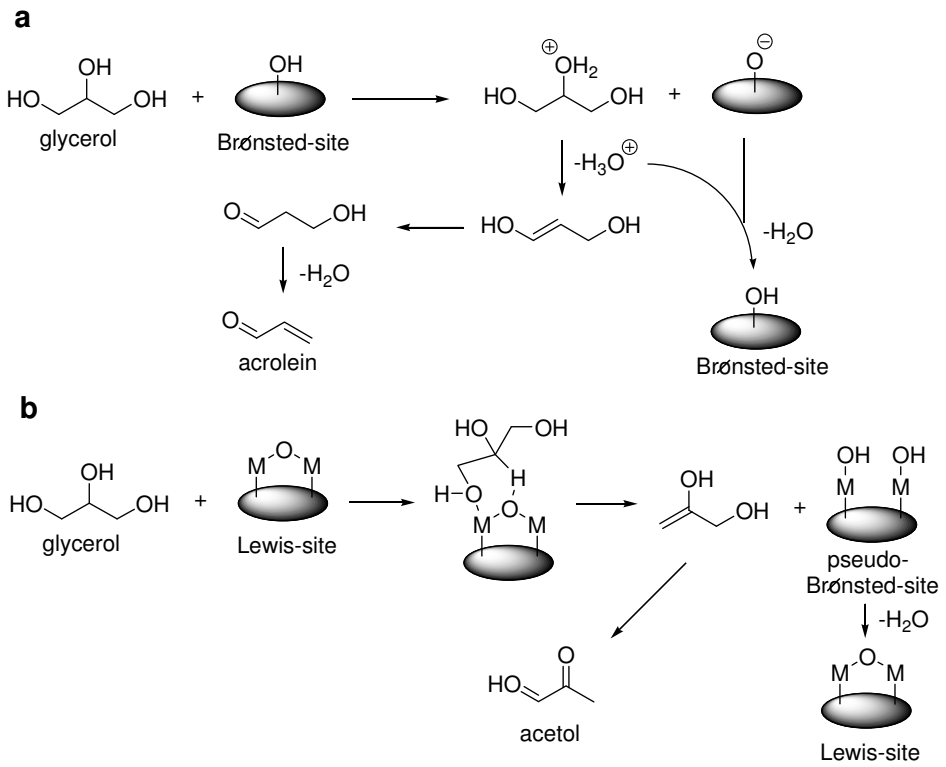

Scheme 2-1: Reaction mechanisms over *(a)* Brønsted and *(b)* Lewisacid catalysts as proposed by Alhanash *et al.*[13]

As catalysts usually contain both acid and basic sites, the influence of the basicity must also be discussed. Kinage *et al.* investigated the selective dehydration of glycerol to acetol, and proposed a reaction mechanism for basic catalysts.[16] In contrast to the mechanisms proposed for acid catalysts, the reaction over basic catalysts does not begin with dehydration but with dehydrogenation (Scheme 2-2). The resulting 2,3-dihydroxy-propanal can either react *via* dehydration and hydrogenation to acetol, or form - *via* retro-aldol-reaction - formaldehyde and hydroxyacetaldehyde, that can be hydrogenated to ethyleneglycol. In the light of this reaction mechanism, one can understand the high selectivity to acetol observed by Chai *et al.* over basic catalysts.[10]

© 2011 Tous droits réservés. http://doc.univ-lille1.fr

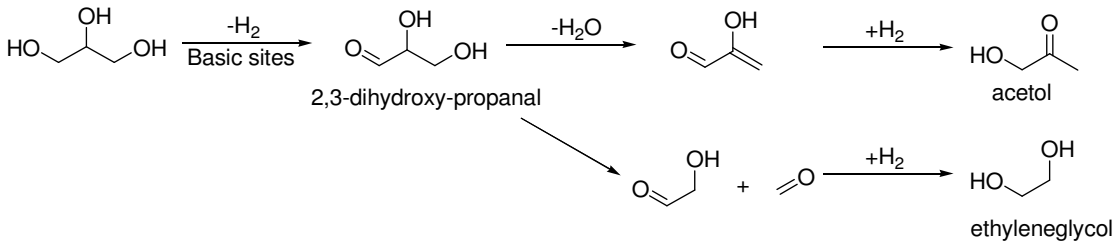

Scheme 2-2: Reaction mechanism over basic catalysts as proposed by Kinage *et al.*[16]

In this section, we have seen that the strength and the type of the catalysts' acidity are of main importance for obtaining good catalytic performances. However, according to the employed catalyst system, this characteristic alone is not sufficient to also get sufficient long-term stability and good selectivity to acrolein. In the next paragraphs, we will discuss in details about the three most widely used catalytic systems for the dehydration of glycerol: Supported heteropoly acids, zeolites and finally the family of metal-oxides, phosphates and pyrophosphates.

2.1.2 Supported heteropoly acids

The use of supported inorganic acids like phosphorous acid or heteropoly acids is one possibility for reaching high performances in the dehydration of glycerol, as shown by Neher and Chai.[4,5,10] However, when using supported catalysts, new parameters beside the aforementioned acidity arise, namely the distribution of the active phase on the support and the pore-size of the support.

Chai *et al.* published two papers in 2008 and 2009 dealing with zirconia- and silica-supported heteropoly acid catalysts.[17,18] These studies showed that the nature of the catalyst support has a significant impact on the thermal stability and on the dispersion of the Keggin-type active phase. The use of zirconia as a support led to better results as far as the deactivation of the catalyst is concerned. The Keggin-anion density at the surface of the support was identified as being a key for tuning the activity and the selectivity of the HPA for acrolein production, which is in good agreement with the conclusions of Ning *et al.* who used activated carbon-supported silicotungstic acid catalysts.[19] The latter claimed that a 10 wt.% silicotungstic acid supported catalyst gives the best acrolein space time yield ever reported in the literature (namely 68.5 mmol acrolein/h·g), but this value is misleading as the calculation was based on the mass of active phase, not on the mass of catalyst. This

© 2011 Tous droits réservés.
http://doc.univ-lille1.fr

promising performance is attributed to the good dispersion of the HPA on the support surface and also to the relative quantities of strong acid sites.

The aspect of the pore-size of the support has been discussed by Tsukuda and coworkers for the first time.[20] This group worked with silica-supported heteropolyacids and focused their study on the influence of the textural properties of the porous support on the selectivity. They used three commercial silica supports with pore sizes of 3, 6 and 10 nm. The active phase was either a heteropoly acid or a conventional inorganic acid like phosphorous or boric acid. Good results were obtained when using Keggin-type heteropoly acids like phosphotungstic acid ($H_3PW_{12}O_{40}$) or silicotungstic acid ($H_4SiW_{12}O_{40}$) on the 6 nm silica-support. At full conversion, the selectivity to acrolein was 65 % and 75 %, respectively (Table2-1), whereas the molybdenum-based homologous heteropoly acid (*i.e.*, $H_3PMo_{12}O_{40}$) did not yield high selectivity (34 %). These values could even be further increased by changing the support with a silica exhibiting alarger pore diameter. The maximum measured selectivity was then 86 % for the silicotungstic heteropoly acid deposited on a 10 nm pore diameter silica with a 30 wt.% loading of active phase (at full glycerol conversion). For very small pore diameters (namely 3 nm), the selectivity remained nearly unchanged with time on stream, whereas the conversion decreased by a factor two probably because of coking related to steric hindrances. The influence of the temperature was also studied and the optimal one in terms of acrolein yield was 275 °C, which is consistent with former studies on Brønsted acid catalysts.

Similar results were obtained by Atia *et al.* who investigated the catalytic performances of the silicotungstic acid supported on alumina with pore sizes of 5 nm and 12 nm.[21] The reaction conditions for the catalytic tests were chosen as the same as those used by Tsukuda[20], for the sake of easier direct comparison. Thereby, one can see that the selectivity to acrolein increased from 65 % for the alumina support with a pore size of5 nm to over 85 % for the alumina support with a pore size of 12 nm, both at full conversion (Table2-1). Furthermore, Atia stated the same activation barrier as Tsukuda, since the alumina based catalysts also showed complete conversion for temperature higher than 275 °C.

These results show that the size of the pores has a direct influence on the selectivity of the catalyst. Actually, if steric limitations do not enable the rapid

© 2011 Tous droits réservés. http://doc.univ-lille1.fr

desorption and diffusion of the products in the porous network of the catalyst, then condensation of reactants and products is more likely to occur, which results in lower selectivity to acrolein and deactivation of the catalyst due to carbon deposit.

Thus, the aforementioned studies point out two important parameters that govern the catalytic performances of supported inorganic acids: the dispersion of the active phase and the textural properties of the catalyst. These two parameters were concomitantly investigated by Chai and Tsukuda, who gathered their efforts, which resulted in the publication of some common patents.[22,23,24] These patents actually focus on supported heteropoly acids as catalysts and on their catalytic performances in relation to the textural properties of the porous support. They carried out a huge number of tests using different catalysts based on various active phases loaded in various amounts on a variety of supports. As previously reported, the phosphomolybdic acid was unselective compared to phosphotungstic acid and silicotungstic acid.[20] With 20-30 wt.% of silicotungstic acid on a porous silica with a pore size of 6 or 10 nm, they obtained a selectivity to acrolein of up to 87 % at 275 °C (Table2-1). Smaller pore diameters (3 nm) or higher reaction temperature (300 °C) always led to a decrease by a factor two in the catalytic performance indicators (selectivity, conversion). The influence of the BET specific surface area of the support was also studied but proved to have little effect. They compared two silica supports with identical pore diameter but with different specific surface areas. A two-fold increase in the surface area did not yield any significant effect on the catalytic performances.

Whereas Chai and Tsukuda[22] showed that silicotungstic acid and phosphotungstic acid gave the best performances, due to their higher acidity, a group around Brückner *et al.*[25] focused on the supported phosphomolybdic acid ($H_3PMo_{12}O_{40}$) and vanado-phosphomolybdic acid ($H_4PMo_{11}VO_{40}$). By electron paramagnetic resonance spectroscopy (EPR) they proved that the Keggin structure of the molybdenum compounds was partially destroyed upon impregnation on silica-alumina support, and that further calcination at 350 °C led to the total decomposition yielding the metal-oxides. These catalysts were then tested in the dehydration reaction, whereby the oxidation state of the metal atoms was followed by *Operando* EPR. The catalytic performance was close to what was already observed for these

© 2011 Tous droits réservés.
http://doc.univ-lille1.fr

Table2-1: Catalytic results for supported heteropoly acids

Catalyst	T_{react} [°C]	m_{Cat} [g]	co-feed	TOS [h]	C [%]	S_{Acro} [%]	S_{Acetol} [%]	Y_{Acro} [%]	STY [mmol /g·h]	ref.
15 wt.% PW/SiO_2	315	0.3	-	10	18	57	7	10	0.6	17
15 wt.% PW/ZrO_2	315	0.63	-	10	76	76	12	58	1.6	17
10 wt.% SiW/AC	330	0.38	-	5	93	67	8	62	11.1	19
20 wt.% PW/Al_2O_3	275	0.3	-	5	99	52	8	51	5.1	21
20 wt.% SiW/Al_2O_3	275	0.3	-	5	98	64	8	63	6.3	21
30 wt.% PMo/Q6	325	0.3	-	5	98	65	7	64	3.8	20
30 wt.% PW/Q6	325	0.3	-	5	100	33	5	33	2.0	20
30 wt.% SiW/Q6	325	0.3	-	5	100	74	7	74	4.4	20
30 wt.% SiW/Q10	275	0.3	-	5	98	86	7	84	5.1	20
CsPW	275	0.3	-	1	100	98	nc.	98	49.0	13

T_{react}=reaction temperature; m_{Cat}=mass of catalyst; co-feed=co-feeding gas; TOS=time on steam; C=conversion of glycerol; S_{Acro}=selectivity to acrolein; S_{Acetol}=selectivity to Acetol; Y_{Acro}=yield of Acrolein; STY=space-time-yield; nc.=not communicated; PW=$H_3PW_{12}O_{40}$; SiW= $H_4SiW_{12}O_{40}$; CsPW= $Cs_{2.5}H_{0.5}PW_{12}O_{40}$; AC=Active carbon; Q6=CARiACT-Q6; Q10=CARiACT-Q10

compounds by Chai[22] and is not really worth mentioning (selectivity to acrolein not exceeding 25 %). On the other hand, the *Operando* screening of the catalyst revealed that the oxidation state of the metals was 3+ for vanadium and 4+ for molybdenum, which indicates that they were reduced during reaction. When oxygen was co-fed, the reduction of vanadium was limited to 4+ and that for molybdenum to 5+, and the coking was slowed down, whereby the authors claim that the carbon is preferentially deposited on the vanadium centers. Moreover, the carbon species present in the coke layer were analyzed. According to the EPR signal, the carbon was mainly in the sp^3 hybridization state, which corresponds to non-double bond C-C chains, like from radical polymerization of the C=C double bond in acrolein. Furthermore, in the presence of oxygen in the feed, the formation of C=O carbonyl groups was detected.

Another idea of using heteropoly compounds was studied by Dubois *et al.*, who used salts of heteropoly acids, obtained by complete or partial substitution of the protons by metal cations.[26] They used silicotungstic or phosphotungstic acid and prepared their according salts with metals from the main group elements, such as caesium, rubidium, calcium or bismuth, or transition metals such as zirconium, lanthanum, iron or hafnium. The partially neutralized heteropoly acids containing caesium ($Cs_{2.5}H_{0.5}PW_{12}O_{40}$ and $Cs_{2.5}H_{1.5}SiW_{12}O_{40}$) and rubidium ($Rb_{2.5}H_{0.5}PW_{12}O_{40}$)

© 2011 Tous droits réservés. http://doc.univ-lille1.fr

required significantly lower reaction temperature (260-280 °C *vs.* 300-350 °C) compared to the proton-free compounds and all showed higher selectivities to acrolein in the so-called oxy-dehydration reaction (90 % vs. 50-70 %). The best result is reported for $Cs_{2.5}H_{1.5}SiW_{12}O_{40}$with a yield of acrolein of 93.1 %. Nevertheless, when this catalyst was used without co-feeding of oxygen, the catalytic performance was much lower with an acrolein yield of no more than 40 %. Comparable results with caesium salt of phoshotungstic acid was reported by Alhanash *et al.*, who also obtained acrolein yields up to 98 % during the first hour of reaction, which is the highest performance ever reported (49 $mmol_{ACRO}\cdot g^{-1}\cdot h^{-1}$; Table2-1).[13] Nevertheless, these authors admit that the catalyst rapidly deactivates, whereby they obtained these performances only for the first hours of reaction.

As a conclusion, one can state that the use of Keggin-type heteropoly compounds is a highly promising way for obtaining high catalytic performances. Due to their composition with central-atom, addenda-atom and counter-ion, they offer many possibilities for tuning their acidity. When these compounds are furthermore deposed on a support, one can even control the pore size of the catalyst, whereby diffusion limitations are reduced and the catalytic performance can be increased. It is also worth mentioning that the support has a significant influence on the long-term performances of the catalysts. In fact, zirconia- and alumina- supported heteropoly acids show increased long-term performances despite average initial performances.

2.1.3 Zeolites

The use of supported heteropoly compounds is not the only way for reaching good catalytic performances. Actually, zeolitic structures are also a promising approach as demonstrated by Dubois *et al.*[8],and are being well studied since then.

Next to the ZSM-5 and β-zeolite, already patented by Dubois *et al.*[8], Li studied other zeolite structures such as MCM-49, MCM-22, MCM-56 and ZSM-11.[27,28] The acrolein yields obtained were in the range of 70-85 % for all the catalysts with nearly no decrease in the catalytic performances during the first 400 h of reaction.

In 2007, Okuno and coworkers patented metallosilicate catalysts with a MFI structure, a typical structure of zeolites with a 3D pore network.[29] Next to aluminosilicates, they also prepared gallosilicates and ferrosilicates. Nevertheless, the tests of the catalytic performances only revealed good results for the first-

© 2011 Tous droits réservés. http://doc.univ-lille1.fr

mentioned aluminosilicates and gallosilicates, whereas ferrosilicates were less selective due to their higher redox-character. The aluminosilicates offered most stable performance without any ion-exchange, and enabled reaching a selectivity to acrolein of around 65 %. In this patent, the results claimed over zeolitic catalysts are quite similar to those reported in Dubois *et al.*'s work (*i.e.*, 70 % of selectivity to acrolein at glycerol full conversion).[8] In further publications, the same team reported the tuning of the acidity by modifying the Si/Al ratio of the zeolite and the best results were achieved using a ratio of 28 with a 71.2 % yield in acrolein (Table2-2).[30,31]

Kim *et al.* picked up the idea of Okuno and studied the influence of the silica/alumina ratio for zeolites of the HZSM-5 type.[14] They chose commercial HZSM-5 catalysts with ratios ranging from 23 to 1000. A detailed characterization of the acid properties using temperature programmed desorption of ammonia revealed an inverse relationship between the total acidity and the silica/alumina ratio. In fact, the catalyst with a silica/alumina ratio of 30 had 9-times more acid sites (66 mmol NH_3/g) than the catalyst with a ratio of 500 (7 mmol NH_3/g). According to the observed desorption temperature, Kim could also show that low silica/alumina ratios result in a larger number of strong acid sites. Nevertheless, these very strong acid catalysts showed only poor selectivity to acrolein of no more than 41.6 % for the catalyst with a silica/alumina ratio of 30 (Table2-2). Therefore, Kim investigated the type of the acid sites and could show that these low silica/alumina ratios lead to Lewis-acid catalysts, whereas higher ratios give Brønsted-acid catalysts as already postulated by Alhanash *et al.*[13] Kim concluded that a Brønsted-acid catalyst with a large number of sites was the most favorable when targeting high acrolein yields. These two conditions were found for a HZSM-5 catalyst with a silica/alumina ratio of 150 which gave 63.8 % of selectivity at a conversion of 75.8 % 315 °C. Furthermore, the influence of the reaction temperature on the last mentioned catalyst was studied, showing that a reaction temperature below 315 °C gave only low conversion of no more than 50.3 %, whereas reaction temperatures above 315 °C resulted in poor acrolein selectivity of no more than 57.4 %.

The idea of tuning the number of Brønsted sites by adjusting the silica/alumina ratio is one possible optimization way. An alternative way was proposed by the research group around Schüth and consists in the replacement of the Brønsted protons at the catalysts' surface by sodium cations using an ion-exchange step.[32]

© 2011 Tous droits réservés.
http://doc.univ-lille1.fr

They used a commercial HZSM-5 catalyst with a silica/alumina ratio of 65 and varied the number of the surface protons between 0.5 and 1. Without any surprise, the catalyst containing no sodium showed the best performance in glycerol dehydration with a 60 % selectivity to acrolein at full conversion, which is explained by the high number of acid sites that are not replaced by sodium (Table2-2).

Further, Zhou and co-workers proposed a synthesis procedure using dual templates of micro- and mesoporous ZSM-5 composites used as catalysts in the dehydration of glycerol to acrolein.[33] The best result achieved with these catalysts was 73.6 % of acrolein selectivity at 98.3 % of glycerol conversion, which is quite a good performance. The influence of the textural parameters is not clear for the used zeolite compounds, but the authors claim that mesopores are more favorable than micropores, as the latter limit the diffusion inside the catalyst. A more detailed analysis on the impact of the pore size of ZSM-5 zeolites on the selectivity was performed by Pathak *et al.*[34] They could show that the selectivity to acrolein increases with the pore size, whereas the selectivities to acetaldehyde, formaldehyde and hydroxyacetone decreases in the meantime. Nevertheless, an optimum pore size cannot be reliably denoted, as only four different pore sizes, namely 0.54, 0.74, 3.15 and 11.2 nm, were investigated.

Table2-2 : Catalytic performances observed over various zeolites

Catalyst	T_{react} [°C]	m_{Cat} [g]	co-feed	TOS [h]	C [%]	S_{Acro} [%]	S_{Acetol} [%]	Y_{Acro} [%]	STY [mmol/g·h]	ref.
β-Zeolite	300	4.2	-	1.5	100	57	10	57	5.8	8
HZSM-5	300	6.4	-	1	79	49	6	39	2.6	8
MFI+Ga	360	9	-	nc.	96	62	nc.	59	4.6	29
MFI28	360	9	-	nc.	92	69	nc.	63	4.8	30
MFI200	360	9	-	nc.	100	61	nc.	61	4.6	30
MFI30	315	0.3	-	2	52	42	7	22	17.0	14
MFI150	315	0.3	-	2	76	64	5	49	37.9	14
MFI500	315	0.3	-	2	39	44	4	17	13.4	14
HZSM-5noNa	320	1.2	-	10	100	60	5	60	0.3	32

T_{react}=reaction temperature; m_{Cat}=mass of catalyst; co-feed=Co-feeding gas; TOS=Time on steam; C=Conversion of glycerol; S_{Acro}=Selectivity to acrolein; S_{Acetol}=Selectivity to Acetol; Y_{Acro}=Yield of Acrolein; STY=Space-time-yield; nc.=not communicated; MFI**=indicates the Si/Al ratio

The use of zeolites as catalysts in the reaction of dehydration of glycerol offers another attractive way due to the possibility of tailor-made acid properties by tuning

© 2011 Tous droits réservés.
http://doc.univ-lille1.fr

the composition of the bulk (silica/alumina ratio), by incorporation of transition-metal oxides (like gallium oxide or iron oxide) or by modification of the surface (ion-exchange). Furthermore, the structure and size of the porous network of zeolites can be tuned, whereby, like in the case of supported inorganic acids, the diffusion limitations can be avoided.

2.1.4 Mixed metal oxides, phosphates and pyrophosphates

As a last group of catalysts employed for the dehydration of glycerol, we summarize various metal oxides, phosphates and pyrophosphates in the following paragraph.

Next to the aforementioned niobium oxide[9], a group around Chai studied binary mixtures of zinc oxide, tin oxide, zirconia, titania, alumina and silica as catalysts in the dehydration reaction.[35] Whereas the catalytic performances of these mixed oxides remains rather low with acrolein yields not exceeding 36 %, the study of the acidity and the textural parameters clearly shows that the less acid catalysts have increased selectivity to hydroxyacetone, whereas small pore diameters lower the selectivity to acrolein.

Suprun *et al.* published a paper on phosphate modified titania, alumina and silica/alumina (SAPO).[36] They found a strong influence of acidity and textural parameters on the catalytic performances. Like in the case of the supported inorganic acids and the zeolites, a relationship between the total acidity and the selectivity to acrolein was observed. In fact, the most acidic catalyst, a silica-alumina phosphate, showed an acrolein selectivity of up to 72 % (Table2-3). Furthermore, Suprun points out that microporous materials (5-6 Å) are less active due to internal diffusion limitations, and tend to increased carbon deposit, as observed on SAPO-34.

A similar catalytic system, namely vanadium oxo-phosphates and oxo-pyrophosphates, was studied by Wang *et al.*[37-38] Like in the case of niobium-oxide, the acidity of these compounds can be tuned by properly adjusting the calcination temperature, but in an inverse relationship, as high calcination temperatures result in a higher number of acid sites. The catalysts were tested in the oxy-dehydration reaction, *i.e.*, with co-feeding of oxygen. The best result was obtained using a vanadium pyrophosphate calcined at 800 °C, which gave a selectivity of 66 % to acrolein at full glycerol conversion (Table2-3). Nevertheless, this result was not

© 2011 Tous droits réservés.
http://doc.univ-lille1.fr

obtained over the catalyst with the largest number of acid sites. As the specific surface area decreases for larger calcination temperatures due to sintering of the solid, the selectivity drops drastically for higher calcination temperature. Dubois continued the study of pyrophosphates using boron and aluminium as cations, whereby the boron-containing compounds showed the highest acrolein yield at a value of 77.8 %.[39]

Other metal pyrophosphates were studied by Liu and coworkers, who used rare earth metals such as lanthanum, neodymium and cerium.[40] All the pyrophosphates show quite high conversions and similar selectivities, whereby the highest yield in acrolein was 80 % achieved over $Nd_4(P_2O_7)_3$. Like concerning the aforementioned vanadium pyrophosphates, the acidity of the neodymium compound is depending on the calcination temperature, whereby the optimum calcination temperature was 500 °C.

The use of phosphates instead of pyrophosphates was studied by Deleplanque *et al.*[41] They prepared iron phosphates using various preparation techniques, such as hydrothermal reaction or precipitation. The highest acrolein yield was 92.1 % in the dehydration reaction. In the oxy-dehydration reaction, *i.e.*, with co-feeding of molecular oxygen, the selectivity to acrolein decreased to 62.5 % at full conversion, due to some total oxidation to carbon oxide species (Table2-3). Therefore, the same group tested the addition of group 1 metal cations, such as caesium, strontium and potassium.[42] The doping with caesium increased the acrolein yield to 72.2 %, which was significantly higher than for the undoped iron phosphate, but still lower than the yield obtained without oxygen co-feeding. The idea of doping the phosphate species was also adopted by Matsunami *et al.*, who used phosphate-modified silica with alkali salts. Nevertheless in this case, the yield in acrolein did not exceed 67 %.[43,44]

Already in 2006, Dubois *et al.* proposed the use of tungsten oxide on zirconia as dehydration catalysts. When a catalyst containing 9 wt% of tungsten oxide was used at 300 °C, total conversion of glycerol was achieved yielding 74 % acrolein.[7] Redlingshofer *et al.* continued the research activities on this kind of binary metal oxide mixtures.[45,46] The reaction was carried out at a relatively lower temperature (260 °C) and they observed good performances with an acrolein yield between 77 and 79 %. Nevertheless, the catalysts tended to deactivate under the stream,

© 2011 Tous droits réservés. http://doc.univ-lille1.fr

whereby the acrolein yield decreased at a rate of 5 % per 10 hours. Additionally, the authors described the possibility of regenerating the catalyst by oxygen treatment at 350 °C for 5 h and claimed recovering the initial catalytic performances after this treatment.[47,48]

This well known combination of tungsten-oxide on zirconia was further studied by Ulgen *et al.*[49] They evidenced a correlation between the increasing amount of tungstenoxide and the increasing acidity. For the catalyst containing 19 wt.% of tungstenoxide, an acrolein yield of 54 % was obtained (Table2-3). Furthermore, the influence of the calcination temperature on the physical properties of the catalyst was studied. Whereas the temperature treatment shows only low impact on the acidity, the number of basic sites is significantly decreased. Moreover, the textural parameters change quite dramatically, as the sintering leads to larger pores but reduced specific surface area. For these two reasons, the thermal treatment has in all cases a positive impact on the catalytic performances, as the decrease in basicity leads to the suppression of acetol and the larger pore size reduces the deactivation due to coking, as internal diffusion limitations are reduced.

Table2-3: Catalytic performance observed over metaloxides, phosphates and oxo-phosphates.

Catalyst	T_{react} [°C]	m_{Cat} [g]	co-feed	TOS [h]	C [%]	S_{Acro} [%]	S_{Acetol} [%]	Y_{Acro} [%]	STY [mmol/g·h]	ref.
Nb_2O_5-350	315	0.56	-	10	75	47	10	35	1.3	9
Nb_2O_5-400	315	0.57	-	10	88	51	12	45	1.6	9
Nb_2O_5-500	315	0.61	-	10	91	35	14	32	1.2	9
TiAl-600	315	0.6	-	2	86	43	17	37	1.1	35
SAPO-11	280	0.2	-	1	66	62	10	41	0.9	36
SAPO-34	280	0.2	-	1	59	72	7	42	0.9	36
VPO-700	300	0.2	O_2	10	81	95	9	77	6.9	37
VPO-800	300	0.2	O_2	10	100	80	6	80	7.1	37
VPO-900	300	0.2	O_2	10	97	58	15	56	5.0	37
$Fe_x(PO_4)_y$	280	0.8	-	5	100	92	0	92	4.1	41
9 wt.%WO_3/ZrO_2	300	17	-	5	100	74	11	74	1.9	7
19 wt.%WO_3/ZrO_2	280	5	-	nc.	83	69	10	57	9.3	49

T_{react}=reaction temperature; m_{Cat}=mass of catalyst; co-feed=Co-feeding gas; TOS=Time on steam; C=Conversion of glycerol; S_{Acro}=Selectivity to acrolein; S_{Acetol}=Selectivity to Acetol; Y_{Acro}=Yield of Acrolein; STY=Space-time-yield; nc.=not communicated; M_xO_y-***=indicates the calcination temperature in °C; TiAl=TiO_2/Al_2O_3 binary mixture; SAPO=silica-alumina-phosphate; VPO=Vanadium oxo-phosphate

© 2011 Tous droits réservés. http://doc.univ-lille1.fr

The family of mixed metal-oxides, phosphates and pyrophosphates is rather heterogeneous. Some compounds, like niobium oxide, tungsten oxide or pyrophosphates, offer the possibility of controlling their acid strength *via* the calcination step. This thermal treatment generally also influences the specific surface area and the pore size as a consequence of sintering, whereby diffusion limitations may arise. In comparison to the aforementioned zeolites and supported HPA, the control of the physical properties of the mixed metal oxides and phosphates is less straightforward.

2.1.5 Reaction mechanism

Whereas the research for an efficient catalyst can follow a more or less purely applied approach, a more fundamental aspect lies in the understanding of the reaction mechanism. This implies the identification of the intermediate steps and the explanation of the formation of the by-products. A first proposal was made by Bühler *et al.* for the glycerol activation in the liquid phase using supercritical water as a catalyst.[15] Two pathways were claimed, either *via* an ionic or a radical mechanism (**Scheme 2-3**). The ionic reaction (**Scheme 2-3a**) begins with the protonation of glycerol either on one primary hydroxyl group or on the secondary hydroxyl group. Afterwards, the elimination of a water molecule leads to the formation of a carbo-cation. In the case of the secondary carbo-cation, the only possible product after cleavage of H_3O^+ is acrolein, whereas either acrolein or acetaldehyde and formaldehyde can be formed starting from the primary carbocation. The radical pathway (**Scheme 2-3b**) starts with the abstraction of an hydrogen from a primary carbon by an $OH^{\bullet}$ radical. The resulting radical species further looses an $OH^{\bullet}$, which leads to the formation of acrolein.

© 2011 Tous droits réservés.
http://doc.univ-lille1.fr

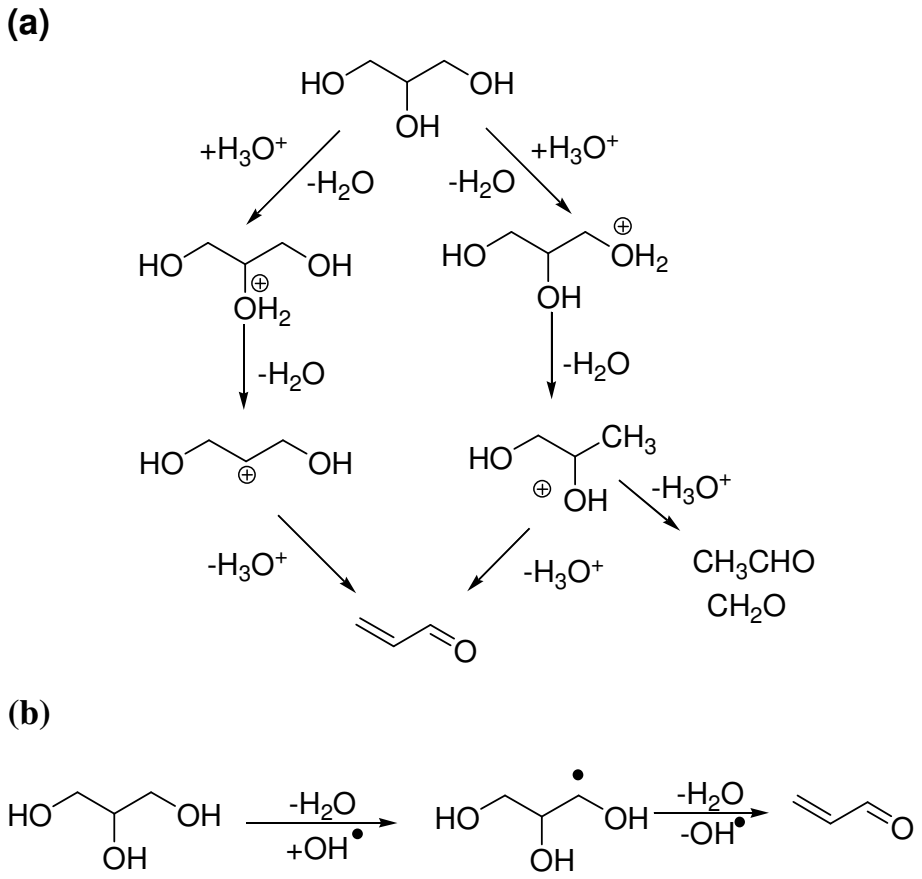

Scheme 2-3: Reaction pathways to the formation of acrolein considering *(a)* an ionic and *(b)* a radical pathway.[15]

Tsukuda *et al.* subsequently proposed a more formal reaction framework (**Scheme 2-4**).[20] The first step of glycerol dehydration leads to the formation of two enols, which are in tautomeric equilibrium with the corresponding ketone (hydroxyacetone) and aldehyde (3-hydroxypropionaldehyde). The latter subsequently reacts in a second step either *via* dehydration to acrolein or *via* retro-aldol reaction to give formaldehyde and acetaldehyde, which may be easily oxidized to acetic acid (in the presence of O_2). As an important conclusion, Tsukuda, in agreement with Bühler's previous proposal[15], points out that the key to obtain high acrolein selectivity lies in the control of the first dehydration step for favoring the formation of 3-hydroxy-propionaldehyde while suppressing the formation of hydroxyacetone, which is identified as the main by-product of the process.

© 2011 Tous droits réservés. http://doc.univ-lille1.fr

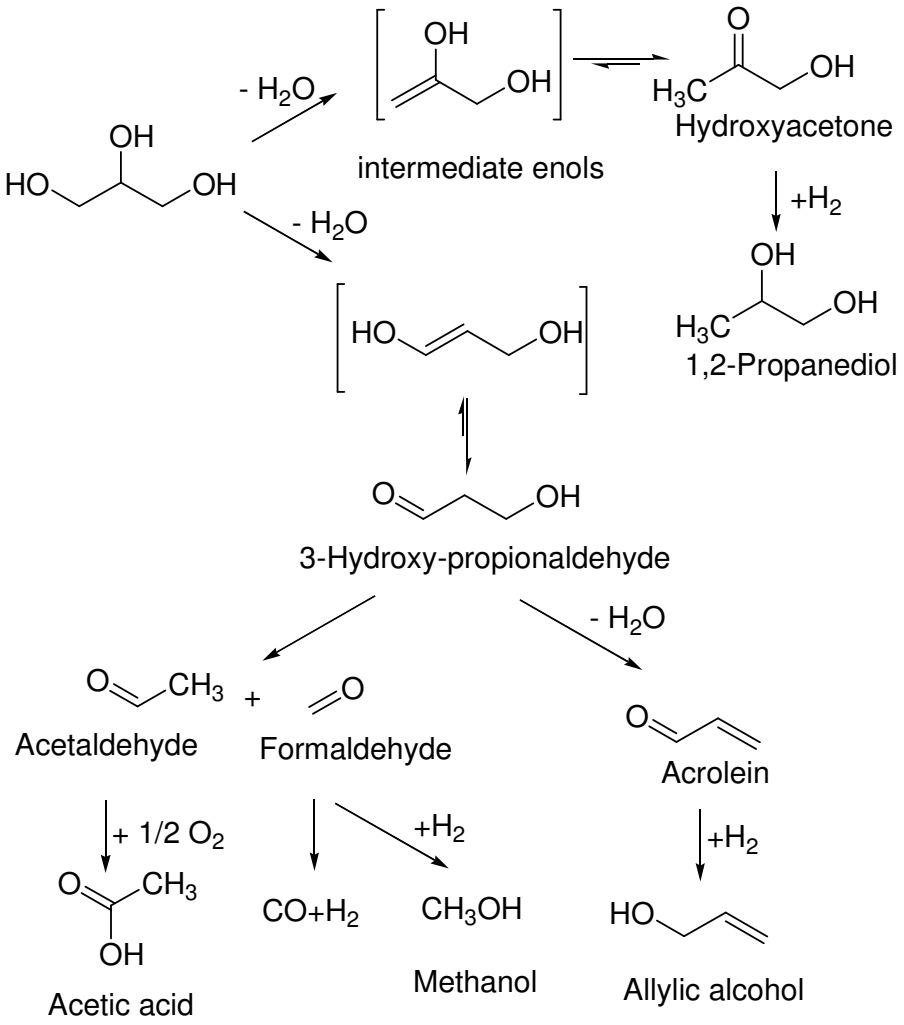

Scheme 2-4: Mechanism proposed by Tsukuda *et al.* and completed by Chai *et al.*[10,20]

The same mechanism has been further completed by Chai *et al.* (**Scheme 2-4**)[10] who added the two hydrogenation steps, which can occur starting from acrolein or hydroxyacetone to respectively form allylic alcohol and 1,2-propanediol, which are sometimes actually observed. The hydrogenation of the formaldehyde to methanol or its decomposition into CO + H_2arealso mentioned.

These schemes are interesting for a first approach, but it is needed to go even deeper in the analysis to explain the formation of all the observed by-products. Corma postulated a more complex reaction framework (**Scheme 2-5**).[50] The first dehydration step is obviously the same as that previously described by Tsukuda and Chai, and leads to hydroxyacetone or 3-hydroxy-propionaldehyde, which further

© 2011 Tous droits réservés.

reacts in a second dehydration step to yield acrolein.[20] In order to go further and investigate the secondary reactions, the authors directly used hydroxyacetone as a reactant at 350 °C and classified the main reaction products in three groups: acids (9.4 %), other aldehydes (52.0 %) and coke (27.7 %). They also observed the formation of low amounts of acetone (4.0 %), acetaldehyde (1.4 %) and carbon monoxide (1.2 %). Nevertheless, the conversion of hydroxyacetone did not exceed 25 %, which means that this compound is quite stable and is thus usually identified as the major by-product of the reaction of dehydration of glycerol to acrolein.

To investigate the consecutive reactions of acetone, they repeated this method by reacting acetone at 350 °C. The resulting product distribution is dominated by unsaturated hydrocarbons like butene (27.9 %), propylene (1.7 %), $C_5 + C_{6\text{-}8}$ aromatics (6.6 %) and coke (31.9 %) (note that this latter is the known consecutive product of unsaturated hydrocarbons). The other identified products were various acids (20.2 %) and other aldehydes (7.3 %) at an overall conversion that did not exceed 14 %. With their findings, they thus completed the reaction scheme proposed by Chai and Tsukuda by adding further side-reactions outgoing from hydroxyacetone. Thereby, they explained the formation of oligomers and coke by consecutive reactions starting from hydroxyacetone *via* acetone and acetaldehyde.

© 2011 Tous droits réservés.
http://doc.univ-lille1.fr

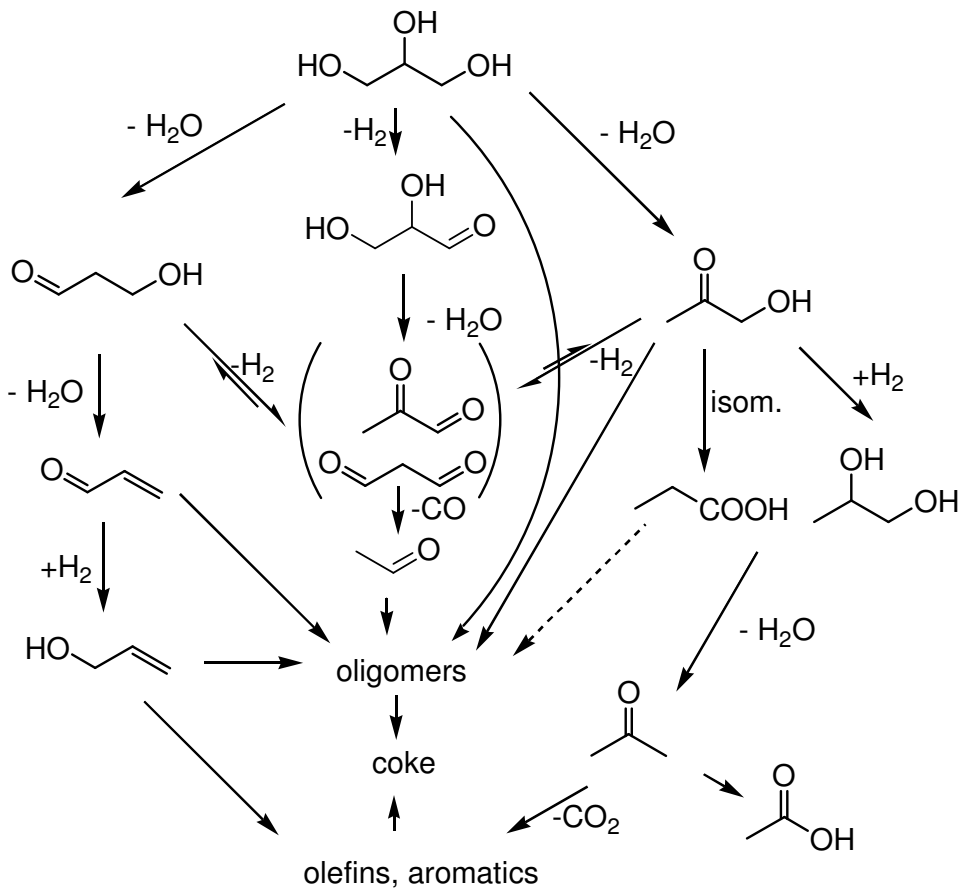

Scheme 2-5: Reaction network proposed by Corma *et al.*[50]

Suprun *et al.* chose a similar approach to investigate the consecutive reactions of 3-hydroxy-propionaldehyde and hydroxyacetone.[36] They could thus confirm the retro-aldol reaction previously postulated by Tsukuda,[20] which leads to the formation of formaldehyde and acetaldehyde issued from 3-hydroxy-propionaldehyde. Additionally, significant amounts of coke were found, which is explained by the formation of cyclic C_6-compounds identified by GC-MS analysis (**Scheme 2-6a**). The authors further identified various furan derivates (**Scheme 2-6b**), which must thus be taken into account when one specifically seeks for fine information on the minor reaction by-products.

© 2011 Tous droits réservés.
http://doc.univ-lille1.fr

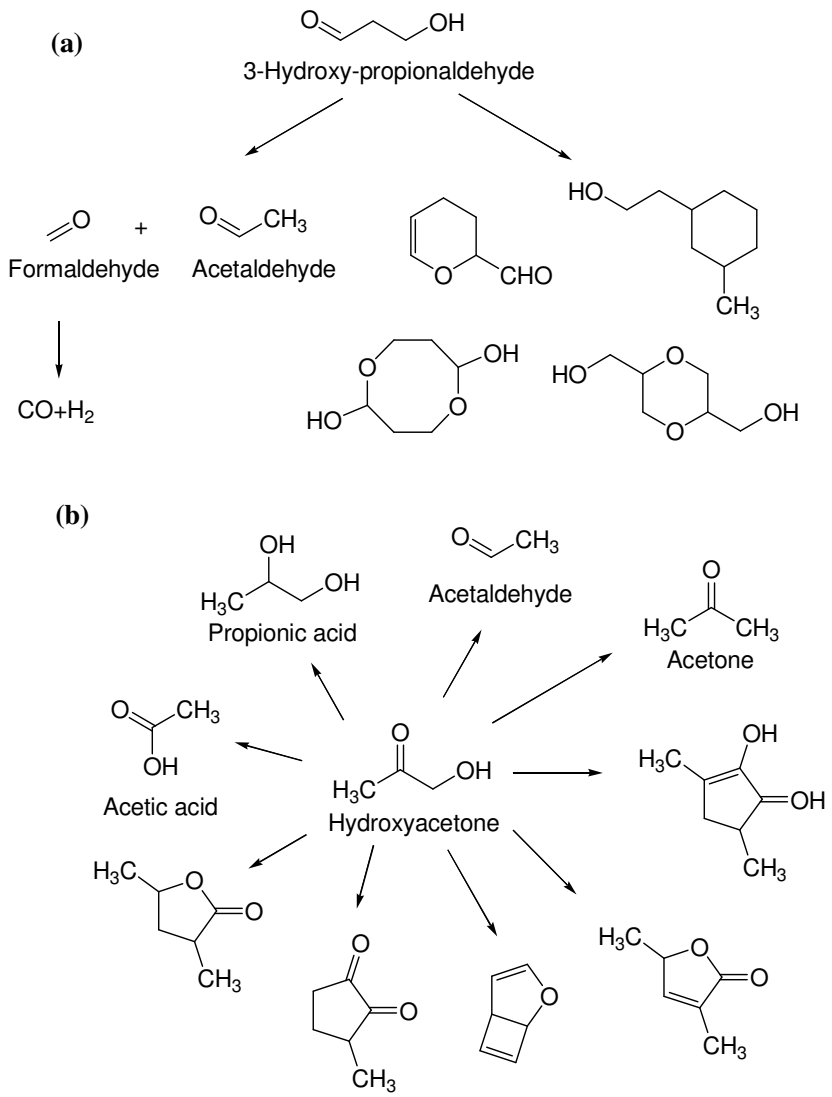

Scheme 2-6: Products derived from *(a)* 3-hydroxy-propionaldehyde and *(b)* hydroxyacetone[36]

In some cases – according to the catalytic system –, the co-feeding of oxygen has a positive impact on the long-term performances. Nevertheless, the presence of oxygen results in a new product distribution. In fact, new by-products, such as organic acids, were observed, whereby a new reaction scheme was proposed by Deleplanque *et al.*(Scheme 2-7).[41] Next to the dehydration reaction yielding the already known products like hydroxyacetone and acrolein, or their reductions to acetone and allylic alcohol, the authors postulate some new oxidation reactions. Starting from formaldehyde – originating from the aforementioned retro-aldol reaction – oxidation leads to the formation of formic acid, which easily decomposes to carbon oxides (CO or CO_2). When acrolein is oxidized, acrylic acid is obtained, which may react through decarbonylation to give acetic acid. Alternatively, the latter can

© 2011 Tous droits réservés. http://doc.univ-lille1.fr

also be formed by oxidation of acetaldehyde. On the other hand, the formation of propanoic acid is explained by the reduction of allylic alcohol in the first step and oxidation of the formed 1-propanol finally yielding the acid. Next to these oxidation reactions, the authors also postulate the formation of acetals issued from the condensation of glycerol with formaldehyde. This may be possible when the glycerol concentration is rather high compared to the oxygen concentration, whereby the oxidation of formaldehyde to formic acid becomes limited. Nevertheless, one can conclude that the presence of oxygen results in a much larger number of by-products, whereby the observed lower selectivity to acrolein can be explained.

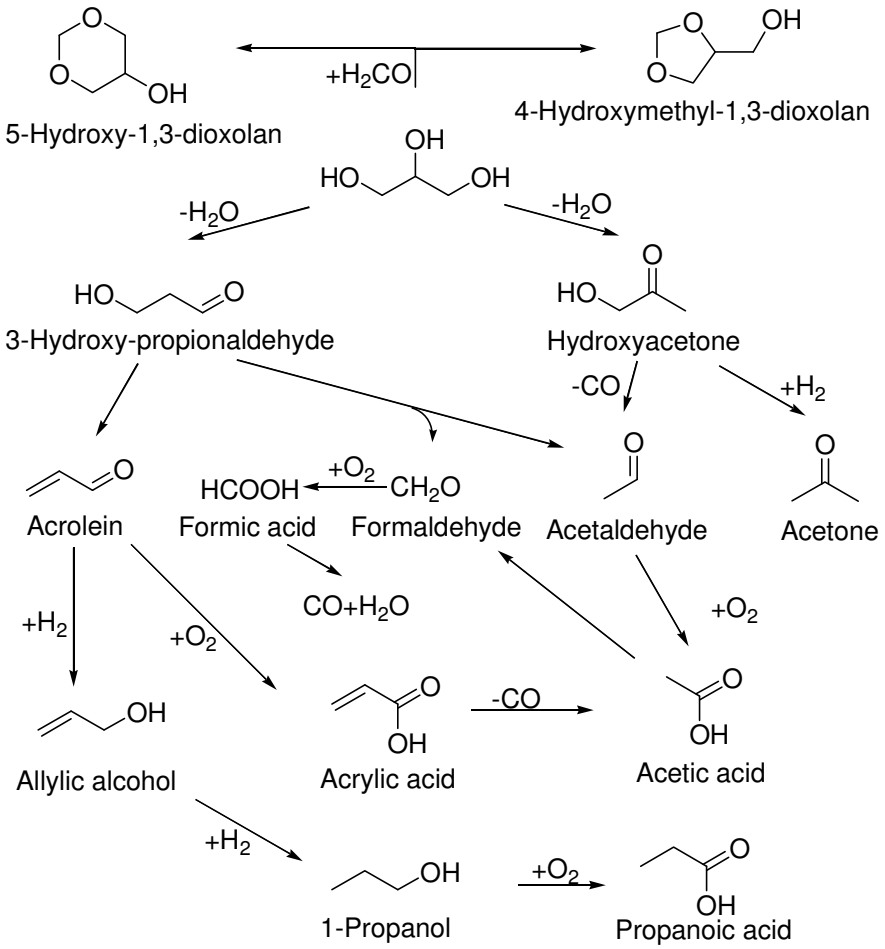

Scheme 2-7: Reaction scheme proposed for dehydration in oxygen-rich atmosphere[41]

All these reaction mechanisms are mostly formal and do not explain the interaction with the solid catalyst. Therefore, Yoda *et al.* developed a mechanism for the dehydration over H-MFI zeolites based on *in-situ* infrared observations.[51] The mechanism is similar to the aforementioned ones, whereby glycerol interacts with the

© 2011 Tous droits réservés.
http://doc.univ-lille1.fr

bridging hydroxyl-group of the zeolite to give alkoxy species (**Scheme 2-8**). When glycerol is bound at the terminal OH-group, acetol is formed upon the known keto-enol-tautomerism. On the other hand, the interaction with the secondary OH-group leads to the formation of a bound intermediate of 3-hydroxypropionaldehyde, and, after a second dehydration step, to the formation of acrolein.

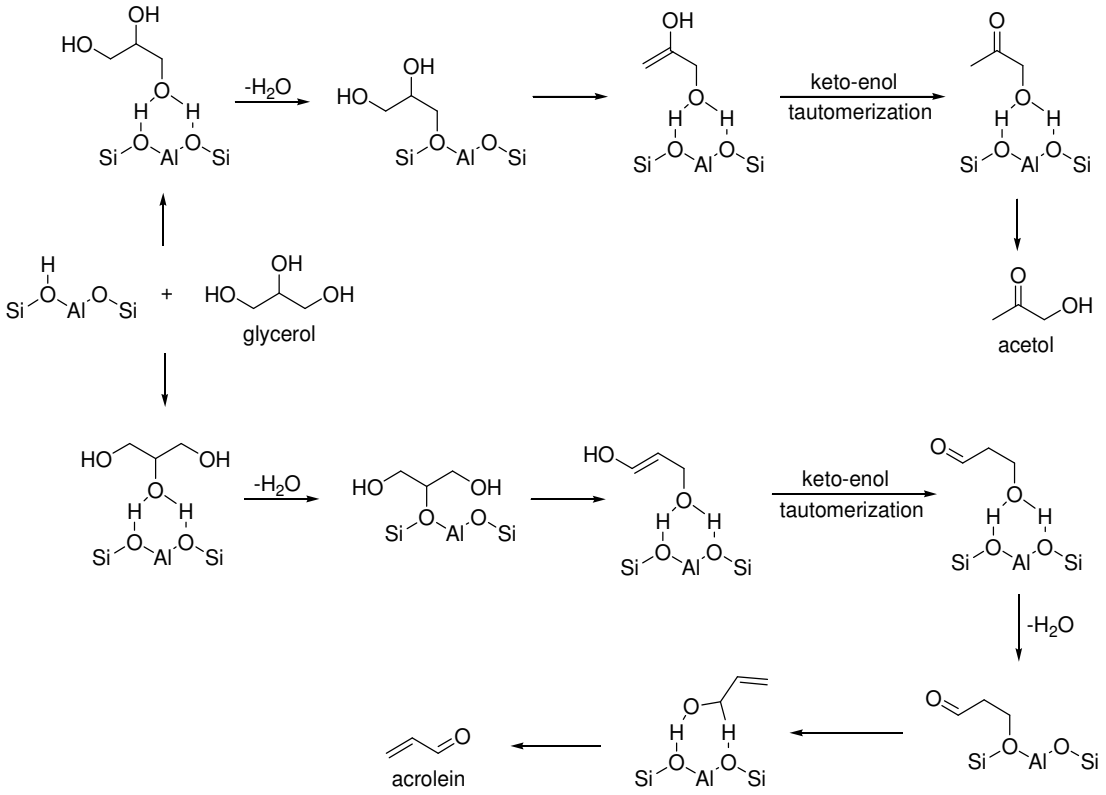

Scheme 2-8: Reaction mechanism over H-MFI catalyst as proposed by Yoda *et al.*[51]

Outgoing from these proposed reaction mechanisms, two research groups calculated the energy-states for the different reaction pathways. Nimlos *et al.* concentrated on the calculations of the neutral and of the protonated reaction pathways using the Gaussian 03 algorithm with B3LYP/6-311G sets for the molecule-orbitals.[52] For the neutral glycerol pathway, they found a very high activation barrier of 70.9 kcal/mol for the dehydration of the secondary hydroxyl-group (**Figure 2-1**). In contrast, the second dehydration step, starting from the intermediate 3-hydroxy-propanealdehyde, required only 29.7 kcal/mol. The dehydration of the primary OH-group, leading to the acetol formation, was found to be energetically even more unfavorable with an activation energy of 73.2 kcal/mol. Nevertheless, the formation of

© 2011 Tous droits réservés.
http://doc.univ-lille1.fr

acetol is exothermic and releases 4.0 kcal/mol, whereas acrolein formation requires 9.3 kcal/mol.

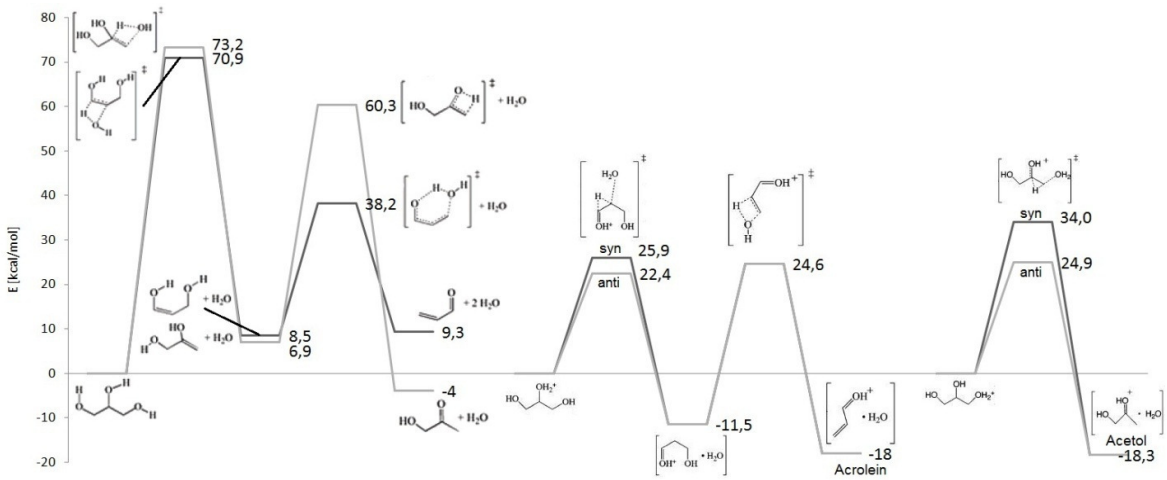

Figure 2-1: Results of thermodynamic calculations for the neutral and the protonated reaction pathways to acrolein and acetol[52]

The calculations for the protonated glycerol pathway, as proposed by Bühler *et al.*[15], show that the activation energies are much lower than for the non-protonated one. Outgoing from the protonated secondary hydroxyl-group of glycerol, the activation energy of the transition-state of the first dehydration is only 22.4 kcal/mol *vs.*70.9 kcal/mol in the case without proton. The activation energy of the second dehydration step, which is calculated at 24.6 kcal/mol in the presence of a proton, is also lower than without. Furthermore, the reaction pathway for protonated glycerol leads to the exothermic formation of acrolein (-18.0 kcal/mol). Like in the case of the non-protonated reaction, the formation of acetol requires - again –a higher activation energy of 24.9 kcal/mol than the formation of acrolein (22.4 kcal/mol). Moreover, the differences in the final energy of the two products are quite low (acetol: -18.3 kcal/mol; acrolein: -18.0 kcal/mol). From these results, one can conclude that the formation of acetol is thermodynamically less favored than the formation of acrolein due to the – slightly - higher activation energy barrier. Nevertheless, the difference is rather small, whereby the formation of acetol cannot be entirely suppressed.

The calculations of the reaction over ZSM-5 zeolite catalysts – as proposed by Yoda *et al.*[51] – was performed by Kongpatpanich *et al.*, who used Gaussian 03 with M06-2X/6-31G set for the zeolite 12T cluster model.[53] For the first dehydration step,

© 2011 Tous droits réservés. http://doc.univ-lille1.fr

they found an activation energy slightly higher than that observed by Nimlos *et al.*for the protonated glycerol pathway(41.4 kcal/mol *vs.*22.4 kcal/mol; **Figure 2-2**).[52] The activation energy of the second dehydration was calculated at 38.5 kcal/mol and the final energy was +19.5 kcal/mol. It is difficult to discuss these divergent results, and, unfortunately, Kongpatpanich missed to calculate the reaction pathway leading to the formation of acetol.

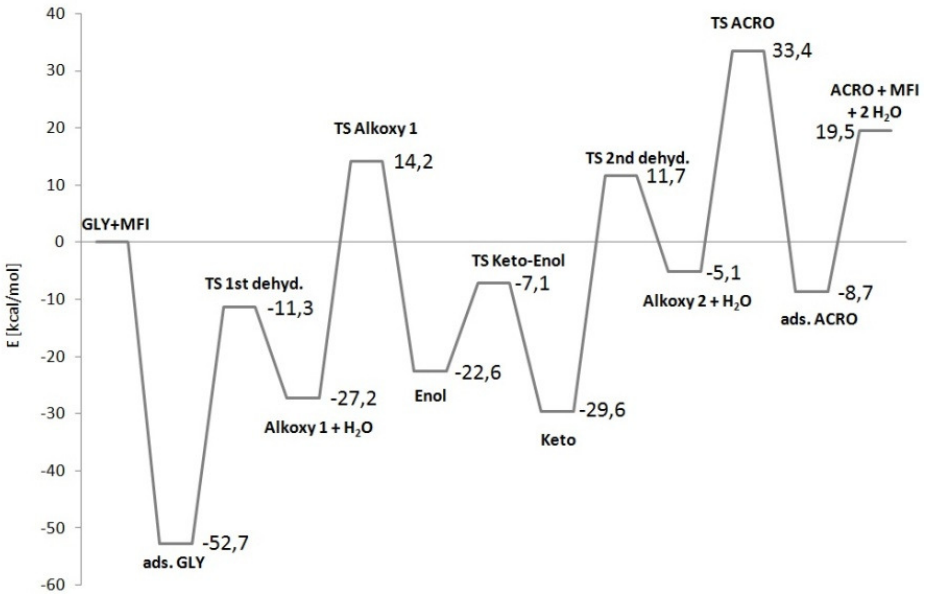

Figure 2-2: Results of thermodynamic calculations for the glycerol dehydration over MFI-zeolite[53]

The described mechanisms give quite good explanations for the observed products in the reaction of glycerol dehydration, such as acrolein, hydroxyacetone, formaldehyde, acetaldehyde, 1,2-propanediol and, of course, coke. The recently published mechanisms over basic catalysts and the different types of acid catalysts are the first attempts for explaining the different product selectivities observed over these types of catalysts. It appears that the influence of thermodynamics on the selectivity of the reaction could not yet be reliably determined by the means of quantum-mechanical calculations.

***

With regards to the catalytic results and the possible reaction mechanisms published in literature, the present work is focused on the dehydration of glycerol using Brønsted acid catalysts. Among those, supported heteropoly acids are outstanding in terms of catalytic performances (activity, selectivity and productivity)

© 2011 Tous droits réservés. http://doc.univ-lille1.fr

compared to other catalytic systems (zeolites, etc.). Furthermore, the acid properties of heteropoly acids can be tuned *via* variation of their composition, which enables obtaining tailor-made properties, whereby optimal conditions for the dehydration reaction can be adjusted. On the other hand, the choice of the support must be carefully performed with regard of the required optimal pore size and the influence on the acidity of the heteropoly acid.

In fact, a pore size of 10 nm was found to be favorable in terms of catalytic performances,[20] which is generally ascribed to reduced diffusion limitations. Among the possible supports, mesoporous silica such as SBA-15 and MCM-41 are already well established in catalysis and offer the possibility of a controlled pore size. On the other hand, zirconia and alumina were identified as supports enabling and increase in the long-term catalytic performance of supported heteropoly acids. Unfortunately, these materials offer less possibility for controlled textural properties, or are not stable under vapor-rich conditions. Thus, in this work, we chose zirconia-modified silica supported heteropoly acids as catalytic systems, as they combine the major advantages separately evidenced for the support and the active phase. In the following two sections, the active phase (heteropoly acid of Keggin type) and the mesoporous silica supports are described in details.

2.2 Keggin-type heteropoly compounds

From the previous paragraphs, one can see that the dehydration of glycerol over heteropoly acids (HPAs) results in high selectivity and conversion. Nevertheless, the catalytic performance is strongly dependant on the type of the used heteropoly compound. In the following section, we will give a detailed description of this family of compounds, with a specific focus on their chemical properties.

Heteropoly compounds (HPCs) are mixed oxides of high molecular weight formed by the condensation of at least two different oxo-anions.[54,55,56] In the solid state, they consist in a combination of heteropoly anions, counter-cations and water of crystallization. Several heteropoly anionic structures have been described, but, among them, the Keggin-type HPAs are the most interesting for catalysis up to now.

These latter HPAs have been discovered by Berzelius in 1826 who synthesized the 12-ammonium phosphomolybdate $(NH_4)_3PMo_{12}O_{40}$ by reacting phosphoric acid with ammonium molybdate. Rosenheim *et al.* proposed to give the name “heteropoly

© 2011 Tous droits réservés. http://doc.univ-lille1.fr

anion" for these compounds in 1917.[57] Some years later, in 1930, Pauling proposed a first hypothesis for the description of the crystallographic structure, but it is Keggin who, in 1934,thanks to the progress made in the XRD technique, correctly identified the structure of the 12-phosphotungstic acid $H_3PW_{12}O_{40}$.[58]Among the HPCs, the Keggin structure is the most studied. These compounds areindeed easy to prepare, quite stable, and are up to now the most interesting ones from a catalysis and industrial point of view. Their raw formula is $XM_{12}O_{40}^{n-}$, where X is the central atom or heteroatom, M the addenda atom and *n* the charge of the heteropoly anion itself.

2.2.1 Structure

The complex structure of these compounds can be divided in two levels of organization[59]:

- The primary structure consisting in the atomic arrangement of the heteropoly anion itself;
- The secondary structure representing the spatial organization of heteropoly anion, the surrounding counter-cations and of the crystallization water.

The primary structure of Keggin-type heteropoly anions consists of a central XO_4 tetrahedron (with X = P, Si, Ge or As), which is linked by the corners with 12 MO_6 octahedra (M = Mo, W, V, Nb, Ni, Co, ...). These octahedra are grouped in four M_3O_{13} ensembles linked by the corners. The octahedra within a same group are linked by the edges as shown in **Figure 2-3**.

© 2011 Tous droits réservés.
http://doc.univ-lille1.fr

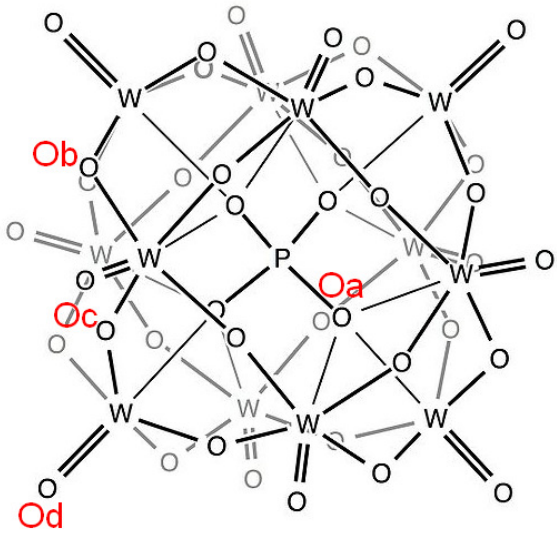

Figure 2-3: Primary structure of a Keggin HPA

This configuration presents four different types of oxygen atoms:

- 4 O_a atoms linking the central tetrahedron with the octahedral;
- 12 O_b atoms linking the M_3O_{13} groups *via* their corners;
- 12 O_c atoms linking the three MO_6octahedra of a same M_3O_{13} group *via* their edges;
- 12 O_d atoms only connected to one M atom (= terminal oxygen atoms).

This regular structure can be included in a sphere, the so-called “Keggin sphere”, of which the diameter is close to 1.2 nm. The electrostatic forces tend to make the M and O_d atoms get closer to one another, which gives to this bound a double bound-like character (thus noted $M{=}O_d$). The $X\text{-}O_a$ bounds are longer and will be more easily cleaved when the Keggin structure is decomposed. Up to six isomers can be obtained by rotating at least one of the M_3O_{13} groups of the primary structure by 60° as the oxygen atoms are not equivalent, which results in a slight distortion of the MO_6 octahedrons. However, at ambient temperature, only two isomers (namely the ‘α’ and the ‘β’ ones) are present unmeasurable quantities. The exchange of one metal addenda atom (*e.g.*, molybdenum) with another metal-atom (*e.g.*, vanadium) does not strongly modify the crystalline network, but results in its slight distortion.

© 2011 Tous droits réservés.
http://doc.univ-lille1.fr

Nevertheless, this modification induces an electronic displacement according to the electron density of the inserted metal.

The secondary structure can be described as a tridimensional arrangement between the heteropoly anions, the cations and the water of crystallization. The observed complex molecular organization is maintained by electrostatic forces or by weak Van-der-Waals or hydrogen bounds. An example of this kind of organization is given in **Figure 2-4**.

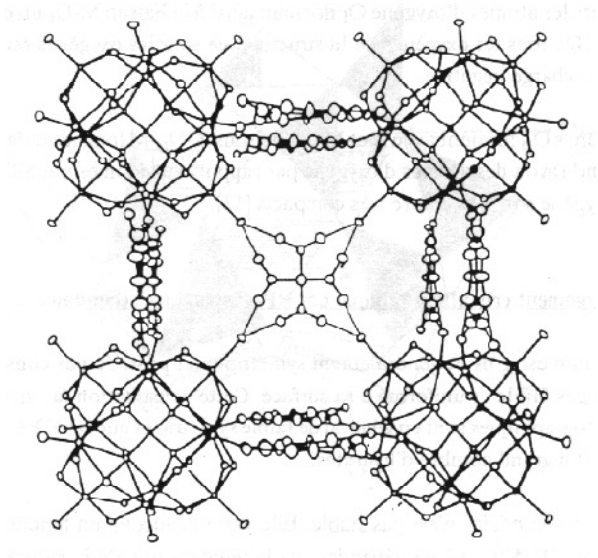

Figure 2-4: Example for a secondary structure of a Keggin-type HPA

Depending on the cations present in the secondary structure, the salts of HPA can be divided in two groups[60]:

- Group A consists of HPA-salts derived from small cations (H^+, Na^+, Cu^+,...).These salts are soluble in water and exhibit low specific surface areas (1~10 m²/g);
- Group B gathers HPA-salts derived from large cations (Cs^+, Ag^+, NH_4^+,...).These salts are insoluble in water and exhibit higher specific surface areas.

The configuration of the secondary structure presents much more varieties than those observed for the primary structure, as it is, *e.g.*, a function of the nature of the counter-cations and of its environment. The secondary structure is a very important

© 2011 Tous droits réservés. http://doc.univ-lille1.fr

feature, as it determines the thermal stability of the compound, which can be an important factor for catalytic applications.

2.2.2 Stability

HPA have proved their remarkable and unique simultaneous acid and redox properties[55], but their rapid degradation at high temperature by decomposition is still a major drawback.[61] The stability of these compounds is thus a critical parameter that has been extensively studied.

In a first step, the water of crystallization is released from the secondary structure at about 200 °C. In the second step, at about 300 °C, the so called "water of constitution" is eliminated, yielding to the formation of lacunary species, whereby the Keggin structure is still kept intact. The third step around 400 °C consists in the irreversible collapse of the Keggin structure, giving simple metal oxides.[56]

For instance, for the silicotungstic acid:

$$H_4SiW_{12}O_{40} \Leftrightarrow SiO_2 + 12\ WO_3 + 2\ H_2O$$

Several ways of enhancement of the stability of the HPAs have been investigated. One way consists in the aforementioned exchange of addenda metal atoms. It is reported that the substitution of a Mo atom by a V atom or by a W atom leads to a more stable HPA.[62] The second way consists on the preparation of HPA salts, which are known to be more stable than their parent acid due to the reduced number of protons needed in the final decomposition step of the HPA. Especially, the insertion of large cation in the secondary structure (type B salts) reinforce the stability of the HPA.[54] On the other hand, the central heteroatom has a quite low influence on the stability of the HPA. However, it seems that phosphorus or arsenic are more favorable than Si. It seems also that the stability of the HPA is linked to the creation of a cubic secondary structure.[63] Some studies were focused on the influence of the support on the thermal stability of the HPA. Apparently, Lewis acid supports (*e.g.*, alumina, zirconia) increase the thermal stability of the HPA by electrostatic interactions.[21] Moreover, the stability can be increased by adapting the reaction conditions of the catalytic process. It was found that reductive conditions (hydrogen) are rather unfavorable,[54] whereas the presence of water and oxygen in the gas phase improves the thermal stability of the HPA at higher temperatures, which can be

© 2011 Tous droits réservés.
http://doc.univ-lille1.fr

explained by the regeneration of partially decomposed Keggin structures and the shift of the equilibrium of the decomposition reaction to the side of the HPA formation.[64]

2.2.3 Chemical properties

As aforementioned, HPAs present simultaneously acid and redox properties. These properties are tunable by modifying their compositions.

2.2.3.1 Acidity

HPA are very strong Brønsted acids, stronger than common inorganic acids (HCl,HNO_3, H_2SO_4 , ...) and are even sometimes classified as super acids.[56,65] The strong delocalization of the charge in the Keggin structure is responsible for this property. In the solid state, these structures present two types of protons:

- delocalized protons, which are rapidly exchanged with those of the water of crystallization;
- more localized protons, which are located near the O_d atoms.

The acidity of the HPAs strongly depends on the nature of the addenda atoms. Hence, the HPAs containing W are more acid than those containing Mo. As a matter of fact, the Mo-O_d bound is more polarizable than the W-O_d bound. The O atoms linked to Mo atoms are negatively charged and protons are less mobile in this case. The Brønsted acidity strongly decreases with the loss of constitutional water because all the residual protons are then localized. The exchange of the protons of the heteropoly acid by cations results in a decreased number of Brønsted acid sites. But, according to Misono *et al.*, the electro negativity of the counter-cation is also an important factor that influences the acidic properties of the HPAs, as some cations can provide their own Lewis acidity (*e.g.*,Al_3^+).[66] When using supported heteropoly acid, the acidity is also depending on the support due to electro-static interactions. It was found that strong interactions result in reduced Brønsted acidity.[21]

2.2.3.2 Redox properties

HPA can also be strong oxidants.[67] This property can also be tuned by judicious changes in the crystal-structure (obtained by tuning the composition of the Keggin heteropoly anion and/or selecting a proper type of counter-cation). Hence, the oxidation power of HPAs increases in the series W, Mo, V for the addenda and B, Si,

© 2011 Tous droits réservés.
http://doc.univ-lille1.fr

P for the central heteroatom. The highest redox potential is observed for the vanado-phosphomolybdic acids, but it rapidly decreases when the corresponding salts are formed.[56]

Molybdenum heteropoly acids are easily reduced, which gives them a blue color: "Molybdenum Blues". The electron in excess is hence localized on a precise metallic site: on V, for instance, in the case of the vanado-phosphomolybdic acids. Misono *et al.* suggested a 2-steps mechanism for the reduction of $H_3PMo_{12}O_{40}$ by molecular hydrogen:[54]

- 1st step: Dissociation of molecular hydrogen as follows:

  $$\text{O-Mo(VI)-O-Mo(VI)-O} + H_2 \rightarrow \text{O-Mo(V)-O-Mo(V)-O} + 2\,H^+$$

  The electrons are then close to the Mo(VI), which takes a Mo(V) character but they remain partially mobile;

- 2nd step: Reaction of the protons with oxygen atoms of the network to form water:

  $$\text{O-Mo(V)-O-Mo(V)-O} + 2\,H^+ \rightarrow \text{O-Mo(V)-Mo(V)-O} + H_2O$$

The excellent redox properties of HPAs give them the ability of catalyzing oxidation reactions as, for instance, the oxy-dehydrogenation of isobutyric acid to methacrylic acid,[68] the oxidation of methacrolein to methacrylic acid,[69] the methanol oxidation to formaldehyde[70] and even the transformation of n-butane to maleic anhydride.[71]

as a conclusion, one can see that heteropoly compounds present an unique combination of acid and redox properties. Moreover, these properties are easily tunable *via*the proper selection of the central atom, the addenda atom, the counter-cations and the support, whereby tailor-made catalysts are feasible.

2.3 Mesostructured silica

According to Tsukuda *et al.*,[20] Atia *et al.*[21]and Zhou *et al.*[33],the porous structure of the support has a significant impact on the catalytic performances, which is mainly ascribed to diffusion limitations. According to the articles of the aforementioned authors, the optimum pore diameter is around 10 nm.[20] Among the various

© 2011 Tous droits réservés.
http://doc.univ-lille1.fr

mesoporous metal-oxide supports, mesostructured silica is most favorable due to its high hydrothermal stability, whereby it has found a wide ranges of applications in catalysis.[72]

Since the discovery of the first mesostructured silica in 1992 by Kresge and Beck,[73,74] various structures have been prepared. Among them, the most popular are SBA-15,[75] MCM-48[74] and MCM-41.[73] All these materials have a well-structured porous network, whereby a very narrow distribution of the pore diameter is obtained.

The general synthesis of mesoporous silica is based on the use of structure-determining templates. The most efficient methods are syntheses based on the use of surfactants. These surfactants consist of a hydrophilic head and a hydrophobic tail within the same molecule. When dissolved in an aqueous reaction media, they will self-organize in such a way that the contact surface between the hydrophobic tail and water is minimized (therefore, the energy of the system is minimal).Depending on the concentration and the temperature, different types of agglomerations can be obtained, like micelles, rods, or lamellar liquid crystals (**Figure 2-5**).[76]

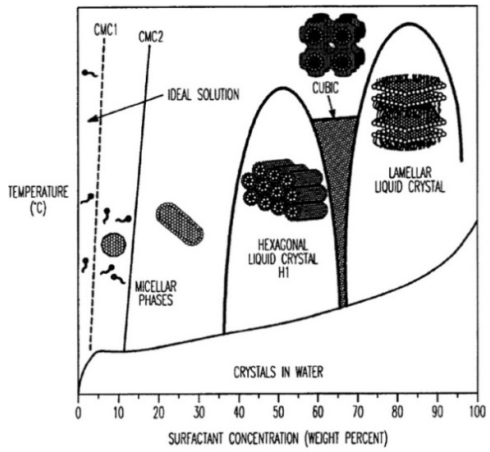

Figure 2-5: Schematic phase diagram for surfactants [77]

The addition of silicaspecies (*e.g.*, tetraethyl-ortho-silicate, 'TEOS') to this mixture leads to the formation of structured silica materials by self-assembly around the surfactant complexes (**Figure 2-6**). This self-organization can take place by two different pathways, in which either the liquid-crystal phase is already formed before the addition of the silicate species (liquid-crystal initiated pathway) or the addition of the silica species induces the agglomeration of isolated silicate-enrobed surfactant

© 2011 Tous droits réservés.
http://doc.univ-lille1.fr

micelles (silicate initiated pathway). The final silica is formed by condensation of the silica species according to the following reaction:

$$Si(EtO)_4 + 4\ H_2O \rightarrow Si(OH)_4 + 4\ EtOH$$

$$n\ Si(OH)_4 \rightarrow OH–(Si(OH)_2)_n–Si(OH)_3 + (n-1)\ H_2O$$

After thermal destruction of the remaining surfactant structure, the mesostructured silica is obtained, whereby the silica structure is the negative pattern of the surfactants' one. Therefore, the silica can be of hexagonal type like MCM-41 and SBA-15, or of cubic type like MCM-48. The structural and physical properties, such as the geometry of the porous-network, the pore-size, the BET specific surface area and the wall thickness, can be controlled *via* modification of the structure (and/or the nature) of the template, which is a function of the surfactants' concentration and the reaction temperature.

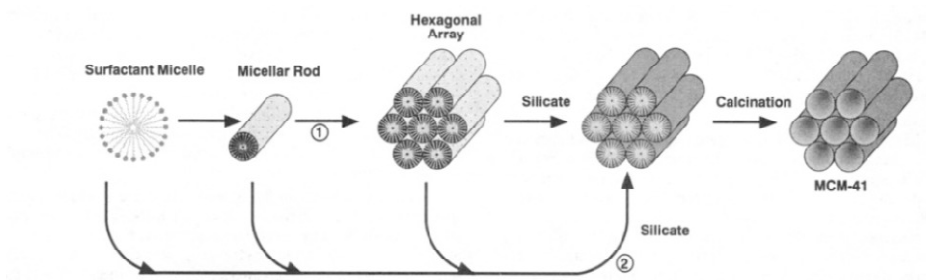

Figure 2-6: Liquid-crystal templating (LCT) mechanism of MCM-41, showing the *(1)* liquid-crystal-initiated and the *(2)* silicate-initiated pathways [73]

In the following section, we will briefly describe the properties of some common mesostructured silica that we used as catalyst supports for the dehydration of glycerol. More detailed information can be found in the well-known review articles from Soler-Illia *et al.*[78], Corma *et al.*[79] or Ciesla *et al.*[80]

2.3.1 MCM-41 and MCM-48

MCM-41 and MCM-48 (Mobile Composition Matters) are the two first discovered mesostructured silica, synthesized in 1992 by the Mobile Research and Development Corporation.[73-74] The surfactant used for their synthesis is a long-chained non-branched amine or ammonium salt (*e.g.*, n-cetyltrimethylammonium bromide).The structural and textural parameters can be controlled by modifying the chain length and/or the concentration of the templating agent: If the amine to silica ratio is less

© 2011 Tous droits réservés.
http://doc.univ-lille1.fr

than 1(excess of Si), hexagonal MCM-41 is formed, whereas higher ratios (excess of amine) lead to the formation of cubic MCM-48.

The structure of MCM-41 can be described as a solid with hexagonal-ordered cylindrical pores without connections between channels and is often compared to a honeycomb (**Figure 2-7**,left). The porous network is 2-dimensional. In contrast, the structure of MCM-48 is classified as a body-centered cubic structure, which is the negative pattern of a micellar-arrangement that is known as gyroid minimum-surface. The MCM-48 network is therefore 3-dimensional. The typical poresize for both types of silica is in the range of 2-10 nm with a specific surface area of more or less 1000 m²/g. Due to a low wall thickness of no more than 0.8-1.2 nm, MCM-41 and MCM-48are quite unstable when exposed to hot water or steam. During 12 h in boiling water, the hydrolysis of the silica proceeds, whereby the highly ordered structure collapses progressively, yielding amorphous silica.

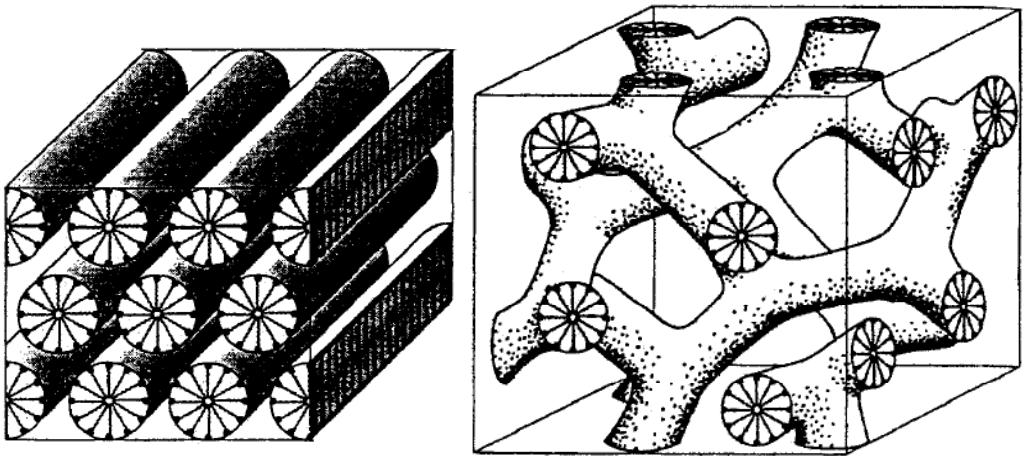

Figure 2-7: Structure of MCM-41(left)[81] and MCM-48 (right)[73]

2.3.2 SBA-15

Similarly to MCM-41, the SBA-15 (Santa Barbara Amorphous) silicate is also of the hexagonal type, but with this small difference that the cylindrical pores have interconnections between each other, and therefore built a 3-dimensional pore-network (**Figure 2-8**). Whereas the cylindrical pores have typical diameters typically from 5 to 30 nm, the interconnections are usually of much smaller diameters and are responsible for the microporosity of SBA-15. Another difference, in comparison to MCM-41, is the larger wall-thickness of 3-6.4 nm, which results in an enhanced tolerance against steam. This is why SBA-15 silica is widely used as a catalyst

© 2011 Tous droits réservés. http://doc.univ-lille1.fr

support for reactions in vapor-rich atmosphere. The specific-surface of SBA-15 can reach1000 m²/g, but this surface decreases when increasing the pore diameter. Like in the case of MCM-41, the textural parameters can be controlled by varying the concentration of the template, which is a poly-triblock copolymer named as 'Pluronic P123' ($EtO_{20}PrO_{70}EtO_{20}$), and/or by tuning the reaction conditions during the hydrothermal treatment[82], and/or by addition of swelling agents such as 1,3,5-trimethylbenzene, 1,3,5-triisopropylbenzene[83] or n-hexane.[84]

Figure 2-8: Schematics of the structure of SBA-15[85]

2.3.3 KIT-6

Similar to MCM-48,KIT-6 has also a body-centered cubic structure, but with thicker walls of *ca.*3.0 nm against *ca.*1.0 nm for MCM-48.[86] The synthesis procedure is similar to that of SBA-15 with P123 as a surfactant and butanol as an additional co-template. Indeed, here butanol plays an important role, which is crucial for the formation of the meso-phase. The cubic phase is only obtained with a butanol/P-123 ratio of1, whereas for lower ratios, a SBA-15-like 2-dimensional hexagonal phase is formed. The obtained silica has a specific surface area of about 800 m²/g and a pore diameter between 4 and 12 nm, depending on the selected reaction conditions.

As a conclusion, mesoporous silica offers the possibility of controlled structure and textural properties. For instance, the pore size can be adjusted within a large range by using adapted reaction conditions. Thereby, these compounds are highly interesting as catalysts supports. Nevertheless, the possible limited hydrothermal stability of silica must be kept in mind when using steam-rich conditions.

© 2011 Tous droits réservés. http://doc.univ-lille1.fr

[1] Schering-Kahlbaum FR695931, **1930**.
[2] H. Groll, G. Hearne (Shell), US 2042224, **1936**.
[3] H. Hoyt, T. Manninen (US Ind. Chemicals. Inc.) ,US 2558520, **1951**.
[4] A. Neher, T. Haas, A. Dietrich, H. Klenk, W. Girke (Degussa), DE 4238493, **1994**.
[5] A. Neher, T. Haas, A. Dietrich, H. Klenk, W. Girke (Degussa), US 5387720, **1995**.
[6] A. Neher, T. Haas (Degussa), US 5426249, **1995**.
[7] J-L. Dubois, C. Duquenne, W. Hoelderich, J. Kervennal (Arkema), WO 2006087084, **2006**.
[8] J-L. Dubois, C. Duquenne, W. Hoelderich (Arkema),WO 2006087083, **2006**.
[9] S-H. Chai, H-P. Wang, Y. Liang, B-Q. Xu, *J. Catal.* **2007**, *250*, 342-349.
[10] S-H. Chai, H-P. Wang, Y. Liang, B-Q. Xu, *Green Chem.* **2007**, *9*, 1130-1136.
[11] Z.H. Chen, T. Lizuka, K. Tanabe, *Chem. Lett.* **1984**, *13*, 1085.
[12] T. Lizuka, K. Ogasawara, K. Tanabe, *Bull. Chem. Soc. Jpn.* **1983**, *56*, 2927.
[13] A. Alhanash, E.F. Kozhevnikova, I.V. Kozhevnikov, *Appl. Catal. A: Gen.* **2010**, *378*, 11-18.
[14] Y.T. Kim, K-D. Jung, E.D. Park, *Micro. Meso. Mater.* **2010**, *131*, 28-36.
[15] W. Bühler, E. Dinjus, H. J. Ederer, A. Kruse, C. Mas, *J. of Supercritical Fluids* **2001**, *22*, 37-53.
[16] A. K. Kinage, P.P. Upare, P. Kasinathan, Y.K. Hwang, J-S. Chang*, Catal. Commun.* **2010**, *11*, 620-623.
[17] S-H. Chai, H-P. Wang, Y. Liang, B-Q. Xu, *Green Chem.* **2008**, *10*, 1087-1093.
[18] S-H. Chai, H-P. Wang, Y. Liang, B-Q. Xu, *Appl. Catal. A: Gen.* **2009**, *353*, 213-222.
[19] L. Ning, Y. Ding, W. Chen, L. Gong, R. Lin, Y. Lü, Q. Xin, *Chin. J. Catal.* **2008**, *29*(3), 212-214.
[20] E. Tsukuda, S. Sato, R. Takahashi, T. Sodesawa, *Catal. Comm.* **2007**, *8*, 1349-1353.
[21] H. Atia, U. Armbruster, A. Martin, *J. Catal.* **2008**, *258*(1), 71-82.
[22] B-Q. Xu, S-H. Chai, T. Takahashi, M. Shima, S. Sato, R. Takahashi (Nippon Catalytic Chem. Ind.), WO 2007058221, **2007**.
[23] T. Sato, R. Takahashi (Nippon Catalytic Chem. Ind.), JP 2008088149, **2008**.
[24] H. Jo, S-H. Chai, T. Takahashi, M. Shima (Nippon Catalytic Chem. Ind.), JP 2007137785, **2007**.
[25] S. Erfle, U. Armbruster, U. Bentrup, A. Martin, A. Brückner, *Appl. Catal. A Gen*, **2010**, doi: 10.1016/j.apcata.2010.04.042 article in press.
[26] J-L. Dubois, Y. Magatani, K. Okumura (Arkema), WO 2009127889 and WO 2009128555, **2009**.
[27] X-Z. Li (Shanghai Huayi Acrylic Acid Co), CN 101070276, **2007**.
[28] A. Zhuang, C. Zhang, S. Wen, X. Zhao, T. Wu (Shanghai Huayi Acrylic Acid Co), CN 101225039, **2008**.
[29] M. Okuno, E. Matsunami, T. Takahashi, H. Kasuga, M. Okada, M. Kirishik (Nippon Catalytic Chem. Ind.), WO 2007132926, **2007**.
[30] M. Okuno, E. Matsunami, T. Takahashi, H. Kasuga (Nippon Catalytic Chem. Ind.), JP 2007301505, **2007**.
[31] M. Okuno, E. Matsunami, T. Takahashi, H. Kasuga (Nippon Catalytic Chem. Ind.), JP 2007301506, **2007**.
[32] C-J. Jia, Y Liu, W. Schmidt, A-H. Lu, F. Schüth, *J. Catal*. **2010**, *269*, 71-79.
[33] C.-J. Zhou, C.-J. Huang, W.-G. Zhang, H.-S. Zhai, H.-L. Wu, Z.S. Chao, *Stud. in Surf. Sci. Catal.* **2007**, *165*, 527-530.
[34] K. Pathak, K.M. Reddy, N.N. Bakhshi, A.K. Dalai, *Appl. Catal. A, Gen.* **2010**, *372*, 224-238.
[35] L-Z. Tao, S-H. Chai. Y. Zuo, W-T. Zheng, Y. Liang. B-Q. Xu, *Catal. Today* **2010**, doi: 101016/j.cattod.2010.03.073 article in press.
[36] W. Suprun, M. Lutecki, T. Haber, H. Papp*, J. Mol. Catal. A: Chem*. **2009**, *309*, 71-78.
[37] F. Wang, J-L. Dubois, W. Ueda, *J. Catal.* **2009**, *268*, 260-267.
[38] F. Wang, J-L Dubois, W. Ueda, *Appl. Catal. A: Gen.* **2010**, *276*, 25-32.
[39] J-L. Dubois (Arkema) WO2010046227, **2010**.
[40] Q. Liu, Z. Zhang, Y. Du, J. Li, X. Yang, *Catal. Lett.* **2008**, *127*(3-4), 419-428.
[41] J. Deleplanque, J-L. Dubois. J-F. Devaux, W. Ueda, *Catal. Today* **2010** doi :10.1016/jcattod.2010.04.012 article in press.

© 2011 Tous droits réservés.
http://doc.univ-lille1.fr

[42] J-L. Dubois (Arkema) WO2009044081, **2009**.
[43] E. Matsunami, T. Takahashi, H. Kasuga (Nippon Catalytic Chem. Ind.), JP 2007268363, **2007**.
[44] E. Matsunami, T. Takahashi, H. Kasuga (Nippon Catalytic Chem. Ind.), JP 2007268364, **2007**.
[45] H. Redlingshoefer, C. Weckbecker, K. Huthmacher, A. Doerflein (Evonik Degussa), WO 2008092533, **2008**.
[46] H. Redlingshoefer, C. Weckbecker, K. Huthmacher, A. Doerflein (Evonik Degussa), DE 102007004351, **2007**.
H. Redlingshoefer, C. Weckbecker, K. Huthmacher, A. Doerflein (Evonik Degussa), EP 2114561, **2009**.
[47] H. Redlingshoefer, C. Weckbecker, K. Huthmacher, A. Doerflein (Evonik Degussa), WO 2008092534, **2008**.
[48] H. Redlingshoefer, C. Weckbecker, K. Huthmacher, A. Doerflein (Evonik Degussa), DE 102007004350, **2007**.
[49] A. Ulgen, W. Hoelderich. *Catal. Lett*. **2009**,*131*,122-128.
[50] A. Corma, G.W. Huber, L. Sauvanaud, P. O'Connor, *J. Catal.* **2008**, *257*, 163-171.
[51] E. Yoda, Y. Ootawa, *Appl. Catal. A : Gen.* **2009**, *360*, 66-70.
[52] M.R. Nimlos, S.J. Blanksby, X. Qian, M.E. Himmel, D.K. Johnson, *J. Phys. Chem. A.* **2006**, *110*, 6145-6156.
[53] K. Kongpatpanich, T. Nanok, B. Boekfa, J. Limtrekul, *Prepr. Pap. - Am. Chem. Soc. Div. Pet. Chem.* **2010**, *55* (1), article in press.
[54] M. Misono, *Catal. Rev., Sci. Eng*. **1987**, *29*, 269-321.
[55] Y. Ono, *Perspectives in catalysis*, London, Blackwell Scientific Publications, **1992**, 431-464.
[56] M. Misono, T. Okuhara, N. Mizuno, *Catalysis by heteropoly compounds, Successful design of catalysis*, Amsterdam, Elsevier Science Publishers, **1988**, 267-278.
[57] A. Rosenheim , J. Jaenicke, *Anorg. Chem*. **1917**, *100*, 304.
[58] J. F. Keggin, *Proc. Roy. Soc*. **1934**, *144*, 75.
[59] D. Casarini, G. Centi, P. Jiru, V. Lena, Z. Tsarugkova*, J. Catal*. **1993**, *143*, 325-344.
[60] N. Niiyama et al., *Nippon Kogaku Kaishi* **1982**, 569.
[61] O. Watzenberger, G. Emig, D. T. Lynch*, J. Catal*. **1990**, *124*, 247-258.
[62] G. Lischke, R. Eckelt, G. Öhlmann, *React. Kinet. Catal. Lett*. **1986**, *31*, 267-272.
K. Brückman, J. Haber, E. Lalik, E. M. Serwicka, *Catal. Lett*. **1988**, *1*, 35-40.
K. Brückman, J. Haber, E. M. Serwicka, *Faraday Discuss. Chem. Soc*. **1989**, *87*, 173-187.
G. A. Tsigidinos, C. J. Hallada, *Inorg. Chem*. **1968**, *7*, 437.
H. G. Jerschkewitz et al., Z. Anorg; *Allg. Chem*. **1985**, *526*, 73.
F. Ritschl, R. Fricke, *J. Chem. Soc., Faraday Trans. 1*, **1987**, *83*, 1041-1053.
[63] F. Cavani, E. Etienne, M. Favaro, A. Galli, F. Trifiro, G. Hecquet, *Catal. Lett*. **1995**, *32*, 215-226.
[64] Y. Konishi, K. Sakata, M. Misono, Y. Yoneda, *J. Catal*. **1982**, *77*, 169-179.
[65] M. Misono, N. Mizuno, K. Katamura, A. Kasai, Y. Konishi, K. Sakata, T. Okuhara, Y. Yoneda, *Bull. Chem. Soc. Jpn.* **1982**, *55*, 400-406.
N. Essayem, G. Coudurier, M. Fournier, J. C. Vedrine, *Catal. Lett*. **1995**, *34*, 223-235.
K. Nowinska, *J. Chem. Soc., Chem. Commun.* **1990**, 44.
[66] N. Mizuno, T. Watanabe, M. Misono, *J. Phys. Chem*. **1985**, *89*, 80-85.
[67] N. Mizuno, T. Watanabe, M. Misono, *J. Phys. Chem*. **1990**, *94*, 890-894.
[68] G. B. Mc Garvey, J. B. Moffat, *J. Catal*. **1991**, *132*, 100-116.
[69] M. Mizuno, T. Watanabe, M. Misono, *Bull. Chem. Soc. Jpn*. **1991**, *64*, 243-247.
[70] K. Brückman, J. M. Tatibouët, M. Che, E. Serwicka, J. Haber, *J. Catal*. **1993**, *139*, 455-467.
[71] M. Ai, *J. Catal*. **1984**, *85*, 324-330.
S. Paul, V. Dubromez, D. Vanhove, *Stud. Surf. Sci. Catal*. **2002**, *143*, 481.
[72] D. Trong On, D. Desplantier-Giscard, C. Danumah, S. Kaliaguine, *Appl. Catal. A: Gen.* **2003**, *253*, 545-602.

© 2011 Tous droits réservés.
http://doc.univ-lille1.fr

[73] J.S. Beck, J.C. Vartuli, W.J. Roth, M.E. Leonowicz, C.T. Kresge, K.D. Schmitt, C.T-W. Chu, D.H. Olson, E.W. Sheppard, S.B. McCullen, J.B. Higgins, J.L. Schlenkert, *J. Am. Chem. Soc.* **1992**, *114*, 10834-43.
[74] C.T. Kresge, M.E. Leonowicz, W.J. Roth, J.C. Vartuli, J.S. Beck, *Nature* **1992**, *359*, 710-712.
[75] D.Y. Zhao, J.L. Feng, Q.S. Huo, N. Melosh, G.H. Frederickson, B.F. Chmelka, G.D. Stucky, *Science* **1998**, *279*, 548-552.
D.Y .Zhao, Q.S. Huo, J.L. Feng, , B.F. Chmelka, G.D. Stucky, *J. Am. Chem. Soc.* **1998**, *120*, 6024-6036.
[76] S. Besson, T. Gacoin, C. Ricolleau, C. Jacquiod, J-P. Boilot, *J. Mater. Chem.* **2003**, *13*, 404-409.
[77] G. Lopez, C. Brinker, H. Fan, Y. Lu (Science and Technology Corporation at the University of New-Mexico), US 6913832, **2005**.
[78] G.J. de A.A. Soler-Illia, E.L. Crepaldi, D. Grosso, C. Sanchez, *Curr. Op. in Coll. Interf. Sci.* **2003**, *8*, 109-126.
[79] A. Corma, *Chem. Rev.* **1997**, *97*, 2327.
[80] U. Ciesla, F. Schüth, *Micro. Meso. Mater.* **1999**, *27*, 131.
[81] K. Schumacher, P.I. Ravikovitch, A. Du Chesne, A.V. Neimark, K.K. Unger, *Langmuir* **2000**, *16*, 4648-4654.
[82] J. Roggenbuck, G. Koch, M. Tiemann, *Chem. Mater.* **2006**, *18*, 4151-4156.
[83] L. Cao, T. Man, M. Kruk, *Chem. Mater.* **2009**, *21*, 1144-1153.
[84] M. Kruk, L. Cao, *Langmuir* **2007**, *23*, 7247-7254.
[85] W.B. Yue, W.Z. Zhou, *Prog. Nat. Sci.* **2008**, *18*, 1329-1338.
[86] F. Kleitz, S-H. Choi, R. Ryoo, *Chem. Commun.* **2003**, *17*, 2136-2137.

© 2011 Tous droits réservés.
http://doc.univ-lille1.fr

3 Synthesis procedures and characterization methods

3.1 Preparation of the catalysts

The preparation of each catalyst is performed in several steps. In the next sub-chapters we describe the complete synthesis of each catalyst, starting from the synthesis of various heteropoly acids, which are used as active phases for all the catalysts. Afterwards, the preparation of the various mesoporous silica, used as catalyst supports, is described, and the zirconia-grafting method is the object of a further specific section. Finally, the impregnation procedure of the supports with the active phases is given.

3.1.1 Preparation of the heteropoly acids

The general synthesis method of the heteropoly acids follows four elementary steps: preparation of the heteropoly anion, protonation of the anion to obtain the acid, isolation of the heteropoly acid, and finally purification by crystallization.

3.1.1.3 Phosphotungstic acid $H_3PW_{12}O_{40}$

The reaction of formation of phosphotungstic acid from simple oxides is as follows:

$$12\ WO_4^{2-} + HPO_4^{2-} + 23\ H_3O^+ \rightarrow PW_{12}O_{40}^{3-} + 35\ H_2O$$

The amounts of the reactants are chosen with regard to the stoichiometry of the reaction:

Reactant	Molar ratio	Moles	Mass/Volume
$Na_2WO_4 \cdot 2\ H_2O$	4.0 eq.	0.06 mol	20 g
H_3PO_4 (85 wt.%, 14.7 M)	1.0 eq.	0.015 mol	1 mL
HCl (37 wt.%)	1.0 eq.	0.165 mol	13.3 mL

The original synthesis by M. Fournier[1] was adapted, and conducted according to the following procedure:

1 mL of phosphoric acid (Riedel) is added dropwise to a solution of 20 g of sodium tungstate dihydrate (Fluka) in 20 mL of hot water. The solution becomes instantly white. Further addition of 13.3 mL of concentrated hydrochloric acid (Fluka) leads to a clear solution followed by the precipitation of the white disodium salt. The obtained

© 2011 Tous droits réservés.
http://doc.univ-lille1.fr

mixture is heated at 60 °C to evaporate half of its volume, before being stored at ambient temperature overnight. The residue is filtered and the solid is dissolved in 33.3 mL of hot hydrochloric acid (0.1 M). The solution is left and cooled to room temperature. If precipitation occurs, more hydrochloric acid is added. The protonated heteropoly anion is extracted with diethylether, in a quantity equivalent to that of added concentrated hydrochloric acid. A heavy phase of HPA etherate is formed next to the aqueous phase. Extraction is stopped when a lighter third phase of pure diethylether becomes visible. The etherate is collected and completed with a half volume of water. The biphasic system is kept at ambient temperature until all diethylether is evaporated. The remaining solution is cooled at 4 °C to achieve crystallization.

3.1.1.4 Silicotungstic acid $H_4SiW_{12}O_{40}$

The reaction of formation of silicotungstic acid from simple oxides is as follows:

$$12\ WO_4^{2-} + SiO_3^{2-} + 22\ H^+ \rightarrow \alpha\text{-}SiW_{12}O_{40}^{4-} + 11\ H_2O$$

The amounts of the reactants are chosen with regard to the stoichiometry of the reaction:

Reactant	Molar ratio	Moles	Mass/Volume
$Na_2WO_4 \cdot 2\ H_2O$	12.0 eq.	0.06 mol	19.9 g
$Na_2SiO_3 \cdot 5\ H_2O$	1.0 eq.	0.005 mol	1.1 g
HCl (37 wt.%)	22 eq.	0.1 mol	13.0 mL

16.5 mL of hydrochloric acid (4 M) are added dropwise to a solution of 18.2 g of sodium tungstate dihydrate (Fluka) in 30 mL of hot water. Afterwards, a solution of 1.1 g of sodium metasilicate pentahydrate (Aldrich) in 10 mL of water is rapidly added followed by further addition of 5 mL of hydrochloric acid (4 M). The mixture is heated and keptin boiling conditions for 1 h to complete the isomerization of the α-form. Then, another solution of 1.7 g of sodium tungstate dihydrate in 5 mL water is added, followed by subsequent addition of 8 mL of hydrochloric acid (4 M). The solution is left to reach room temperature.

If precipitation occurs, the mixture has to be filtered before further treatment. The solution is heated to 65 °C to evaporate half of its volume. Then, the protonated heteropolyanion is extracted with diethylether, using a quantity equivalent to that of

concentrated hydrochloric acid. It occurs a heavy phase of the HPA etherate next to the phase of water. The extraction is stopped when a lighter third phase of pure diethylether becomes visible. The etherate is collected and completed with a half volume of water. A blue solution is obtained. The biphasic system is kept at ambient temperature until all the diethylether is evaporated. The remaining solution is cooled at 4 °C to achieve crystallization.

3.1.1.5 Phosphomolybdic acid $H_3PMo_{12}O_{40}$

The reaction of formation of phosphomolybdic acid from simple oxides is as follows:

$$12\ MoO_4^{2-} + HPO_4^{2-} + 23\ H_3O^+ \rightarrow PMo_{12}O_{40}^{3-} + 35\ H_2O$$

The amounts of the reactants are chosen with regard to the stoichiometry of the reaction:

Reactant	Molar ratio	Moles	Mass/Volume
$Na_2MoO_4 \cdot 2\ H_2O$	12.0 eq.	0.09 mol	21.1 g
H_3PO_4 (85 wt.%, 14.7 M)	1.0 eq.	0.0075 mol	0.5 mL
$HClO_4$ (70 wt.%)	38 eq.	0.285 mol	24.3 mL

0.5 mL of phosphoric acid (Riedel) is added dropwise to a solution of 21.1 g of sodium molybdate dihydrate (Fluka) in 30 mL of hot water. Addition of 24.3 mL of concentrated perchloric acid (Fluka) leads to a canary-yellow solution with slight precipitation. The mixture is kept overnight at ambient temperature.

The residue is filtered and the solid is dissolved in hydrochloric acid (1.5 M). The protonated heteropoly anion is extracted with diethylether. A heavy phase of HPA etherate is formed next to the aqueous phase. Extraction is stopped when a lighter third phase of pure diethylether becomes visible. The etherate is collected and completed with half volume of water. The biphasic system is kept at ambient temperature until all diethylether is evaporated. The remaining solution is cooled at 4 °C to achieve crystallization.

3.1.1.6 Vanado-substituted phosphomolybdic acids ($H_4PMo_{11}VO_{40}$ and $H_5PMo_{10}VO_{40}$)

The reactions of formation of vanado-phosphomolybdic acid and di-vanado-phosphomolybdic acid from simple oxides are as follows:

$$PMo_{11}O_{39}^{7-} + VO_3^- + 4\ H_3O^+ \rightarrow PVMo_{11}O_{40}^{4-} + 6\ H_2O$$

$$PMo_{10}O_{38}^{11-} + 2\ VO_3^- + 4\ H_3O^+ \rightarrow PV_2Mo_{10}O_{40}^{5-} + 6\ H_2O$$

The amounts of the reactants are chosen with regard to the stoichiometry of the reactions:

Reactant	Molar ratio	Moles	Mass/Volume
$Na_2HPO_4 \cdot 2H_2O$	1.0 eq.	0.1 mol	17.8 g
$Na_2MoO_4 \cdot 2\ H_2O$	11.0 eq.	1.1 mol	266 g
$NaVO_3$	1.0 eq.	0.1 mol	12.2 g
HCl (37 wt.%)	1.2 eq.	0.12 mol	10 mL

The original synthesis by Rabia *et al.*[2] was adapted and conducted according to the following way:

17.8 g of sodium phosphate dihydrate (Fluka) are added to a solution of 12.2 g of sodium metavanadate (Aldrich) in 500 mL of boiling water. After cooling to room temperature, 10 mL of concentrated hydrochloric acid (Fluka) are added. The addition of an aqueous solution of 266 g of sodium molybdate dihydrate (Fluka) in 500 mL of water results in a change of color from yellow to brown. Afterward, the reaction mixture is acidified with 400 mL of hydrochloric acid, which results in an orange solution. The mixture was further kept at room temperature overnight. The preparation of di-vanado-phosphomolybdic acid is performed in the same way, but with twice the amount of sodium metavanadate.

The protonated heteropoly anion is extracted with diethylether. A heavy phase of HPA etherate appears next to the aqueous phase. Extraction is stopped when a lighter third phase of pure diethylether becomes visible. The etherate is collected and 75 mL water are added. The biphasic system is kept at room temperature until all diethylether is evaporated. The remaining solution is cooled at 4 °C to achieve crystallization.

© 2011 Tous droits réservés.
http://doc.univ-lille1.fr

3.1.2 Silica supports

The synthesis of the silica supports consists of four elementary steps: Preparation of the template solution based on micelles formed by the surfactants, addition of the silica precursor, hydrothermal treatment, and finally elimination of the template by calcination. Furthermore, three commercially-available silica supports were also used: CARiACT Q-10 (Fuji Silysia), TMPS-4 and TMPS-2.7 (both from Taiyo Kagaku). Whereas CARiACT has an hexagonal structure, the TMPS support is a tetragonal structured mesoporous silica.

3.1.2.1 SBA-15 with a pore size between 4 and 9 nm

The preparation of SBA-15 with a pore size between 4 and 9 nm is performed following the procedure of Roggenbuck *et al.*[3] The amounts of reactants are chosen with regard to the desired molar ratios, which determine the coordination of the micelles in hexagonal arrays:

Reactant	Molar ratio	Moles	Mass/Volume
P123 (M_W 5400)	0.018 eq.	0.022 mol	12.0 g
$Si(OEt)_4$ (TEOS)	1.0 eq.	0.115 mol	24.0 g
Water	191 eq.	22.0 mol	370 mL
HCl (32 wt.%)	2.82 eq.	0.325 mol	37.0 mL

12.0 g of triblock-copolymer P123 (Aldrich) are dissolved in a mixture constituted of 370 mL of distilled water and 37 mL of HCl (32 % - Riedel de Häen) at 40 °C. When the solution becomes clear, 24.0 g of tetraethyl-orthosilicate (TEOS - Fluka) are added. The resulting molar ratio is 1.0 TEOS : 0.018 P123 : 2.82 HCl : 191 H_2O. The reaction mixture is left under moderate stirring at 40 °C overnight (24 h) before being subsequently transferred in a teflon-lined autoclave. According to the desired poresize, the silica-gel is hydrothermally treated for 24 h at 50, 100 or 140 °C, whereby high temperature leads to increased pore diameter (e.g. 140°C for 9 nm pore diameter). After filtration, the silica is dried at 80 °C and finally calcined at 550 °C for 3 h (1 °C/min.).

© 2011 Tous droits réservés.
http://doc.univ-lille1.fr

3.1.2.2 SBA-15 with a pore size of 13 nm

The preparation of SBA-15 with the large pore size of 13 nm is performed following the procedure of Kurk *et al.*, using hexane as a micellar expander.[4] The amounts of the reactants are chosen with regard to their desired molar ratio, which determines the coordination of the micelles in hexagonal arrays, with the hexane located inside the micelles:

Reactant	Molar ratio	Moles	Mass/Volume
P123 (M_W 5400)	0.017 eq.	0.45 mmol	2.4 g
$Si(OEt)_4$ (TEOS)	1.0 eq.	0.026 mol	5.5 g
Water	170 eq.	4.5 mol	75 mL
HCl(37 wt.%)	4.1 eq.	0.11 mol	9.0 mL
NH_4F	0.030 eq.	0.73 mmol	0.027 g
hexane	5.7 eq.	0.15 mol	13.0 mL

2.4 g of triblock-copolymer P123 (Aldrich) and 0.027 g of ammonium fluoride (Aldrich) are dissolved under stirring in a mixture constituted of 75 mL of distilled water and 9 mL of hydrochloric acid (37 wt.%- Fluka) at 25 °C. The temperature is then decreased to 15 °C. After one hour, a mixture of 5.5 g of tetraethyl-orthosilicate (TEOS - Fluka) in 13 mL hexane (≥ 95 % - Carlo Erba/SDS) is added. The resulting molar ratio is 1.0 TEOS : 0.017 P123 : 0.030 NH_4F : 4.1 HCl : 170 H_2O : 5.7 n-hexane. The reaction mixture is kept under stirring at 15 °C during 24 h before being subsequently transferred in a teflon-lined autoclave. The silica-gel is heated for hydrothermal treatment during 24 h at 80 °C. After filtration, the silica is washed with distilled water and dried at 80 °C. Calcination is performed under static air at 550 °C for 3 h (heating ramp of 1 °C/min.).

3.1.2.3 KIT-6

The synthesis of KIT-6 is based on the procedure described by F. Kleitz *et al.*[5] The amounts of the reactants are chosen with regard to their desired molar ratios, which determine the coordination of the micelles in cubic arrangement:

Reactant	Molar ratio	Moles	Mass/Volume

© 2011 Tous droits réservés.
http://doc.univ-lille1.fr

P123 (M_W 5400)	0.018 eq.	0.022 mol	9.0 g
$Si(OEt)_4$ (TEOS)	1.0 eq.	0.115 mol	19.5 g
Water	200 eq.	22.0 mol	325 mL
n-Butanol (BuOH)	1.3 eq.	0.122 mol	9.0 g
HCl (32 wt.%)	1.7 eq.	0.325 mol	18.0 mL

9.0 g of triblock-copolymer P123 (Aldrich) are dissolved in a mixture constituted of 325 mL of distilled water and 18 mL of HCl (32 % - Riedel de Häen) at 35 °C. When the solution becomes clear, 9 g of n-Butanol (99 % - Acros) are added and the resulting mixture is further stirred for 1.5 h before subsequent addition of 19.5 g of tetraethyl-orthosilicate (TEOS- Fluka). The resulting molar ratio is 1.0 TEOS : 0.018 P123 : 1.7 HCl : 200 H_2O : 1.3 BuOH. The reaction mixture is left under reduced stirring at 35 °C overnight (24 h) before being subsequently transferred to a teflon-lined autoclave in which hydrothermal treatment is performed for 24 h at 100 °C. After filtration, the silica is dried at 80 °C and then calcined at 550 °C for 3 h (heating ramp of 1 °C/min.).

3.1.2.4 HMS

The amounts of the reactants are chosen with regard to their desired molar ratios, which determine the coordination of the micelles in hexagonal arrays:

Reactant	Molar ratio	Moles	Mass/Volume
n-Dodecylamine	0.3 eq.	0.039 mol	7.19 g
$Si(OEt)_4$ (TEOS)	1.0 eq.	0.129 mol	26.8 g
Water	32.7 eq.	4.2 mol	76 mL
Ethanol (EtOH)	8.8 eq.	1.13 mol	66 mL

A solution of 7.19 g of n-dodecylamine (98 % - Acros) in 66 mL of ethanol (VWR) and 76 mL of water is prepared at room temperature. Afterwards, 26.8 g of tetraethyl-orthosilicate (Fluka) are added. The resulting molar ratio is 1.0 TEOS : 0.3 n-dodecylamine : 8.8 EtOH : 32.7 H_2O. The reaction mixture is kept under moderate stirring at 35 °C during 18 h and then filtered, washed with water and dried at 80 °C before calcination in static air at 600 °C for 2 h (heating ramp of 1 °C/min.).

© 2011 Tous droits réservés. http://doc.univ-lille1.fr

3.1.2.5 MCM-41

The synthesis of MCM-41 is based on the procedure described by Selvam *et al.*[6]The amounts of the reactants are chosen with regard to their desired molar ratios, which determine the coordination of the micelles in a cubic arrangement:

Reactant	Molar ratio	Moles	Mass/Volume
$C_{16}H_{33}N(CH_3)_3Br$	0.21 eq.	0.021 mol	7.66 g
$Si(OEt)_4$ (TEOS)	1.0 eq.	0.10 mol	20.8 g
Water	100 eq.	10.0 mol	180 mL
NaOH	0.41 eq.	0.041 mol	1.64 g

A solution of 1.64 g of NaOH (PROLABO) and 7.66 g of hexadecyltrimethylammonium bromide (Acros) in 180 mL of distilled water is stirred until it becomes clear. Afterwards, 20.8 g of tetraethyl-orthosilicate (TEOS - Fluka) are added. The resulting molar ratio is 1.0 TEOS : 0.21 amine : 0.41 NaOH : 100 H_2O. The reaction mixture is left under reduced stirring at room temperature overnight (24 h) before being subsequently transferred in a teflon-lined autoclave for hydrothermal treatment for 24 h at 100 °C. After filtration, the silica is washed with water and then dried at 80 °C and calcined at 550 °C for 3 h (heating ramp of 1 °C/min.).

3.1.3 Zirconia grafting

The preparation of the zirconia-grafted samples was performed following the method described by Gutiérrez *et al.*[7] 1.0 g of freshly calcined silica support is slurried in 10 mL of dry ethanol (Riedel) to obtain a gel. After addition of the desired amount of zirconium-(IV)-propoxide [$Zr(n\text{-}PrO)_4$; 70 wt.% solution in n-propanol- Aldrich)], the slurry is left under stirring for 8 h. After filtration, the solid is washed with ethanol and dried at 80 °C. Calcination is performed in static air at the desired temperature for 3 h (heating ramp of 1 °C/min).

3.1.4 Impregnation procedure

The impregnation with heteropoly acid is performed as follows: a solution of 0.2 g of heteropoly acid dissolved in 2 mL of distilled water are added to a slurry of 0.8 g of support in 20 mL water. Afterwards, the reaction mixture is stirred for another 2 h

© 2011 Tous droits réservés.
http://doc.univ-lille1.fr

before the solvent is evaporated under vacuum. The obtained catalyst is dried for 24 h at 70 °C before use.

3.2 Characterization Techniques

The prepared supports and catalysts were characterized using Nitrogen physisorption, X-Ray diffraction, Electron microscopy, Infrared Spectroscopy and Nuclear Magnetic Resonance. The atomic composition was determined by elementary analysis and the acidity of some significant selected samples was measured by temperature programmed desorption of ammonia. In the following paragraphs these techniques are explained.

3.2.1 Textural parameters

A Micromeritics ASAP 2000 was used to measure the specific surface area, poresize distribution and pore volume using N_2 adsorption-desorption experiments on outgassed supports and catalysts. The specific surface area, S_{BET}, was calculated using the linear part of the BET plot. The isotherms were obtained at -196 °C. The mesoporous size distributions were obtained by applying the Barrett-Joyner-Halenda (BJH) equation to the desorption branch of isotherms. The estimation of the total pore volume was made from the N_2 uptake at a P/P_0 value of 0.995.

Figure 3-1: Photograph of theMicromeritics ASAP 2000 apparatus

3.2.2 X-Ray Diffraction

Powder X-Ray Diffraction patterns of the supports were collected on a D8 Bruker diffractometer equipped with a Cu K*α* radiation (λ=1.5406 Å) as an X-ray source. The diffractograms were recorded for 2θ values comprised between 10 and 80° using a 0.01° step with an integration time of 1 s. Phase identification was carried out by comparison with the JCPDS database. If diffraction peaks attributed to tetragonal zirconia were detected in the wide angle region, crystal domain size was estimated using the Scherrer equation after Warren's correction for instrumental broadening according to:

© 2011 Tous droits réservés.
http://doc.univ-lille1.fr

$$D = \frac{K\lambda}{\beta \cos\theta}$$

With the correction factor K assumed equal to 0.86 and λ being the wavelength of the X-ray source. β is the effective line width of the X-ray reflection, calculated by the formula $\beta^2 = B^2 - b^2$ where B is the full width at half maximum (FWHM) of the reflection and b is the instrumental broadening determined by the FWHM of X-ray reflection of quartz having particles larger than 150 nm.

3.2.3 Transmission Electron Microscopy

For the high-resolution imaging of supports, an electron microscope from TECNAI with an accelerating voltage of 200 kV, and equipped with a LaB6 filament, was used. At least 20 images were taken for each sample to validate the pore structure of the supports and the distribution of the ZrO_2 crystallites inside the silica.

Figure 3-2: Photograph of the Tecnai TEM apparatus

3.2.4 Fourier transform Infrared spectroscopy

The IR spectra were recorded with a spectral resolution of 4 cm^{-1} and 256 scans (acquisition time 52 s) using a Thermo Nicolet 460 Protégé FTIR spectrometer equipped with a MCT detector. A KBr spectrum was used as a background for the post-processing of spectra.

Figure 3-3: Photograph of the Thermo Nicolet 460 FTIR spectrometer

© 2011 Tous droits réservés.
http://doc.univ-lille1.fr

3.2.5 Nuclear magnetic resonance

Distribution of the types of silica species was determined using nuclear magnetic resonance with cross polarization and magic angle spinning (^{1}H->^{29}Si CP-MAS NMR) on a Brüker spectrometer operating at the Larmor frequency of 75.4 MHz. Isotopic chemical shift (δ_{iso}) was referenced to tetramethyl silane (TMS).The efficiency of zirconia grafting on the SBA-15 surface was thus investigated using ^{29}Si MAS NMR spectroscopy.

3.2.6 Inductively Coupled Plasma Mass spectroscopy

The calcined samples were thereafter analyzed by ICP-Mass spectroscopy using a Thermo-Fisher X7 ICP-MS to determine the experimental quantity of zirconia and heteropoly acid of the catalyst. The zirconium content was determined by inductively coupled plasma-mass spectroscopy (ICP-MS) using a Thermo-Fisher X7 ICP-MS apparatus. The experiments were performed at the central analyses Center of the National French Research Foundation (CNRS) at Solaize.

Figure 3-4: Photograph of the Fisher X7 ICP-MS apparatus

3.2.7 Temperature programmed desorption of ammonia

The acidity of the samples was determined by temperature programmed desorption of ammonia using a Micromeritics AutoChem II 2920 connected to a mass spectrometer (VARIAN). The samples were outgassed at 300 °C, before being flushed with ammonia at 100 °C. The desorption of ammonia was performed with a temperature ramp of 10 °C/min up to 900 °C, and followed by a TCD detector and a mass-spectrometer.

© 2011 Tous droits réservés.
http://doc.univ-lille1.fr

3.3 Description of the catalytic test

The catalytic performances of the catalysts are determined in a micro-pilot test rig using 300 mg catalyst in a fixed-bed down-flow reactor. The complete reaction setup is shown in Figure 3-5.

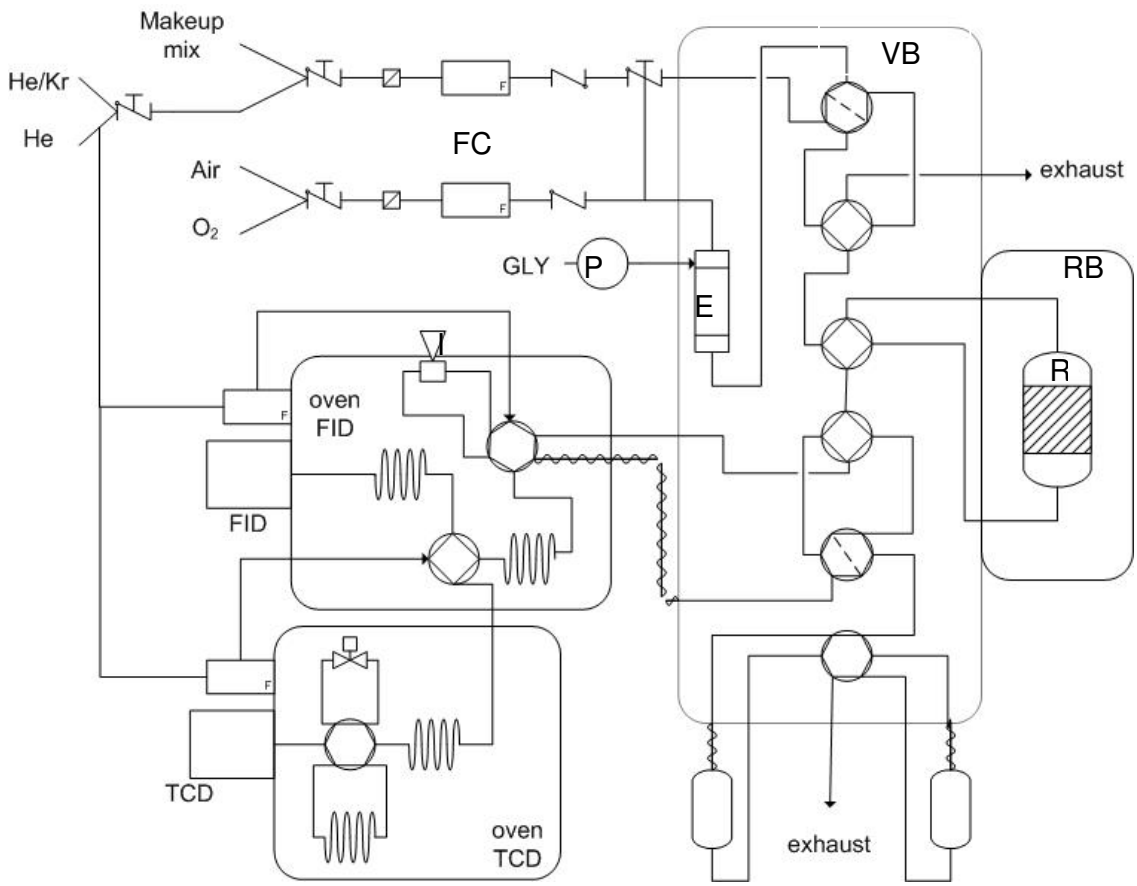

Figure 3-5: Scheme of the catalytic test rig

The evaporator (E) for the glycerol solution is located inside a heated valve-box (VB; 210 °C). It is manufactured from a 1/4" stainless steel tube of 0.46 mm inner diameter filled with glass-wool and carborundum. The glycerol solution is injected into the evaporator via a HPLC pump (P - Gilson HPLC 305). The reactant is then diluted in a helium flow that is controlled by a mass-flow controller (FC – BROOKS). By the same way, an air or oxygen flow can also be fed into the installation for regenerating the spent catalyst. The reactor (R) is implemented into a heating block made from aluminum, which is located in a separate compartment (RB). The block is heated by three heating-cartridges (250 W each) regulated by a PID thermostat (TEMPATRON) that is connected to a thermocouple type K inside the reactor. The reactor itself is

© 2011 Tous droits réservés.
http://doc.univ-lille1.fr

shown in Figure 3-6. It is made from a stainless steel tube of 25 mm outer diameter (15 mm inner diameter) and 120 mm length. The reaction temperature can be followed by two thermocouples inside the reactor whereof one is exclusively used for the regulation of the aforementioned heating-cartridges.

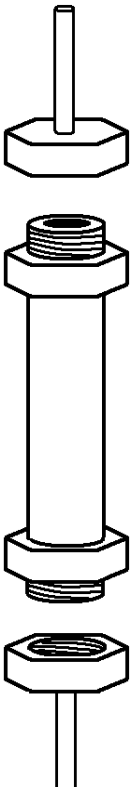

Figure 3-6: Reactor

Even though an online analysis system is present on the reaction setup, results with better precision were obtained using offline sampling with ice-traps. The reaction products are therefore condensed during 1 h and further quantitatively analyzed by high performance liquid chromatography (HPLC) using a THERMO SpectraSystem with a THERMO HyperRez XP column (250 mm length, 8 µm particle size) as a stationary phase and sulfuric acid (5 mmol/L; 0.5 mL.min-1; isocratic) as an eluting agent. The system was equipped with a refractometer (THERMO Surveyor Plus RI) used as detector. The typical sampling frequency was 5 traps during the first 5 h of reaction and further one trap after 24 h of reaction.

Unless otherwise noted, the reaction conditions are as follows:

Reaction temperature	275 °C
Glycerol feed	1.5 mL/h (10 wt.%)
Helium feed	30 mL/min
Mass of catalyst	300 mg – not diluted
Gas hourly space velocity (GHSV)	220 h^{-1}
Contact time	0.18 s

The conversion of glycerol and the selectivity of the products were calculated as follows:

$$\text{Glycerol conversion } (\%) = \frac{n_{\text{Feed, inlet}} - n_{\text{Feed, outlet}}}{n_{\text{Feed, inlet}}} \times 100$$

$$\text{Selectivity } (\%) = \frac{n_{\text{Product, outlet}}}{n_{\text{Feed, inlet}} - n_{\text{Feed, outlet}}} \times 100$$

Where $n_{Feed,inlet}$ and $n_{Feed,outlet}$ are the number of moles of carbon in glycerol at the inlet and the outlet, and $n_{Product,outlet}$ is the number of moles of carbon in the product at the outlet.

[1] C. Rocchiccioli-Deltcheff, M. Fournier, R. Franck, R. Thouvenot, *Inorg. Chem*. **1983**, *22*, 207.
[2] C. Rabia, M. M. Bettahar, S. Launay, G. Hervé, M. Fournier, *J. Chim. Phys.* **1995**, *92*, 1442.
[3] J. Roggenbuck, G. Koch, M. Tiemann, *Chem. Mater.* **2006**, *18*, 4151.
[4] M. Kurk, L. Cao, *Langmuir* **2007**, *23*, 724.
[5] F. Kleitz, S-H. Choi, R. Ryoo, *Chem. Com.* **2003**, *17*, 2136.
[6] T. Selvam, M. Köstner, G.T.P. Mabande, W. Schweiger, N. Pfänder, R. Schlögl, *J. Porous. Mater.* **2007**, *14*, 263.
[7] O.Y. Gutiérrez, D. Valencia, G.A. Fuentes, T. Klimova, *J. Catal.* **2007**, *249*, 140.

4 Characterization results

4.1 Bare silica supports

4.1.1 Textural parameters

In Table4-1, the results of the nitrogen adsorption-desorption experiments for all the prepared supports and the commercial supports are summarized.

Table4-1: Textural parameters of the various used silica supports.

Sample	S_{BET} [m²/g]	$V_{micropore}$ [cm³/g]	V_p [cm³/g]	D_p [nm]
SBA-15 4nm	798	0.12	0.69	4.0
SBA-15 5nm	919	0.12	0.85	4.8
SBA-15 6nm	703	0.02	0.95	5.6
SBA-15 8nm	593	0.00	1.31	7.6
SBA-15 9nm	499	0.00	1.30	8.9
SBA-15 13nm	376	0.00	1.38	13.4
KIT-6	663	0.00	0.90	4.9
CARiACT Q-10	272	0.01	1.26	14.9
HMS	817	0.00	0.70	2.9
MCM-41	644	0.00	0.40	2.8

From the results one can see, that all silica supports have high specific surface (S_{BET}) reaching from 272 m²/g (CARiACT Q-10) to 919 m²/g (SBA-15 with 5nm poresize). This value is significantly higher than the specific surface for heteropoly acid which typically does not exceed 10 m²/g. Therefore these silica are potential supports for the catalysts.

Furthermore, from the textural properties of SBA-15 with different pore diameters, one can state a linear relationship between the pore volume (V_p) and the pore diameter (D_p) and an inverse linear relationship between the specific surface area and the pore diameter (Figure **4-1**). Furthermore, the micro porosity ($V_{micropore}$) in the wall progressively decreases from 0.12 cm³/g for SBA-15 with 4 nm poresize to 0.00 cm³/g for SBA-15 with 8 nm poresize. Indeed, the increase of the synthesis temperature during the hydrothermal step, leads to the progressive decrease of the microporosity in the wall originating from the hydrophilic nature of poly(ethylene oxide) (PEO) blocks of the template.[1,2]

© 2011 Tous droits réservés.
http://doc.univ-lille1.fr

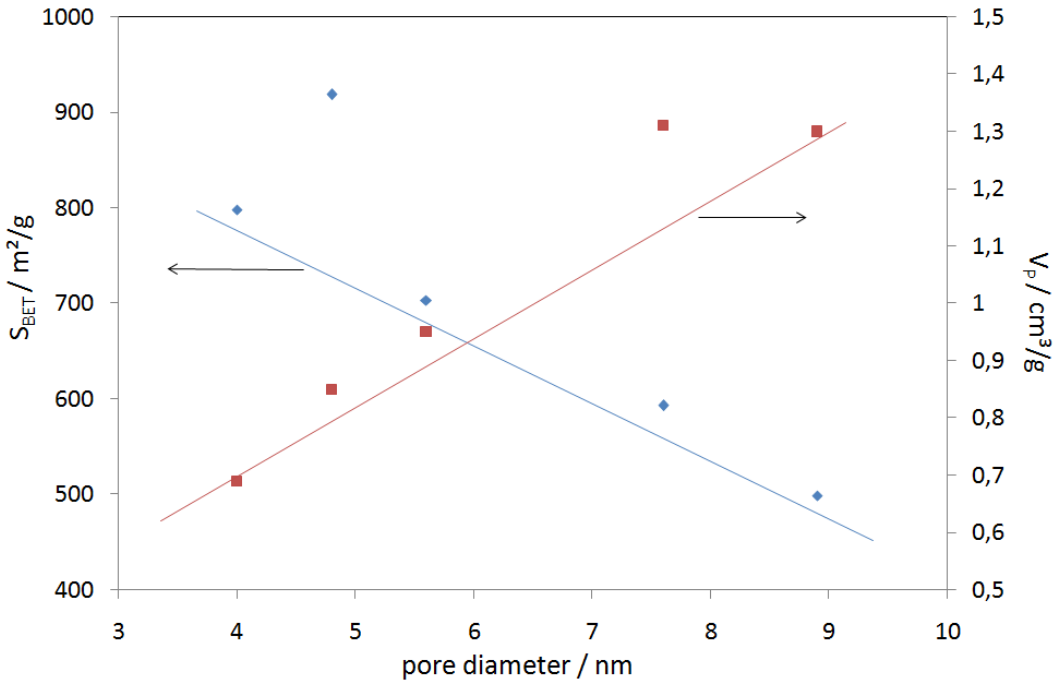

Figure 4-1: Correlation between the pore diameter and: the specific surface area (S_{BET}) and the porous volume (V_P) of SBA-15 supports.

As aforementioned, the performances are closely depending on the poresize of the catalysts, and thus of the support. Therefore, the distribution of the poresize has to be as narrow as possible to enable fine control of this property and establishing reliable correlations between pore size and catalytic performances. In Figure **4-2**, the poresize distribution (according to the BJH formula) is reported for various SBA-15 supports showing the obtained well-controlled narrow distributions.

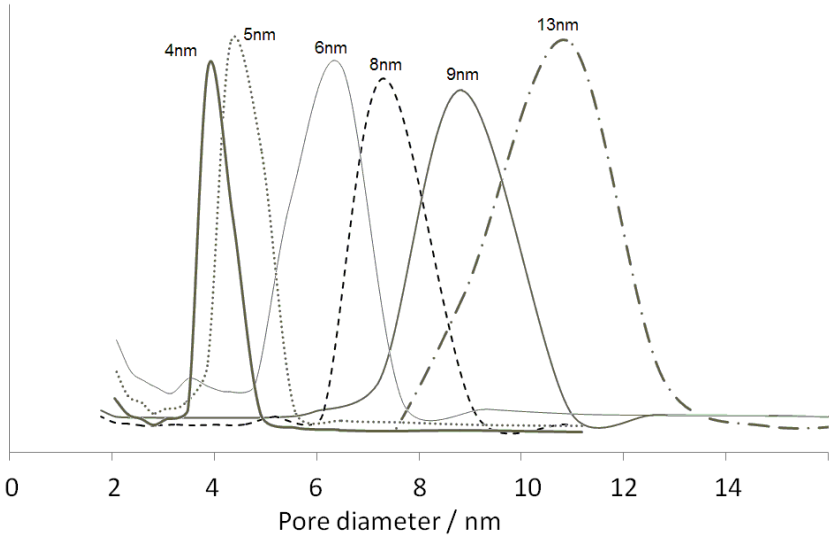

Figure 4-2: Distribution of the pore diameter for the various SBA-15 supports.

4.1.1 Test of the hydrothermal stability of the silica supports

As aforementioned, the silica support can be hydrolyzed under hydrothermal reaction conditions according to the following mechanism:

$$OH–(Si(OH)_2)_n–Si(OH)_3 + (n-1)\ H_2O \rightarrow n\ Si(OH)_4$$

Even though a complete hydrolysis to the silols species $[Si(OH)_4]$ is rather theoretical, a partial collapse of the silica is well described for hot, vapor-rich atmosphere. The reaction conditions used for the catalytic test are close to these limits, as a 10 wt.% glycerol solution results in a partial molar ratio of vapor of 50.7 % at 275 °C. Therefore, all the silica supports were tested on their resistance against steam before considering their further use as supports for catalysts. The reaction conditions for these hydrothermal stability tests were chosen with regard to the conditions of the catalytic test. About 1 g of silica support was loaded in the reactor and flushed with helium. Then, the reactor was heated to 275 °C before a mixture of steam (54 Vol.%) and helium was passed through the reactor for 16 h. Afterwards, the silica was isolated and the structural properties were analyzed by nitrogen adsorption-desorption measurements. In **Table 4-2** are shown the results from textural analyses before and after test under steam.

Table 4-2: Textural parameters of silica before and after steam treatment

support	BET [m²/g]	V [cm³/g]	Ø diameter [Å]
CARiACT	272	1.26	149
- After steam	272	1.25	146
TMPS4	1051	1.21	40
- After steam	1079	1.25	40
TMPS2.7	1075	1.15	32.5
- After steam	1024	0.98	33.5
MCM-41	644	0.7	20
- After steam	650	0.4	30
SBA-15 8nm	523	1.12	80
- After steam	570	1.25	78
SBA-15 6nm	703	0.95	54
- After steam	709	0.94	55
SBA-15 4nm	650	0.68	50
- After steam	604	0.74	44
Kit-6	663	0.89	50
- After steam	731	0.93	50

Most of the supports show a slight change in the textural parameters. Nevertheless, only MCM-41 and SBA-15 with 4 nm pore size show important change in all the three controlled values. Due to the well-founded doubt in their hydrothermal stability, these supports were therefore not used for further preparations of catalysts.

4.2 Zirconia-grafted silica

With regard to the catalytic results obtained for zirconia supported heteropoly acids (cf. 2.1.2), the current work was focused on the use of zirconia grafted silica as support for heteropoly acids. The grafting method, as described in chapter 3.1.3, allows to vary the amount of zirconia, the calcinations temperature and the silica host support. To determine the influence of each parameter, the studies were performed changing only one parameter at one time, leaving the other two constant. The constant values are 20 wt.% for the amount of zirconia, 650°C for the calcinations temperature and SBA-15 with 8 nm poresize for the silica host support. In the following sections the influence of these parameters on the chemical and physical properties is discussed.

© 2011 Tous droits réservés. http://doc.univ-lille1.fr

4.2.1 SBA-15 loaded with zirconia

A SBA-15 support with 8 nm poresize was grafted with theoretical zirconia loadings ranging from 10 wt.% to 40 wt.%. The calcined samples were thereafter analyzed by ICP-Mass spectroscopy to determine the experimental quantity of zirconia. Experimental zirconia contents were found to be in all cases lower than the theoretical ones (Table 4-3). The loss can be easily explained by the washing of the grafted samples with ethanol before drying and calcination, which is suggested to remove unreacted zirconium-propoxide precursor.

Table 4-3: Theoretical and experimental amount of zirconia on SBA-15

Theoretical ZrO_2 loading/ wt.%	ICP ZrO_2 loading/ wt.%
10	7.2
20	18.1
40	36.6

4.2.2 Evolution of the silica surface coverage with zirconia loading

The efficiency of the zirconia grafting on the SBA-15 surface was investigated using ^{29}Si MAS NMR spectroscopy. Figure 4-3 presents the MAS spectra obtained for the SBA-15 sample with a pore size of 8 nm, which was loaded with 0 to 40 wt.% of zirconia, in the dried state (*i.e.*, before calcination). The signal of the initial SBA-15 support consists of overlapping resonance bands centered around -105 ppm. The fit of the spectrum using the DMfit program enables quantification, and the results are given in

Table 4-4. The assignments to the Q_x, where x represents the number of SiO_4 tetrahedra sharing a corner with the tetrahedron under consideration, have been done using the studies of Mägi *et al.*[3] Comparison of the initial SBA-15 spectrum with the zirconia containing samples shows that grafting leads to a progressive decrease in the $Q_2[(SiO)_2\text{-}Si\text{-}(OH)_2]$ and $Q_3[(SiO)_3\text{-}Si\text{-}OH]$ signal intensity (Figure 4-3) to the benefit of an increase in the intensity of signal in the range between -110 and -120 ppm, which is clearly visible for the sample containing 40 wt.% of zirconia. Such signal intensity increase is easily attributed to the progressive coverage of the silanol-groups (Si-OH) from the SBA-15 surface by zirconia.[3] This result clearly shows that most of the SBA-15 surface is available for the zirconia precursor, even if a small fraction of Q_2 type species remains unreacted. The increase in the intensity and the

© 2011 Tous droits réservés.
http://doc.univ-lille1.fr

broadening of the Q_4[Si-$(SiO)_4$] signal located around -112 ppm in the case of the zirconia grafted samples can be assumed by a similar chemical shift for the Q_4[*i.e.*, Si-$(SiO)_4$] signal and for the Q_3-Zr [$(SiO)_3$-Si-OZr] signal, making difficult the differentiation between these two species. Thereby, the decrease in the intensity of the Q_2 and the Q_3 with the increase in the zirconia loading will obviously give rise to the Q_2-2Zr and Q_3-Zr signals, while the Q_4 signal will remain quite unchanged since grafting could only occur on silica surface and not in the bulk of silica [Si-$(OSi)_4$].

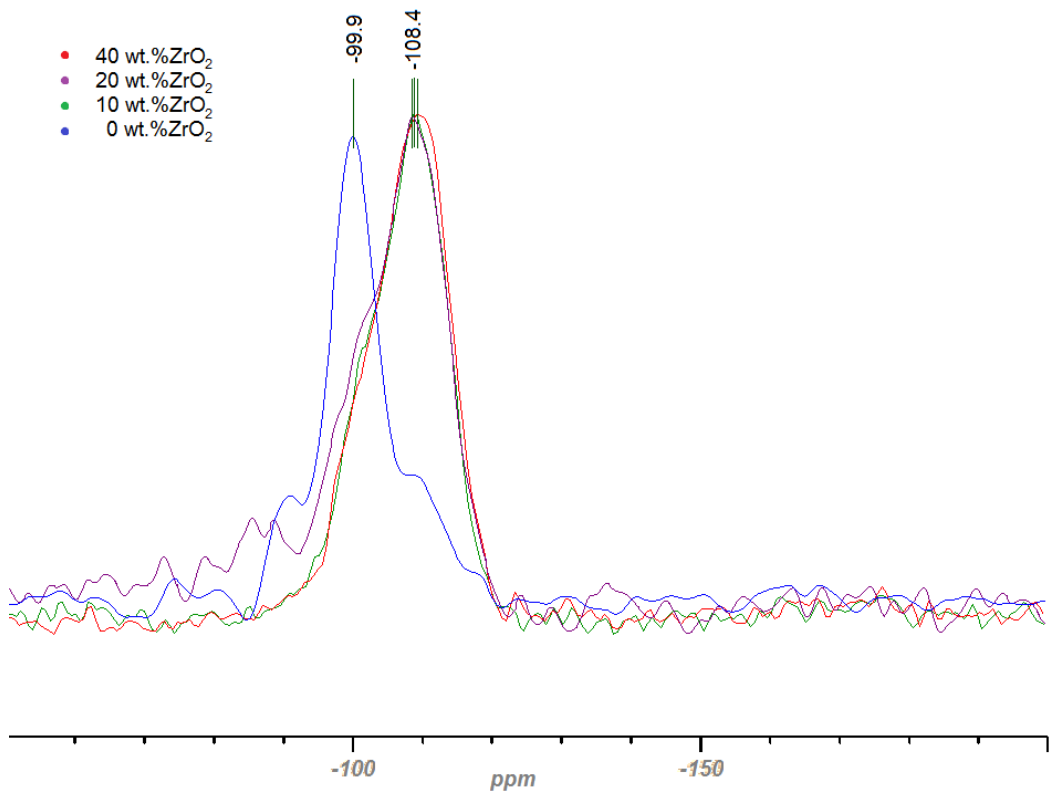

Figure 4-3: ^{29}Si-MAS NMR spectra of SBA-15 containing 0 wt.% - 40 wt.% of zirconia.

Table 4-4: Results of the deconvolved ^{29}Si-MAS-NMR spectra

δ / ppm	ZrO_2	0wt.%	10wt.%	20wt.%	40wt.%
-94	(Q2)	14.6%	2.4%	2.0%	1.1%
-102	(Q3)	67.8%	26.3%	25.2%	24.6%
-108	(Q3-Zr) or (Q2-2Zr)	-	51.3%	52.5%	53.8%
-112	(Q4)	17.6%	20.0%	20.3%	20.5%

© 2011 Tous droits réservés.
http://doc.univ-lille1.fr

4.2.3 Influence of the thermal treatment temperature

The effect of the thermal stabilization of the nanocomposites is reported for the sample containing 20 wt.% of zirconia on SBA-15 with 8 nm pore diameter. First, the TGA measurement shows five decomposition steps (Figure **4-4**). A first weight loss is observed on the differential mass signal at temperature below 100 °C, which is attributed to the loss of physisorbed water and/or residual solvent evaporation. Three successive decomposition steps are visible at 250 °C, 350 °C and 440 °C, respectively. These three steps are logically attributed to the decomposition of the zirconia precursor grafted on the silica surface. Finally, a small decomposition is noticed at a temperature close to 900 °C. Such decomposition is assigned to condensation of residual SiOH from the structure.[4,5]

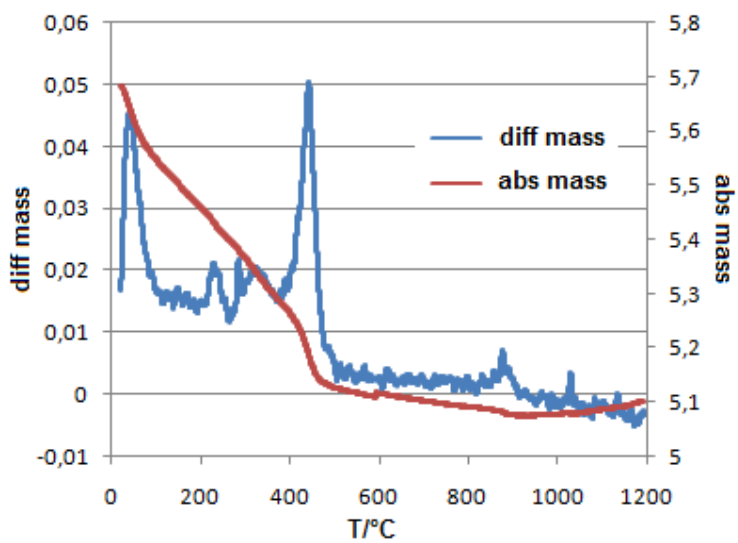

Figure 4-4: TGA results obtained over SBA-15 (8 nm poresize) grafted with 20 wt.% zirconia.

The evolution of the physical properties with the calcination temperature is given in Table 4-5. A small decrease in the specific surface area is observed up to 650 °C (< 20 %), while further increasing the calcination temperature to 950 °C leads to adrastic fall of the surface area value. Similar observations are found on the pore volume and poresize evolution with the calcination temperature. The more marked decreases in surface area, pore volume and pore size values after calcination at 950 °C could be partially explained by the lower values obtained for the silica alone after calcination at the same temperature (Table 4-5, line 5). Indeed, comparing these two last solids shows that the difference remains similar, whereby the

© 2011 Tous droits réservés.
http://doc.univ-lille1.fr

significant decrease in the specific surface area can be ascribed to the contraction of silica at high temperature.

The isotherms for the samples containing 20 wt.% ZrO_2 on SBA-15 (8 nm poresize), calcined between 400-950°C are reported in Figure **4-5**. The shape of the isotherms remains unchanged irrespective of the calcination temperature, and corresponds to type IV according to the IUPAC classification. A slight difference in the hysteresis form can be however remarked. For the initial SBA-15 and the samples calcined at 400 °C and 650 °C, the hysteresis loop is of the H1 type (parallel adsorption and desorption branch, characteristic for cylindrical pores), whereas the sample calcined at 950 °C shows an hysteresis loop of the H2 type (non-parallel), which is typical for tubular pores with narrow constrictions.

Table 4-5: Textural parameters for different calcination temperatures

Amount ZrO_2 / wt.%	$T_{calcination}$ / °C	S_{BET} [m²/g]	V_p [cm³/g]	D_p [nm]
0	550	593	1.31	7.6
20	400	587	1.11	6.2
20	650	518	1.06	6.8
20	950	279	0.46	5.0
0	950	332	0.39	4.4

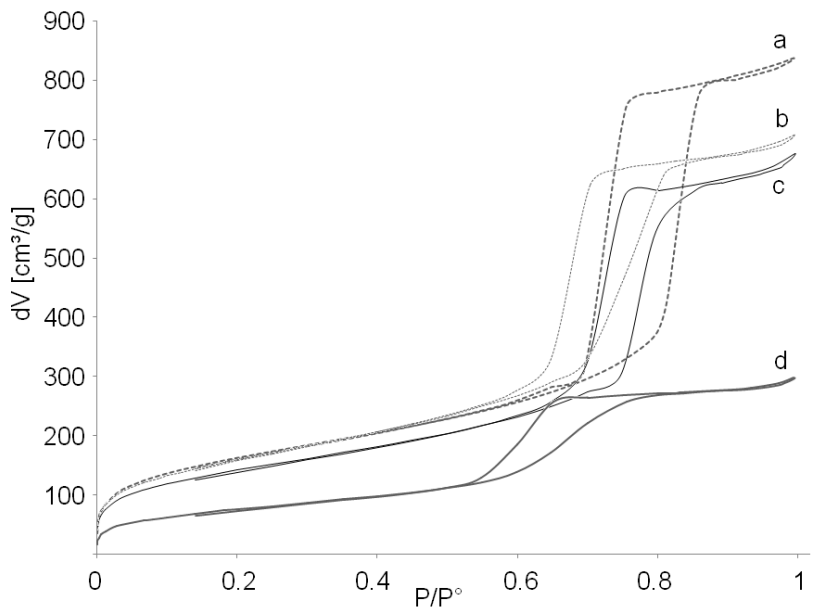

Figure 4-5:Nitrogen adsorption-desorption isotherms of *(a)* the initial SBA-15 (8 nm poresize) and of the same SBA-15 grafted with 20 wt.% zirconia and calcined at *(b)* 400 °C, *(c)* 650 °C and *(d)* 950 °C.

The XRD analysis (Figure **4-6**) does not allow the detection of any crystallized zirconia phase over the samples calcined at 400 °C and 600 °C. In contrast, the diffractogram of the solid calcined at 950 °C shows the presence of broad and poorly defined peaks characteristic of tetragonal zirconia (JCPDS card 17-0923). The average crystal size of zirconia was calculated using the Sherrer equation at 3.7 nm,[6] which is a value largely lower than the pore size of the initial parent support (8 nm). Therefore, no pore plugging could arise from nanosized zirconia crystals aggregated in the mesopores of SBA-15. In conclusion, the significant decrease in the textural parameters for the high temperature calcined sample is more likely attributed to the contraction of the silica at 950 °C (Table 4-5).

© 2011 Tous droits réservés.

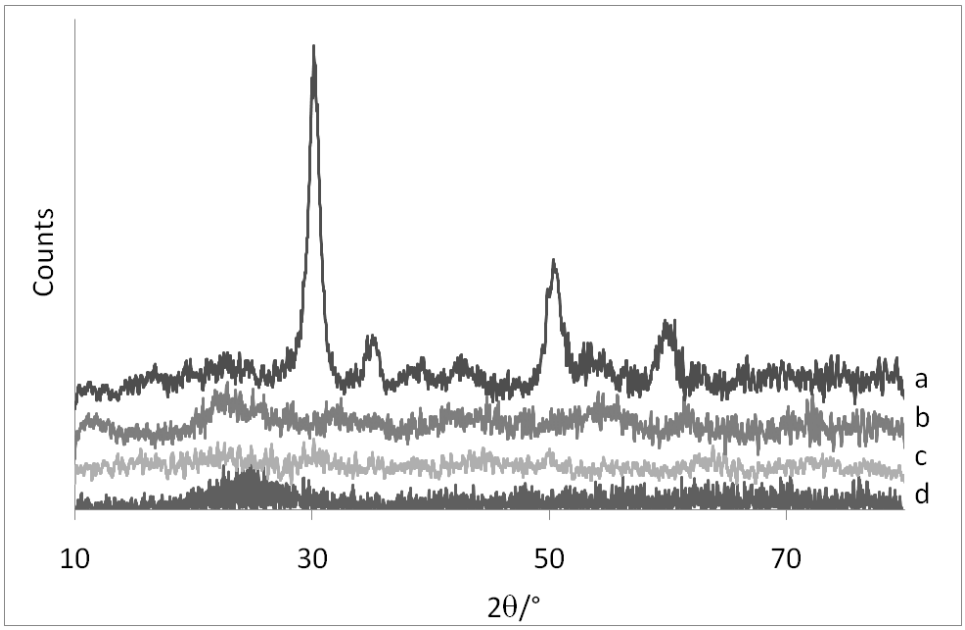

Figure 4-6: XRD patterns of *(a)* the initial SBA-15 (8 nm poresize) and of the same SBA-15 grafted with 20 wt.% zirconia and calcined at *(b)* 400 °C, *(c)* 650 °C and *(d)* 950 °C.

TEM suggests the formation of an uniform zirconia-crystal layer on the silica surface after calcination at low temperature (< 650 °C). Indeed, a homogeneous contrast is observed at low magnification (Figure **4-7**a), suggesting a homogeneous dispersion of the zirconia phase on the silica surface. In addition, the high magnification images show the formation of a regular zirconia crystal film homogenously covering the surface of the SBA-15 channels (Figure **4-7**b). An increase in the calcination temperature to 950 °C leads to the migration of the ZrO_2 crystals outside the porous network, as described by Gutiérrez *et al.*[7] Indeed, important crystalline domains are observed by TEM at low magnification, located just at the entrance of the porous network (Figure **4-7**c). A focus on these regions allows us to detect a few nanometers ZrO_2 crystallized particles (Figure **4-7**d). These observations and the sintering of the ZrO_2 film into small particles are consistent with the results obtained by nitrogen physisorption and XRD analysis.

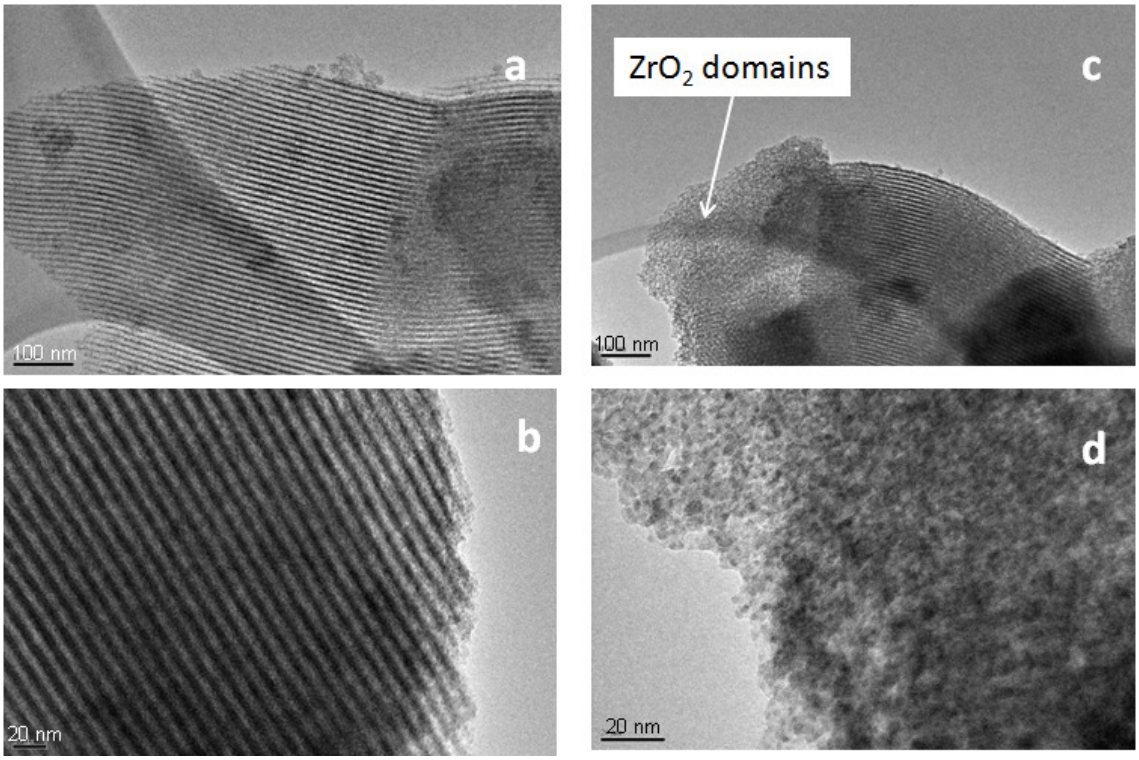

Figure 4-7: Electron microscope picture at low and high magnification obtained for SBA-15 (8 nm poresize) containing 20 wt.% zirconia and calcined at *(a, b)* 650 °C and *(c, d)* 950 °C

4.2.4 Effect of the zirconia loading

The effect of the zirconia loading on the morphological, textural and structural properties of the nanocomposites was studied for zirconia loading ranging from 10 wt.% to 40 wt.% on the SBA-15 with a pore size of 8 nm (SBA-15 8nm). Note that these loadings are larger than those generally studied (22 wt.%),[7],[8] since the objective of our work is to obtain porous composites exhibiting chemical properties of a zirconia phase. The supports grafted using different zirconia loadings were calcined at 650 °C, which leads to the formation of zirconia nanocrystals homogeneously dispersed inside the SBA-15 channels, as demonstrated in section 4.2.2. The SBA-15 with 8 nm poresize, synthesized at high hydrothermal temperature – *i.e.*, 140 °C, was selected as a host support with regard to the absence of micropores (cf. 4.1.1).

The main physical characteristics, obtained by N_2-physisorption, of the nanocomposites are gathered in Table 4-6 and the evolution of the physical properties is plotted as a function of the zirconia loading in Figure 4-9. We observed

a slight decrease in the specific surface area of the nanocomposites with respect to the surface area of the initial SBA-15 support. Nevertheless, this decrease remains below 10 %. In contrast to the results obtained for silica supported heteropoly acids (*cf.* 4.3.2), no linear relationship between the specific surface and the amount of zirconia can be established in the current case. This fact is ascribed to the porous properties of zirconia, whereby the theoretical decrease of the specific surface is partially compensated by new generated surface from zirconia.

On the other hand, a linear decrease in pore volume and pore size is observed with the increase in the zirconia loading (Figure 4-9). Such an evolution is consistent with the progressive loading of the channels of the initial host support, while increasing the zirconia quantity. We can note that the decrease in pore volume remains limited even at the highest loading (< 20 % for the 40 wt.% loading), suggesting a satisfying homogeneity for the deposited phase with limited pore plugging. Indeed, a sample having inhomogeneous dispersion, with aggregates blocking the pore, would obviously present largely lower surface area and pore volume than the initial support, which is not observed in our case.

The evolution of the pore size with the zirconia loading has to be carefully observed. Indeed, the BJH analysis with model assumption will obviously lead to the underestimation of the pore size if the spherical properties of the pores are changing. The deposition of zirconia cluster in the silica pores will obviously lead to the formation of constriction, and consequently to an error on the pore size value. This hypothesis is confirmed by the analysis of the N_2-sorption isotherms (Figure 4-8). Indeed, the isotherms remain of type IV, irrespective ofthe loading, with a brutal adsorption followed by a long plateau suggesting that the integrity of the silica porosity is preserved. Nevertheless, the progressive change of the hysteresis shape from H1 (for the silica support) to type H2 (for the 40 wt.% loading) confirms the formation of constriction in the pores. The constriction is suggested to remain limited in the case of these solids since the decrease in pore size remains itself limited (-1.9 nm at 40 wt% loading from an initial value of 7.6 nm at 0 wt.% loading), but this means that the pore size of the solids has to be considered to be comprised between 5.9 nm (at constriction points) and 7.8 nm (pore size of the support, where no zirconia is located).

© 2011 Tous droits réservés.
http://doc.univ-lille1.fr

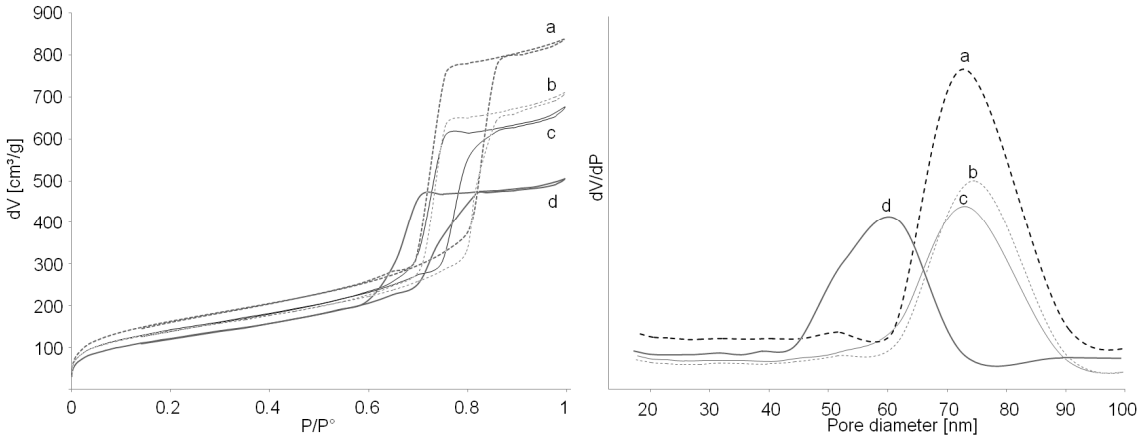

Figure 4-8: Nitrogen adsorption-desorption isotherms and BJH pore distribution for *(a)* the initial SBA-15 (8 nm poresize) and the SBA-15 containing *(b)* 10 wt.%, *(c)* 20 wt.% and *(d)* 40wt.% of zirconia

Table 4-6: Textural parameters SBA-15 (8 nm poresize) with zirconia amount between 0 wt.% and 40 wt.%

Amount of ZrO_2	S_{BET} [m²/g]	V_p [cm³/g]	D_p [nm]
0 wt.%	593	1.31	7.8
10 wt.%	510	1.11	7.4
20 wt.%	518	1.06	6.8
40 wt.%	446	0.80	5.9

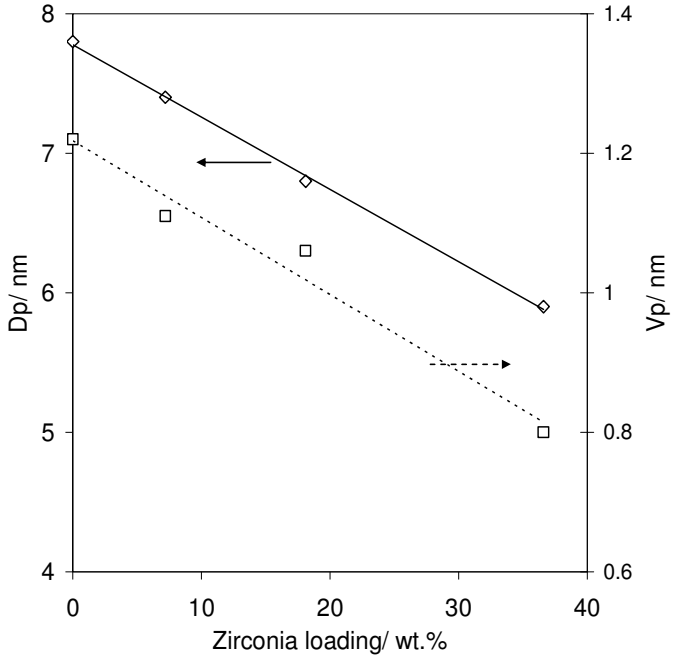

Figure 4-9: Evolution of the physical properties for SBA-15 (8 nm poresize) with zirconia loading from 0 wt.% to 40 wt.%

© 2011 Tous droits réservés.
http://doc.univ-lille1.fr

The XRD does not show any zirconia diffraction peak for samples containing up to 20 wt.% ZrO_2, whereas the presence of a crystallized tetragonal zirconia phase was revealed for the sample grafted with 40 wt.% ZrO_2 (Figure 4-10). The crystal size, calculated using the Scherrer equation (applied to the 220 reflection at $2\theta = 50°$)[6], is estimated at 6.8 nm, which is a value consistent with the hypothesis of a good dispersion of nanoparticles inside the silica cylindrical pores, since it remains lower than the silica pore size of 8 nm. In addition, the formation of 6.8 nm nanocrystals in the porosity will obviously lead to the formation of constrictions, as suggested by the shape of the nitrogen adsorption-desorption isotherms at this high loading. For lower zirconia amounts, the lack in reflection can originate from: *(i)* a too low amount of zirconia in the composite; *(ii)* the formation of an amorphous phase; *(iii)* the crystallization of the zirconia phase at a size below the detection limit. Nevertheless, analysis of the sample containing 20 wt.% zirconiaand calcined at 950 °C shows the possibility to detect a crystallized phase at this temperature, leading the exclusion of point *(i)*. Only the formation of an amorphous phase or a crystallization at a size below the detection limit (< 3 nm) can be thus envisaged. Nevertheless, the TEM analysis of the nanocomposites (already shown in Figure 4-7 for the sample containing 20 wt.% zirconia),enabled an easy detection of lattice plan in all cases, which suggests that the zirconia phase crystallizes in particles of a size below the XRD detection limit. In addition, TEM analysis clearly shows two different morphologies. Indeed, while nanometric particles with high contrast in TEM are clearly identified for the sample containing 40 wt.% zirconia (Figure 4-11), the formation of a zirconia crystal layer is suggested for the two lower loadings (10 and 20 wt.%).

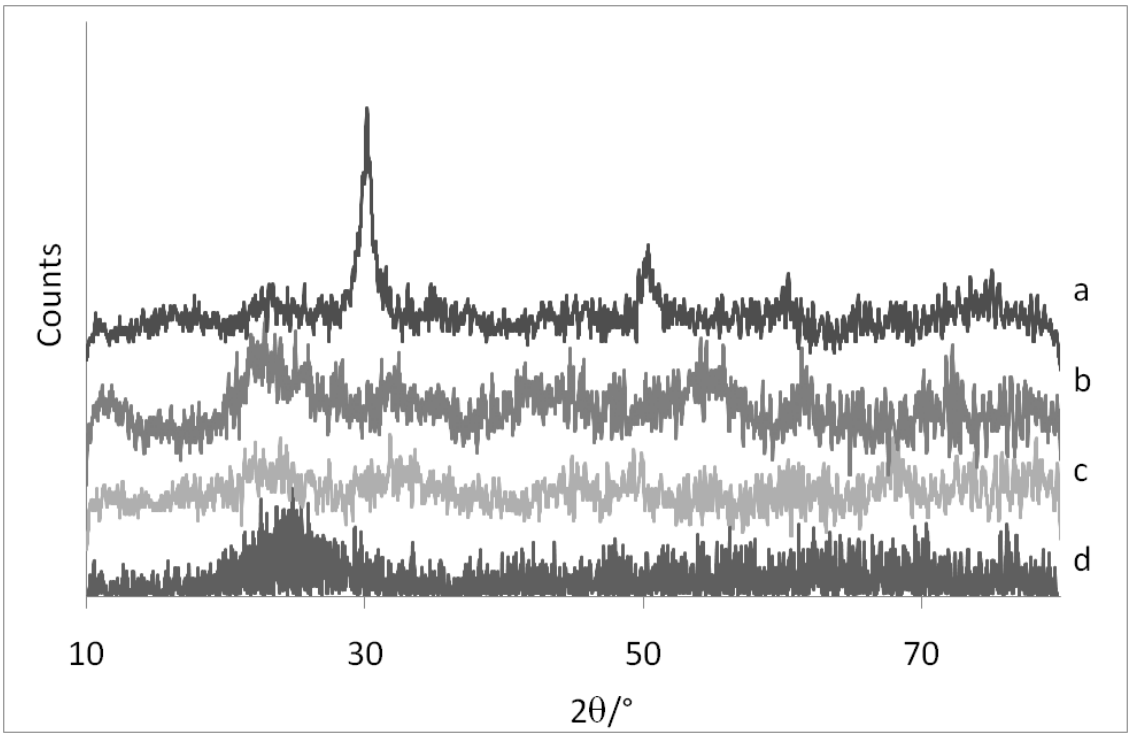

Figure 4-10: XRD patterns for different zirconia amounts, initial SBA-15 of 8 nm poresize (d) and SBA-15 containing (c) 10wt.%, (b) 20wt.% and (a) 40wt.% zirconia

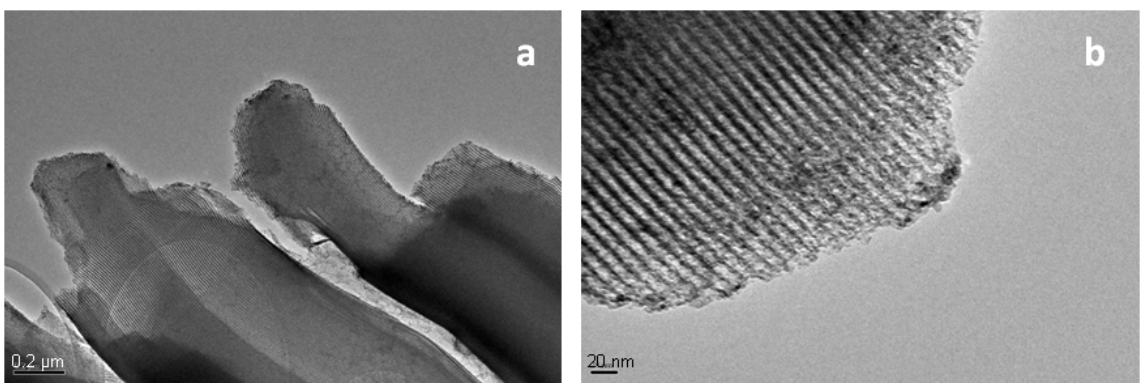

Figure 4-11:TEM image obtained for the sample containing 40 wt.% zirconia on SBA-15 (8 nm poresize) at low (a) and high (b) magnification

4.2.5 Influence of the pore size of the silica host support

In order to confirm the limited pore plugging occurring in large pores SBA-15 supports (as suggested for the composites prepared from SBA-15 8nm), the impact of the pore diameter on the formation of zirconia nanocrystals and the effect on the physical properties were studied over supports exhibiting pore size ranging from 4 nm to 13 nm. The solids were grafted with a constant amount of 20 wt% zirconia, and further thermally stabilized at 650 °C. The results of the textural analyses are shown in Table **4-7**. The grafting always leads to decreases in specific surface area,

porous volume and pore diameter. The impact of the grafting on the specific surface area is important in the case of supports with small diameters were the relative decrease is nearly 40 % against only 10 % in the case of SBA-15 with 9 nm pore size. This result can be explained by the higher contribution of micropores to the specific surface area in the case of SBA-15 with small pore diameter. Indeed, the grafting/calcination cycle leads in all cases to a decrease in the micropore volume (Table **4-7**). Thus, the micropore fraction present in the initial supports is filled with zirconia, and the fraction of surface developed in these micropores disappears. Therefore, the impact of zirconia grafting on the surface area is less important for the supports with large pore sizes (> 6 nm), since these solids present no microporosity.

Table 4-7: Textural parameters for SBA-15 silica of different pore diameter containing no or 20 wt.% zirconia

sample	S_{BET} [m²/g] (ΔS_{BET} [%])	$V_{micropore}$ [cm³/g]	V_p [cm³/g] (ΔV_p [%])	D_p [nm]
Initial SBA-15 4nm	798	0.12	0.69	4.0
- with 20wt.% ZrO_2	507 (-36)	0.05	0.54 (-22)	4.0
Initial SBA-15 5nm	919	0.12	0.85	4.8
- with 20wt.% ZrO_2	576 (-36)	0.06	0.63 (-26)	4.4
Initial SBA-15 6nm	703	0.02	0.95	5.6
- with 20wt.% ZrO_2	572 (-19)	0.02	0.74 (-22)	4.8
Initial SBA-15 8nm	593	0.00	1.31	7.6
- with 20wt.% ZrO_2	518 (-13)	0.00	1.06 (-19)	6.8
Initial SBA-15 9nm	499	0.00	1.30	8.9
- with 20wt.% ZrO_2	465 (-7)	0.00	1.15 (-12)	7.9
Initial SBA-15 13nm	376	0.00	1.38	13.4
- with 20wt.% ZrO_2	284 (-24)	0.00	0.97 (-30)	11.4

The XRD diffractograms do not show any diffraction peaks of zirconia, except for the samples based on SBA-15 with 4 nm and 5 nm poresize (Figure 4-12). The application of the Scherrer equation[6] leads to a crystal domain size of 9.1 nm for the zirconia phase on SBA-15 with 4 nm poresize , and 5.6 nm on SBA-15 with 5 nm poresize, suggesting in both cases the formation of zirconia crystal outside the silica pores. TEM analysis (Figure 4-13) confirms the formation of external particles for these samples, while such observation was not made for the other samples (with poresize ranging from 6 to 13 nm). TEM analysis then suggests the formation of an

© 2011 Tous droits réservés.
http://doc.univ-lille1.fr

uniform zirconia-crystal layer inside the SBA-15 network when the support pore size exceeds 5 nm (Figure **4-7** and Figure **4-11**).

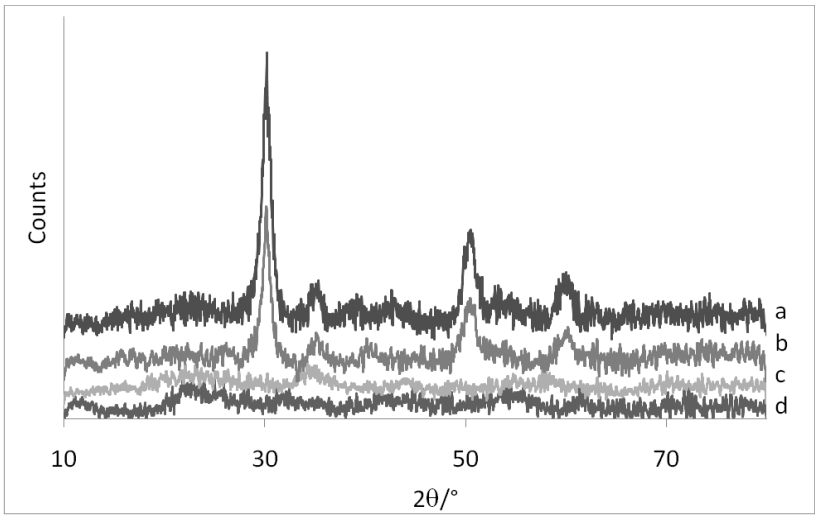

Figure 4-12: XRD patterns for zirconia (20 wt.%) grafted SBA-15 of (a) 4nm, (b) 5nm, (c) 6nm and (d) 8nm pore size.

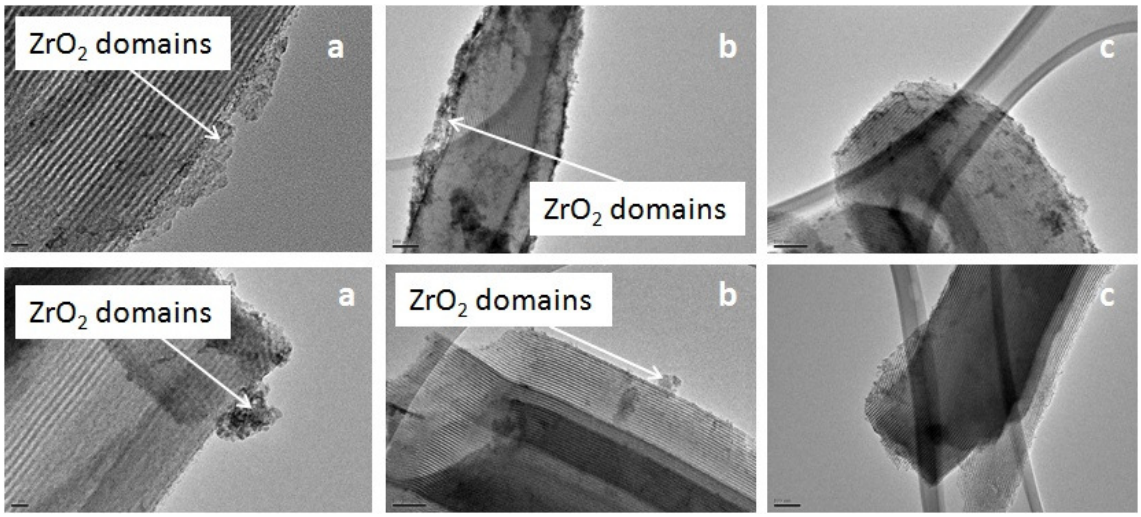

Figure 4-13:RepresentativeTEM pictures obtained for zirconia (20 wt.%) grafted SBA-15 of (a) 4nm, (b) 5nm and (c) 6nm pore size

4.2.6 Acid properties of the zirconia-grafted samples

The acidic properties of samples based on SBA-15 (8 nm poresize) containing between 0 wt.% and 40 wt.% zirconia were measured using temperature programmed desorption of ammonia, in order to evaluate the surface chemical

© 2011 Tous droits réservés.
http://doc.univ-lille1.fr

properties brought by zirconia in the nanocomposites. As expected, the zirconia grafting leads to a significant increase in the number of acid sites (Table **4-8**). Furthermore, the total acidity increases with the amount of zirconia, and shows a nearly linear relationship (Figure 4-14). This linear evolution of the acidity with the zirconia loading suggests a constant accessibility of the zirconia phase per gram and also the maintaining of a high and similar degree of dispersion of the zirconia phase in all the composites.

Furthermore the influence of the calcination temperature on the acidity was subsequently studied on the samples containing 20 wt.% zirconia. Calcination at low temperature (400 °C) results in a quantity of chemisorbed ammonia of 77.6 µmol/g, which is low compared to that obtained after calcination at 650 °C (177.7 µmol/g). As shown by TGA, the decomposition of the zirconia alkoxide is rather incomplete at temperatures below 400 °C, whereby the formation of carbonaceous residues on the composite surface and thus the poisoning of the acidic sites can explain the low total acidity of no more than 77.6 µmol/g after calcination at 400 °C. Similarly, the calcination of the sample at 950 °C leads to a decrease in the total acidity (98.1 µmol/g against 177.7 µmol/g at 650 °C). Nevertheless, the total acidity normalized per m² of solid remains constant (Table **4-8**). This means, as suggested by the physical and textural evolutions, that the zirconia phase accessibility remains constant. In other words, the increase in the calcination temperature results in *(i)* a limited zirconia crystal growth and *(ii)* a limited pore plugging.

Table 4-8: Total amount of chemisorbed ammonia over samples based on SBA-15 (8 nm poresize) containing 0-40 wt.% zirconia calcined at temperatures ranging from 400-950 °C

Amount ZrO_2 / wt.%	$T_{calcination}$ / °C	µmol NH_3/g	10^{-3}µmol NH_3/m^2
0	-	3.9	7
10	650	78.0	153
20	650	177.7	343
40	650	368.2	826
20	400	77.6	132
20	950	98.1	352

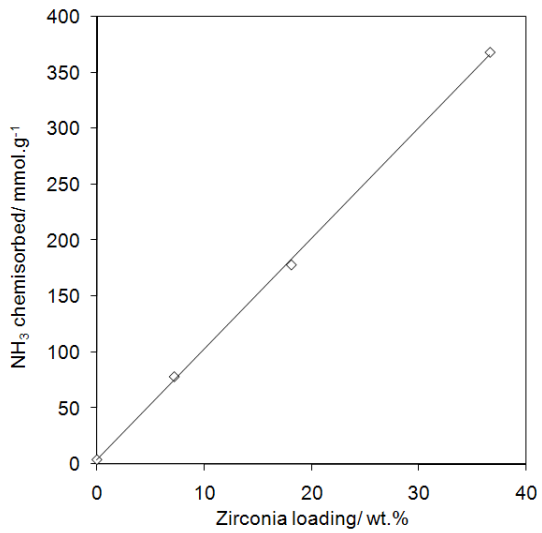

Figure 4-14: Evolution of the quantity of NH_3 chemisorbed with the zirconia loading of SBA-15 (8 nm poresize, calcinations temperature 650°C)

4.3 Characterization of the catalysts and comparison between catalysts based on bare silica and zirconia-grafted silica

4.3.1 Quantity of active phase

A series of catalysts based on SBA-15 of 8 nm poresize with calculated amount of 10-30 wt.% of silicotungstic acid was prepared. The samples were analyzed by inductively coupled plasma-mass spectroscopy to determine the experimental ratio of tungsten and silicium and therefore the actual quantity of active phase. Experimental contents of heteropoly acids were found to be very close to the theoretical ones (Table **4-9**). The deviation remains within the order of magnitude, which is typically observed for wet-impregnation techniques. The larger discrepancy is observed for the lowest loading of HPA with an experimental value of 7.7 wt.% *vs.* 10 wt.% theoretically.[9]

Table 4-9:Theoretical and experimental amount of silicotungstic acid on SBA-15 (8 nm poresize)

Theoretical HPA loading/ wt.%	ICP HPA loading/ wt.%
10	7.2
20	17.4
30	32.0

© 2011 Tous droits réservés.
http://doc.univ-lille1.fr

4.3.2 Dispersion of the active phase

The nitrogen physisorption technique was used in order to measure the textural parameters of the catalysts after impregnation with different amounts of silicotungstic acid as an active phase. Starting from the idea that the active phase will form a kind of homogenous layer on the support, it is possible to calculate the theoretical specific surface area of the catalyst as follows: The support of the catalyst has a known BET surface (for example 100 m²/g). The impregnation with active phase (for example 10 wt.%) leads ideally to the formation of the aforementioned homogenous layer (Figure **4-15**). Normally, this layer does not generate new surface due to the non-porous character of the heteropoly acid. Thereby, the specific surface area decreases, relatively to the amount of introduced active phase (for our example 91 m²/g). Very high loadings of active phase can even provoke the plugging of pores, whereby the experimental surface decreases more than predicted by calculation. Therefore, the comparison between the calculated theoretical specific surfaces and the experimental ones allows us to draw reliable conclusions on the dispersion of the active phase on the support.

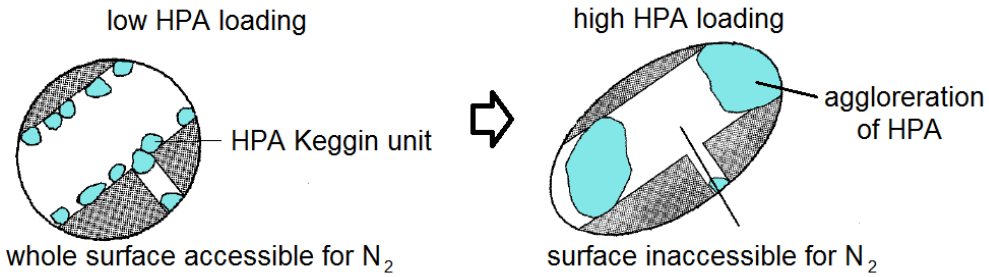

Figure 4-15: Schematical representation of the distribution of the HPA active phase in case of low (right) and high amounts of HPA

The results of the nitrogen physisorption and the calculated theoretical surface for silicotungstic acid on SBA-15 (8 nm poresize) are reported in Table **4-10**.

© 2011 Tous droits réservés.
http://doc.univ-lille1.fr

Table 4-10: Experimental and theoretical specific surface area for catalysts with various amounts of active phase on SBA-15 (8 nm poresize)

Amount of $H_4SiW_{12}O_{40}$	BET exp. m^2/g	BET calc. m^2/g	Ratio exp/calc.
0%	540	540	1.00
10%	480	486	0.99
20%	431	432	1.00
30%	340	378	0.90

From the above results, we can see that up to 20 wt.% of active phase on SBA-15-8nm, the whole surface remains accessible for nitrogen. At higher loading of 30 wt.%, we observe a decrease in the experimentally determined specific surface area, which can be explained by the aforementioned blocking of pores with silicotungstic acid, whereby some surface becomes inaccessible.

In a second series, a commercial silica (CARiACT Q-10, Fuji Silysia) with a mean pore diameter of 15 nm was used as a support and similarly impregnated with 10-30 wt.% of silicotungstic acid. Again, the specific surface area was measured and calculated. The results are reported in Table **4-11**. Due to the larger pore diameter of this carrier, the blocking of the porous network is not observed within the range of studied active phase amounts. Therefore, the calculated and experimental specific surface area remain close even at 30 wt.% loading with silicotungstic acid.

Table 4-11:Experimental and theoretical specific surface area for catalysts with various amounts of active phase on CARiACT Q-10

Amount $H_4SiW_{12}O_{40}$	BET exp. m^2/g	BET calc. m^2/g	Ratio exp/calc.
0%	272	272	1.00
10%	245	245	1.00
20%	209	218	0.96
30%	185	190	0.97

Furthermore, the dispersion of silicotungstic acid on SBA-15-8nm was studied by ^{29}Si-MAS-NMR. In Figure **4-16**, the spectra of the initial SBA-15-8nm support and of

© 2011 Tous droits réservés. http://doc.univ-lille1.fr

the catalyst containing 20 wt.% silicotungstic acid are reported. Thereby, one can see that the impregnation leads to a decrease in the intensity of the Q_2[$(SiO)_2$-Si-$(OH)_2$; -94 ppm] and Q_3 signals [$(SiO)_3$-Si-OH; -104 ppm] of the initial SBA-15 host support, which means that the silol-groups (Si-OH) on the surface are covered with silicotungstic acid. Furthermore, one can observe an increased and broadened Q_4 [Si-$(SiO)_4$; -113 ppm] signal in the case of the catalyst. We consider that the signal broadening is caused by a similar chemical shift of the Q_4 signal, the Q_2-2HPA [$(SiO)_2$-Si-2HPA] and Q_3-HPA [$(SiO)_3$-Si-HPA] signal so that one cannot clearly differentiate between these two. To quantify the decrease in the Q_2 and the Q_3 signal areas, the spectra were deconvolved (Figure **4-17**).

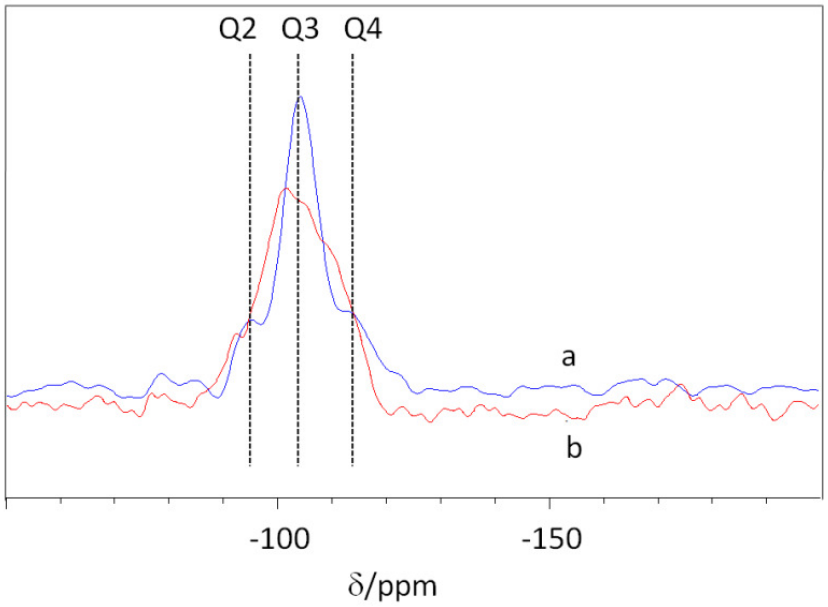

Figure 4-16: ^{29}Si-MAS NMR of (a) SBA-15 and (b) catalyst containing 20 wt.% $H_4SiW_{12}O_{40}$ on SBA-15 (8 nm poresize)*

* The NMR signal of the silicium atom from silicotungstic acid (-85 ppm) is not detected on the catalyst. This fact is attributed to the low amount of silicotungstic acid (20 wt.%) and its high molar mass of 2878 g/mol. Thereby, the molar ratio of Si from silicotungstic acid to Si from SBA-15 is no more than 0.52 %, which is underneath the detection limit for this technique.

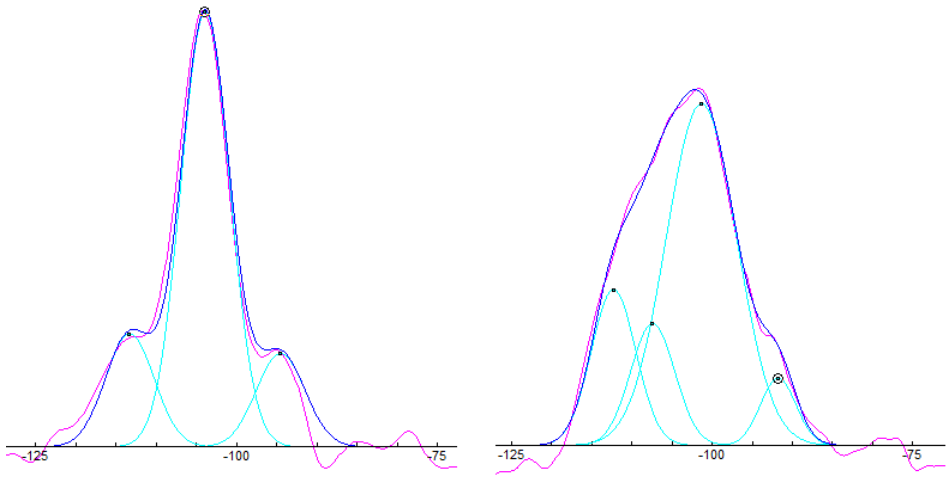

Figure 4-17: Deconvolution of the spectra obtained for SBA-15-nm (left) and the catalyst containing 20 wt.% $H_4SiW_{12}O_{40}$ on SBA-15-8nm (right).

Table 4-12: Results of the deconvolution of the ^{29}Si-MAS NMR spectra of Figure 4-17

δ / ppm	species	SBA-15-8nm	20 wt.% $H_4SiW_{12}O_{40}$/SBA-15-8nm
-94	(Q2)	14.6%	6.2%
-102	(Q3)	67.8%	62.1%
-108	(Q3-HPA) or (Q2-2HPA)	-	13.9%
-112	(Q4)	17.6%	17.9%

From the results of the deconvolution, one can see that the decrease in the Q_2 and the Q_3 signal intensities is accompanied with the appearance of the combined Q_3-HPA/Q_2-2HPA signals (Table 4-12). The experimentally coverage of the surface is determined as the loss in the Q_2 and Q_3 signal which gives a value 14.1 %. Taking into account a mean diameter of the Keggin unit of 12 Å, one can evaluate the theoretical coverage of the support.[10] The calculated theoretical surface coverage of the SBA-15-8nm support with silicotungstic acid is, with this method, of 16.7 %, which is in the same order of magnitude as the aforementioned experimental value.

4.3.3 Structural integrity of the active phase upon impregnation

The structural integrity of the Keggin unit, and thereby of the active phase, was studied using Fourier transform infra-red spectroscopy on a catalyst containing

© 2011 Tous droits réservés.
http://doc.univ-lille1.fr

20 wt.% silicotungstic on SBA-15 with a mean pore diameter of 8 nm. The IR spectra recorded for the aforementioned catalyst containing 20 wt.% silicotungstic acid on SBA-15-8nm, for the initial support SBA-15-8nm and for the pure active phase are reported in Figure **4-18**.In the spectrum of the catalyst one can clearly identify the characteristic absorption bands at 981 and 928 cm^{-1} attributed to the Keggin unit.[1] Hereby, one can confirm the structural integrity of the heteropoly acid after impregnation.

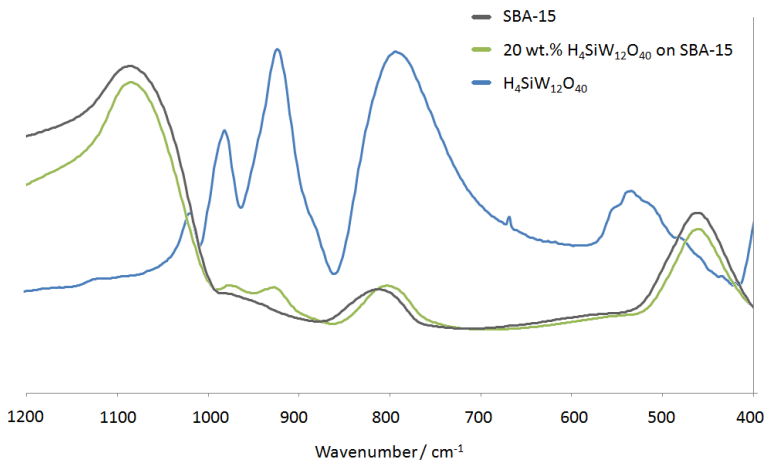

Figure 4-18: FT-IR spectra of silicotungstic acid, SBA-15 (8 nm poresize) and catalyst containing 20 wt.% silicotungstic acid on SBA-15 (8 nm poresize)

4.3.4 Acidity of the catalysts

The acidity of two catalysts containing 20 wt.% of silicotungstic acid on a zirconia-grafted (20 wt.%) SBA-15 (8 nm poresize) and the same bare SBA-15 were measured by ammonia-TPD. The two catalysts were chosen with regard of the difference in their long-term catalytic performance (cf. 5.3.1).

From the Figure **4-19**, one can see that the initial bare SBA-15 support (Figure **4-19**a) shows nearly no acidity, whereas the zirconia-grafting (Figure **4-19**b) leads, as mentioned before, to a significant increase in the number of acid-sites (cf. 4.2.6). Due to the nature of zirconia, one can assume that these new acid-sites are of the Lewis type. When these two respective supports are impregnated with silicotungstic acid, the number of acid sites increases. Nevertheless, the catalyst prepared on SBA-15 (Figure **4-19**c) has slightly less but, according to the desorption temperature,

© 2011 Tous droits réservés.
http://doc.univ-lille1.fr

significantly stronger sites than the catalyst based on zirconia grafted SBA-15 (Figure **4-19**d) (ΔT=25 °C).

The first effect - higher total number of acid sites - is explained by the fact that the catalyst based on zirconia-grafted silica contains the Lewis-sites from the support plus the Brønsted-sites of the silicotungstic acid. Nevertheless, the total number of acid sites found for this catalyst is only slightly increased as some Lewis sites of the support are covered with Brønsted-sites from silicotungstic acid.

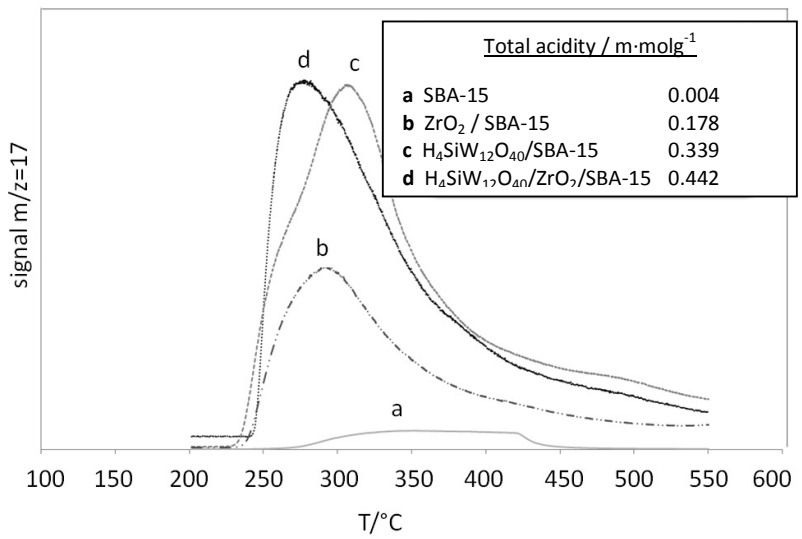

Figure 4-19: Temperature programmed NH_3 desorption of initial SBA-15 (8nm poresize) (a), ZrO_2 grafted SBA-15 (8nm poresize) (b), $H_4SiW_{12}O_{40}$ on SBA-15 (8nm poresize) (c) and $H_4SiW_{12}O_{40}$ on ZrO_2 grafted SBA-15 (8nm poresize) (d).

This second effect is attributed to the electronic interaction of the heteropoly acid and the support. Similar to what was proposed for alumina-supported heteropoly acids by Atia *et al.*,[11] silicotungstic acid shows stronger interaction with zirconia than with silica. In contact with water, the hydroxyl groups at the surface of the metaloxide support are protonated, yielding positively charged $M\text{-}OH_2^+$ (M = Zr, Al or Si) species (Scheme **4-1**). These species strongly interact *via* electronic effects with the negatively charged heteropoly anion as postulated by Wu *et al.*[12] Depending on the acid character of the support, the interaction can be rather strong, like in the case of zirconia and alumina, or weak, like in the case of silica. As a result of this interaction between the support and the heteropoly anion, the Keggin structure is distorted, which results unmodified Brønsted acidity of the active phase. Strong interaction, like

© 2011 Tous droits réservés.
http://doc.univ-lille1.fr

in the case of zirconia, leads to the aforementioned decrease in the force of the Brønsted acid sites.

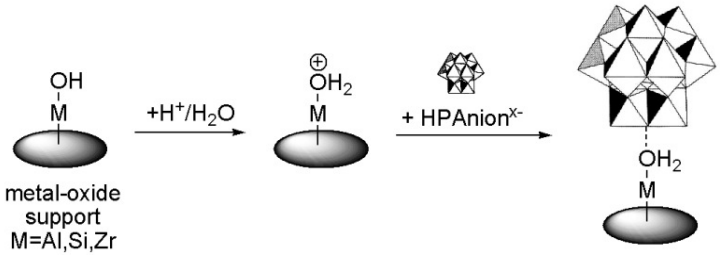

Scheme 4-1: Schematic view of the influence of the support on the heteropoly acid, which leads to the distortion of the Keggin structure

4.3.5 Thermal stability of the catalysts

The thermal stability of two catalysts based on supported silicotungstic acid over SBA-15 and zirconia grafted SBA-15 was determined by TGA analyses. These two catalysts were chosen with regard to their different behavior in the regeneration reaction (cf. 5.4). From Figure **4-20**, one can see that, in both cases, the silicotungstic acid loses its crystalline water between 50 and 100 °C. Afterwards, the catalyst based on non-grafted SBA-15 shows a second loss of weight starting from 350 °C. This is explained by the loss of constitutional water (protons + oxygen), which is characteristic of the beginning of the HPA decomposition process. In contrast, the silicotungstic acid supported on zirconia-grafted SBA-15 remains stable up to 500 °C.

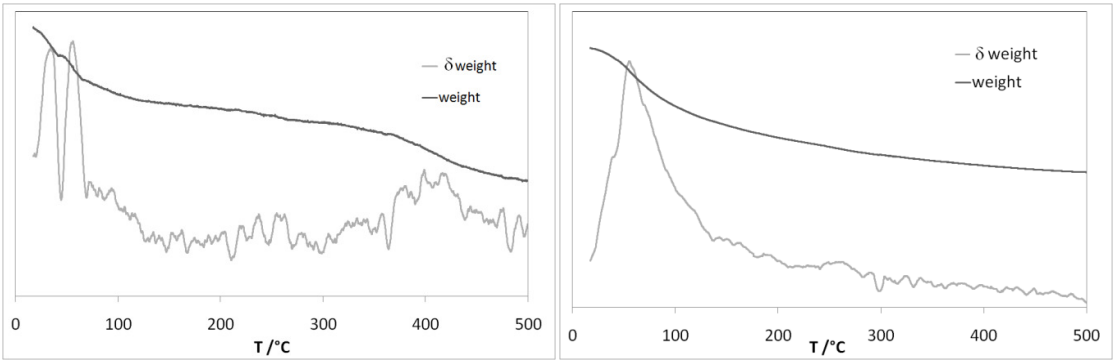

Figure 4-20:Thermogravimetric analyses for silicotungstic acid (20 wt.%) supported on SBA-15 (8nm poresize) (left) and zirconia grafted SBA-15 (8nm poresize) (right)

The increased thermal stability is ascribed to the aforementioned interaction between the support and the heteropoly anion (cf. 4.3.4 and Scheme **4-1**). On the one hand, the strong interactions between zirconia and heteropoly anion decreases the acidity strength of the HPA due to the distortion of its structure, but, on the other

© 2011 Tous droits réservés.
http://doc.univ-lille1.fr

hand, this interaction also stabilizes the Keggin structure and hinders its thermal decomposition. This effect was also described by Atia *et al.* for alumina supported heteropoly acids.[11]

‘’’

The choice of a support is generally guided by the increased specific surface area, which leads to a high number of accessible active sites. It has been demonstrated that mesoporous silica provide this high specific surface. Furthermore these supports offer a narrow pore distribution, which was shown to have important impact on the catalytic performance. On the other hand, not all tested supports show high resistance against hydrothermal treatment. Therefore MCM-41 was excluded from further studies.

Afterwards the zirconia grafting was applied with varying parameters, such as zirconia amount, calcination temperature and silica host support. From the characterization one can conclude, that high amounts (*i.e.* 40 wt.%), a high calcination temperature (*i.e.* 950°C) and silica supports with small pore diameter (*i.e.* 4 nm) lead to the formation of large zirconia domains detected by TEM and XRD. In the other cases, a homogeneous zirconia layer was found. Further the acidic properties of the zirconia grafted supports were determined, showing a linear relationship between the amount of zirconia and the total number of acid sites.

Based on zirconia-grafted and non-grafted SBA-15 (8 nm poresize), two catalysts were prepared by impregnation with 20 wt.% silicotungstic acid. It was found that the zirconia grafting had impact on the strenght of the acid sites of the supported silicotungstic acid and also on the thermal stability of the latter. In fact, when supported on zirconia-grafted silica, the acid strenght was decreased whereas the thermal stability was increased, which was explained by electronic interactions between the support and the heteropoly anion.

© 2011 Tous droits réservés.
http://doc.univ-lille1.fr

[1] M. Kruk, M. Jaroniec, C.H. Ko, R. Ryoo, *Chem. Mater.* **2000**, *12*, 1961.
[2] M. Kurk, V. Antochshuk,M. Jaroniec, *J. Phys. Chem. B* **2000**, *104*, 11465.
[3] M. Mägi, E. Lippmaa, A. Samoson, G. Engelhardt, A.R. Grimmer, *J. Phys. Chem.* **1984**, *88*, 1518.
[4] F. Zhang, Y. Yan, H. Yang, Y. Meng, C. Yu, B. Tu, D. Zhao, *J. Phys. Chem.* **2005**, *109*, 8723.
[5] R. Vérubé, S. Kaliaguine, *Micro. Meso. Mat.* **2008**, *3*, 469.
[6] P. Scherrer, *Göttinger Nachrichten* **1918**, *2*, 98.
[7] D.P. Sawant, A. Vinu. F. Lefebvre, S.B. Halligudi, *J. Mol. Catal. A.* **2007**, *262*, 98.
[8] R. Akkari, A. Ghorbel, N. Essayem, F. Figueras, *Micro. Meso. Mat.* **2008**, *111*, 62.
[9] D.P. Sawan, A. Vinu, S.P. Mirajkar, F. Lefebvre, K. Ariga, S. Anandan, T. Mori, C. Nishimura, S.B. Halligudi, *J. Mol. Catal. A : Chem.* **2007**, *271*, 46.
[10] M. Misono, T. Okuhara, N. Mizuno, *Catalysis by heteropoly compounds, Successful design of catalysis*, Amsterdam, Elsevier Science Publishers, **1988**, 267.
[11] H. Atia, U. Armbruster and A. Martin, *J. Catal.*, **2008**, *258*, 71.
[12] Y. Wu, X. Ye, X. Yang, X. Wang, W. Chu and Y. Hu, *Ind. Eng. Chem. Res.*, **1996**, *35*, 2546.

5 Catalytic performance tests

Parts of this chapter are published in:

B. Katryniok, S. Paul, M. Capron, C. Lancelot, V. Bellière-Baca, P. Rey and F. Dumeignil, *GreenChem.*12, ***2010***, 1922-1925.

5.1 Preliminary tests

5.1.1 Test on mass transfer limitations

The possible existence of external diffusion limitations was studied by variation of the gas-flow and of the volume of the catalytic bed (**Figure 5-1**). When the flow of the reactant gas (F) is changed, the linear velocity changes proportionally, whereby the volume of the catalytic bed (V) must be adapted to ensure constant contact time. In practice, the catalyst quantity and flow were doubled in one case, and decreased by a factor 0.6 in the second case (**Table 5-1**). The catalyst used for this test was 20 wt.% silicotungstic acid supported on CARiACT Q-10.

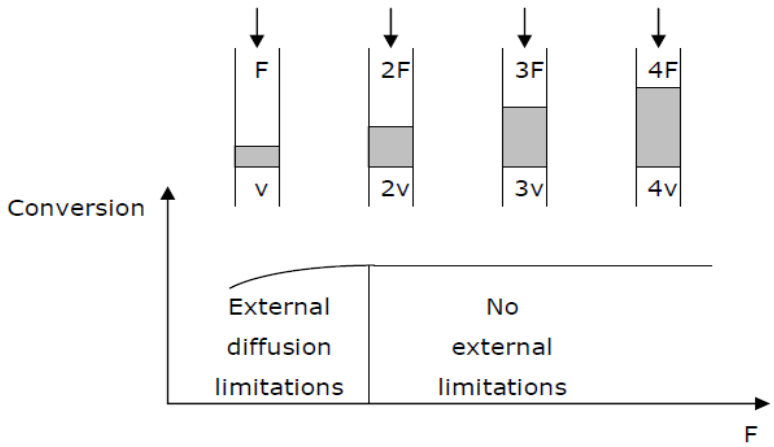

Figure 5-1: Experimental approach for determining potential external mass-transfer limitations

Table 5-1: Parameters and results of the experiments on mass transfer limitations

	V (mg)	liq. F_{GLY} (mL/min)	gas F_{He} (ml/min.)	gas F_{total} (mL/min.)	Glycerol Conversion (%)
A	180	0.9	18	60.0	87
B	300	1.5	30	99.9	87
C	600	3.0	60	199.9	89

© 2011 Tous droits réservés.
http://doc.univ-lille1.fr

From the results, one can see that the conversion after 5 h of reaction is nearly identical for all three conditions and remains close to 87 % (**Table 5-1**). As a conclusion, one can state that the reaction is not limited by external diffusion for gas-flows between 60 - 200 mL/min. An investigation of the internal mass transfer limitations was not done, as the small particle size (< 100 µm) enables the assumption that the internal diffusion is negligible.

5.2 Performance tests of non-zirconia-grafted catalysts

In the following section, the catalytic performances of the catalysts based on non-zirconia-grafted silica are presented and discussed.

5.2.1 Variation of the active phase

In a first series, the influence of the active phase nature was studied. As aforementioned, the physical and chemical properties of heteropoly compounds are depending on the central atom (Si, P…), the addenda atom (W, Mo, V…) and the presence of counter cations (Cs, Rb …) in replacement of protons. Therefore, catalysts with five different active phases (silicotungstic acid, phosphotungstic acid, phosphomolybdic acid, vanado-phosphomolybdic acid and di-vanado-phosphomolybdic acid) were prepared using CARiACT Q-10 as a support. The catalysts were tested using the aforementioned standard reaction conditions.

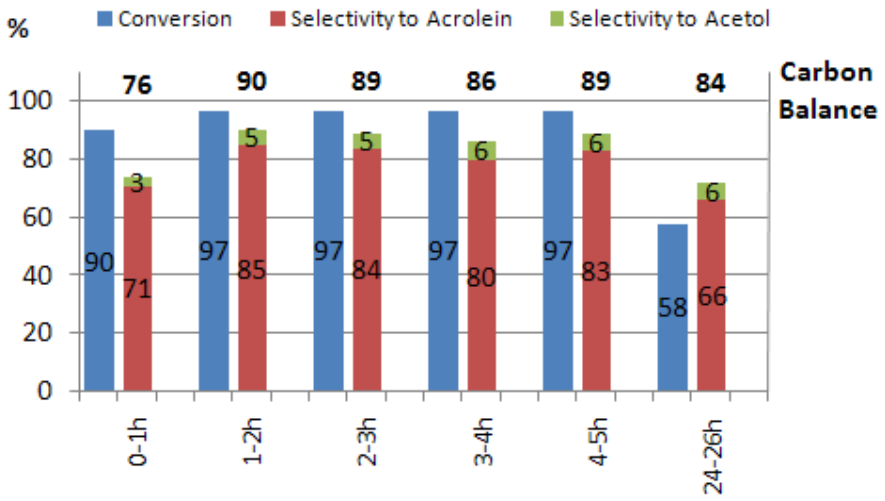

Figure 5-2: Catalytic performance for 20 wt.% silicotungstic acid on CARiACT Q-10

© 2011 Tous droits réservés.
http://doc.univ-lille1.fr

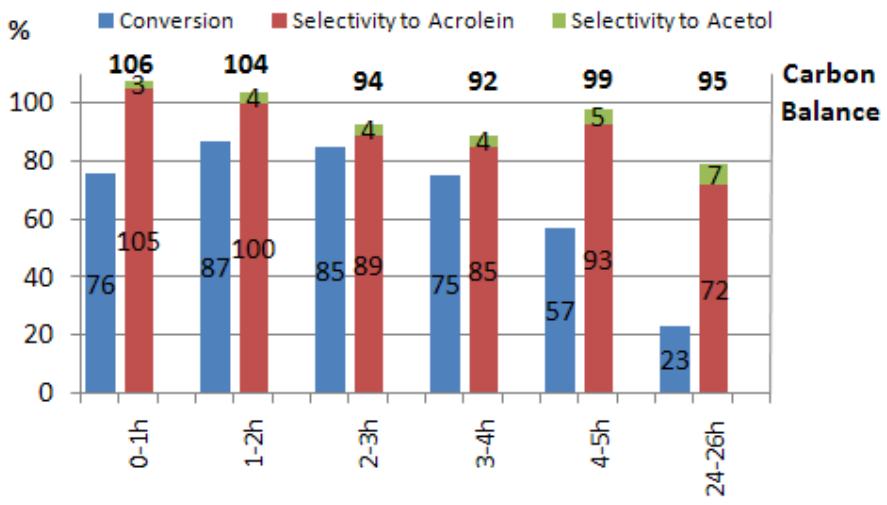

Figure 5-3: Catalytic performance for 20 wt.% phosphotungstic acid on CARiACT Q-10

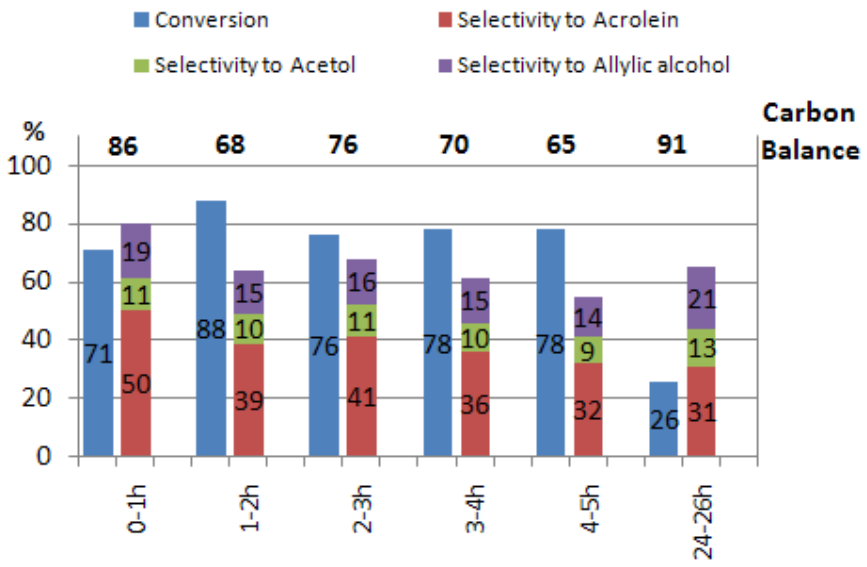

Figure 5-4: Catalytic performance for 20 wt.% phosphomolybdic acid on CARiACT Q-10

© 2011 Tous droits réservés.
http://doc.univ-lille1.fr

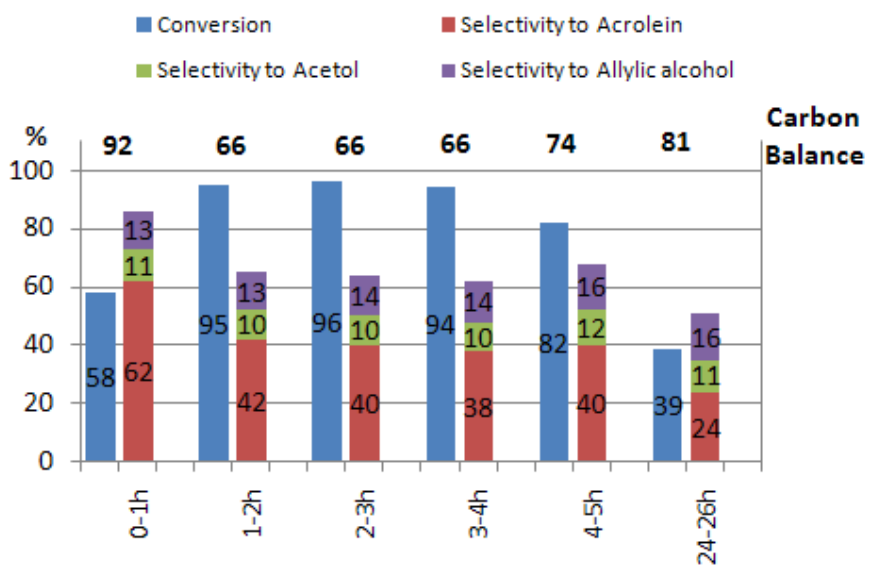

Figure 5-5: Catalytic performance for 20 wt.% vanado-phosphomolybdic acid on CARiACT Q-10

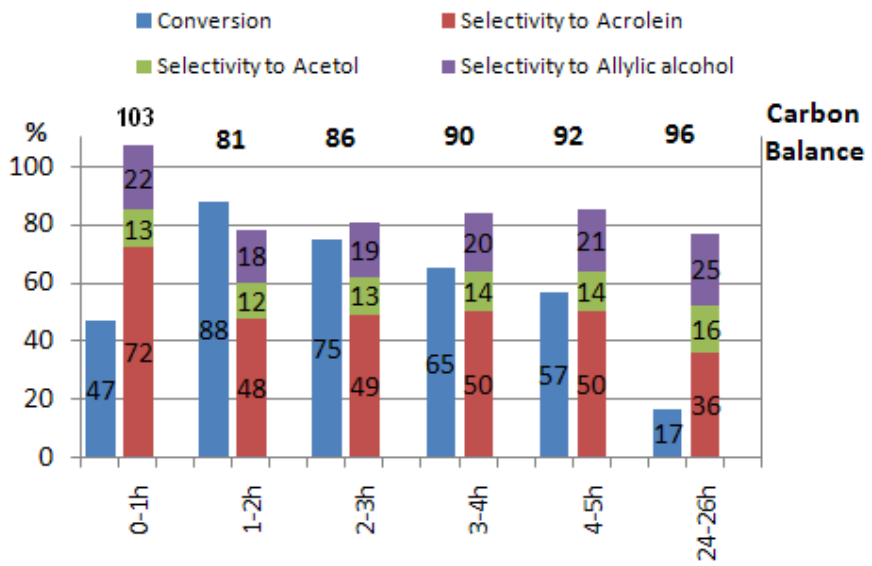

Figure 5-6: Catalytic performance for 20 wt.% di-vanado-phosphomolybdic acid on CARiACT Q-10

From the results, one can see that all the catalysts show a high activity in the dehydration of glycerol, reaching generally about 90 % conversion during the 2 first hours of the reaction. Afterwards, a decrease in conversion can be stated for all the catalysts, which is ascribed to the deactivation by carbon deposit. In fact, when the

© 2011 Tous droits réservés.
http://doc.univ-lille1.fr

catalysts are recovered after test, they are deep black, whereas the initial color varies between white (silico- and phosphotungstic acid), green (phosphomolybdic acid) and yellow-orange (vanadium containing compounds). Nevertheless, the catalyst containing silicotungstic acid still shows 58 % of conversion after 24 h of reaction (**Figure 5-7**), whereas the other catalysts give only between 17 % (di-vanado-phosphomolybdic acid - **Figure 5-6**) and 39 % (vanado-phosphomolybdic acid - **Figure 5-5**) of conversion at the same time-on-stream.

Whereas the catalytic activity is quite similar for all the catalysts, the selectivity to acrolein is strongly depending on the choice of the active phase. The tungsten-containing compounds show very high selectivity to acrolein with values of 80-85 % (silicotungstic acid - **Figure 5-2**) and 85-90 % (phosphotungstic acid - **Figure 5-3**). The formation of acetol (also known as hydroxyacetone) is also observed but remains quite low with a selectivity of no more than 6 % on these samples.

On the other hand, the molybdenum-containing heteropoly compounds exhibit lower selectivity to acrolein of only 50 % and significantly increased formation of acetol with selectivity between 10 and 15 %. Moreover, for these catalysts the formation of allylic alcohol is observed, which was not the case for the tungstic-HPAs. In fact, allylic alcohol and not acetol, is the major by-product in these cases with a selectivity of 14 to 20 % (*cf.* **Figure 5-6**). Even though no other by-products were detected, the carbon-balance for the molybdenum-containing catalysts was significantly lower than that observed for tungsten-containing heteropoly acids.

From these results, one can discuss the influence of the two chemical properties present in heteropoly acids, namely acidity and redox character, on their catalytic performances. The first effect, the higher deactivation rate observed over phosphotungstic acid, is attributed to the increased acid strength compared to silicotungstic acid. As aforementioned, Chai *et al.* demonstrated that strong acid catalysts exhibit increased carbon deposit and therefore faster deactivation.[1]

On the other hand, the decreased selectivity to acrolein and the formation of allylic alcohol over molybdenum-based heteropoly acids can be ascribed to the aforementioned higher redox potential of molybdenum and vanadium in comparison to tungsten.[2]This redox character facilitates the reduction of acrolein to allylic alcohol as proposed by Chai and Tsukuda (cf. **Scheme 2-4**), whereby one can also explain

© 2011 Tous droits réservés. http://doc.univ-lille1.fr

the decrease in the selectivity to acrolein at the same time.[1,3] This increased redox potential may also be responsible for the lower carbon balance observed for the molybdenum based catalysts. In fact, the redox properties give access to a large number of by-products as seen from the reaction mechanisms in section 2.1.5.

5.2.2 Influenceof the reaction temperature

To study the influence of the reaction temperature on the catalytic performances, a catalyst containing 20 wt.% silicotungstic acid on CARiACT Q-10 was chosen. This catalyst can be seen as benchmark catalyst, as it was already studied by Tsukuda *et al.*[3] The sample was tested under standard reaction conditions, but with three different reaction temperatures of 225 °C, 250 °C and 275 °C.

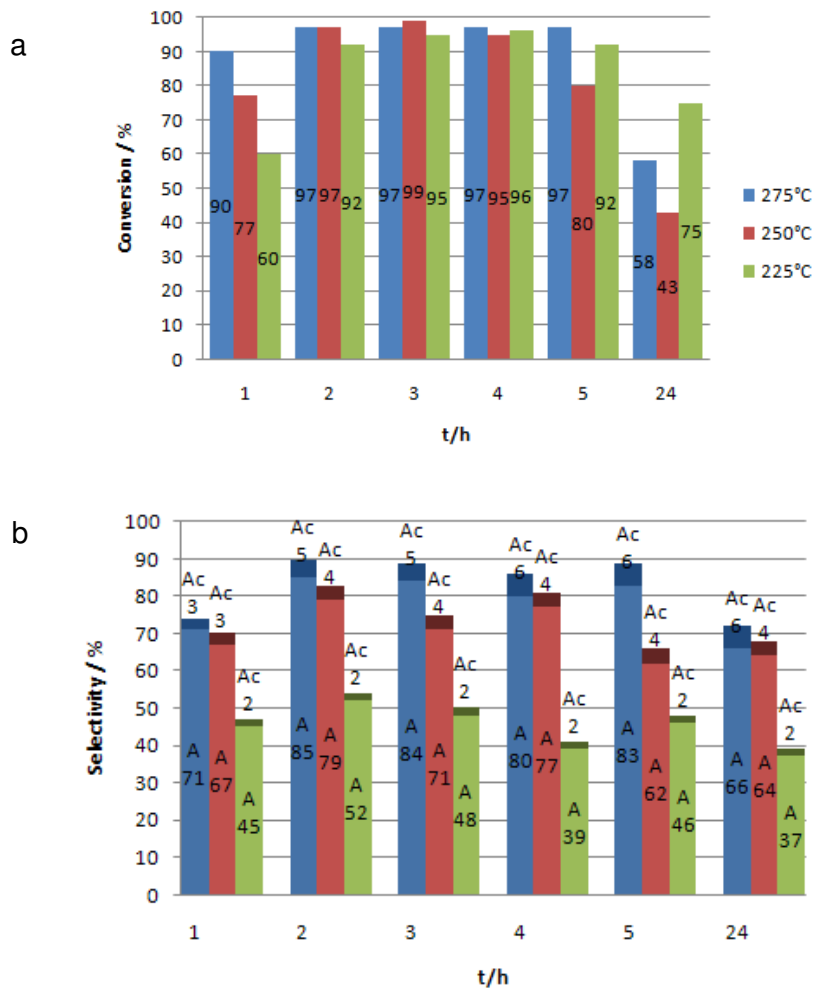

Figure 5-8: Conversion (a) and selectivity (b) for 20 wt.% silicotungstic acid on CARiACT Q-10 at different reaction temperatures (A=Acrolein; Ac=Acetol)

© 2011 Tous droits réservés. http://doc.univ-lille1.fr

From Figure 5-8, one can see that the reaction temperature has only a little influence on the activity, as complete conversion is obtained even at 225 °C. Nevertheless, the selectivity is importantly affected. Whereas the highest selectivity to both acrolein and acetol is observed for the highest reaction temperature of 275 °C, these values are divided by a factor two, when the temperature is decreased to 225 °C.

According to the thermodynamical calculations by Nimlos *et al.*, one can see that the reaction is classified as endothermic (*cf.* Figure 2-1).[4] Therefore, the dehydration reaction requires a high temperature to overcome the activation energy barrier. The activation energy for the acetol pathway is given at 73.2 kcal/mol, which is even higher than the activation energy determined for the acrolein pathway, which is 70.9 kcal/mol. As a result, both selectivities decrease with the reaction temperature, whereby the decrease in the acetol selectivity is even more important as one can see from the selectivity ratio (Figure 5-9).

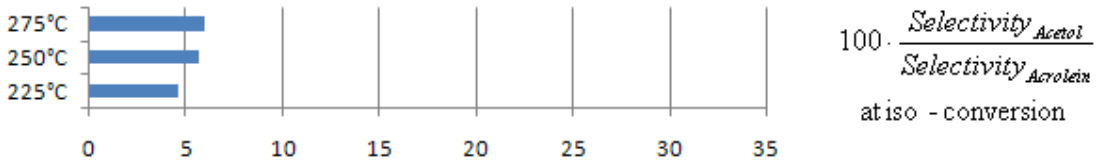

Figure 5-9: Selectivity ratio for 20 wt.% silicotungstic acid on CARiACT Q-10 at different reaction temperatures

On the other hand, we have seen that even at a lower reaction temperatures, the glycerol conversion remains quite high. This is attributed to the fact that, at low temperature, the intermolecular dehydration of glycerol is favored over the intramolecular one. The resulting products are oligomers of glycerol (oligoglycerine), as postulated by Ulgen *et al.*(**Scheme 5-1**).[5]

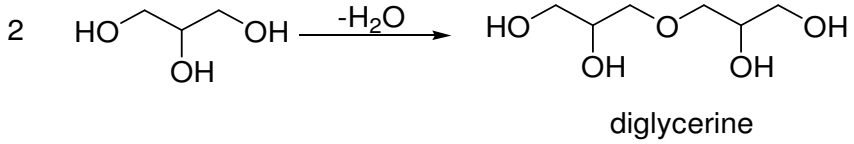

Scheme 5-1: Intermolecular condensation of glycerol

© 2011 Tous droits réservés.
http://doc.univ-lille1.fr

5.2.3 Variation of the silica support

To study the influence of the support on the catalytic performance five other silica - next to the already tested CARiACT Q-10 (5.2.2) – were chosen: KIT-6, SBA-15 (8 nm poresize), TMPS-4, TMPS-2.7 and HMS. The supports represent different poresizes reaching from 3 nm (HMS and TMPS-2.7) to 15 nm (CARiACT Q-10). Like for CARiACT Q-10, the supports were impregnated with 20 wt.% of silicotungstic acid as an active phase and the catalytic performance was determined under the aforementioned standard reaction conditions.

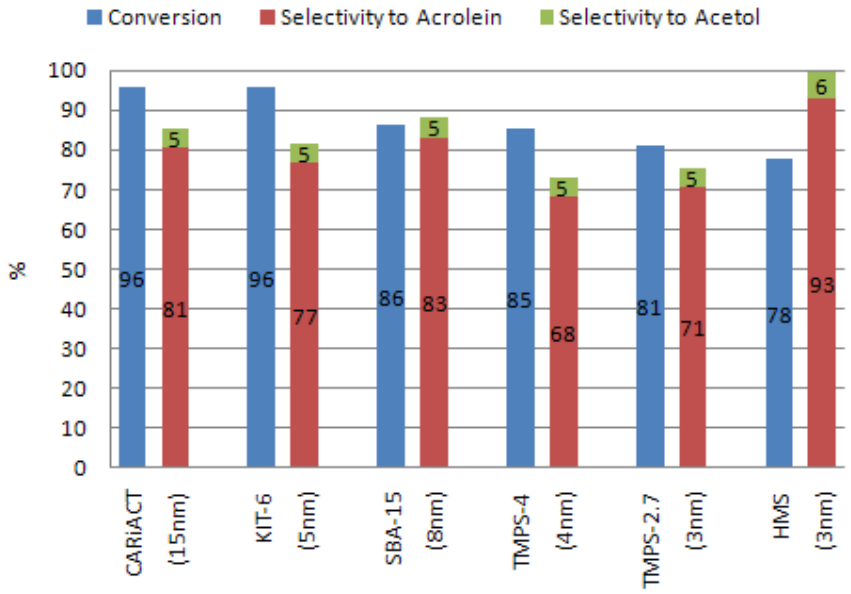

Figure 5-10: Catalytic performance during the first 5 h of reaction for catalysts containing 20 wt.% silicotungstic acid

© 2011 Tous droits réservés.
http://doc.univ-lille1.fr

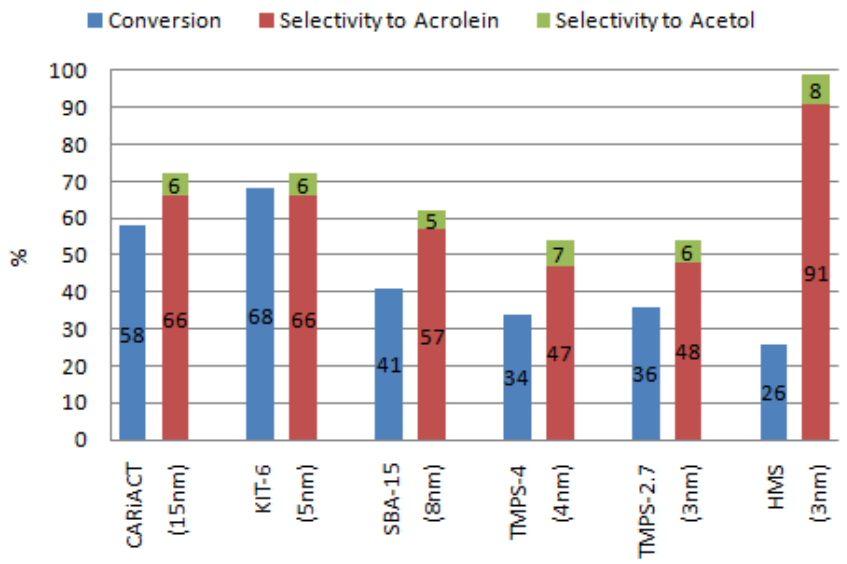

Figure 5-11: Catalytic performance after 24 h of reaction for catalysts containing 20 wt.% silicotungstic acid

From the results, one can see that during the first 5 h on stream, the catalytic performances are quite similar between all the catalysts with conversion between 85 and 95 % (**Figure 5-10**). Only TMPS-2.7 and HMS showed lower activity of only 80 %. On the other hand, the selectivity to acrolein was generally around 80 % the exceptions of for TMPS-4 and TMPS-2.7, on which it did not exceed 70 % and HMS, which showed a superior selectivity to acrolein of over 90 %. After 24 h of reaction (**Figure 5-11**), all the catalysts exhibited a significant decrease in conversion, but whereas the conversion over SBA-15 (8 nm poresize), TMPS-4 and TMPS 2.7 drastically decreased by a factor two (34-41 % *vs.* 81-85 % initially), the decrease was more moderate over the catalysts based on CARiACT Q-10 and KIT-6, which still conserved two-third of their initial conversion (58-68 % *vs.* 96 % initially). On the other hand, the HMS-supported sample had no more than one third of its initial activity during the first 5 h of reaction (26 % *vs.* 78 % initially). Concerning the selectivity after 24 h on stream, one can see that all the catalysts exhibited a significantly loss in selectivity except the catalyst based on HMS, which still exhibited 91 % of selectivity to acrolein.

As a conclusion, one cannot state a direct relation between the pore size and the catalytic performances as postulated by Tsukuda *et al.*[3] Nevertheless, Tsukuda used silica supports from the same type (CARiACT), but with different pore sizes. Thereby, one cannot directly compare his findings with our results, as the geometry of our

© 2011 Tous droits réservés. http://doc.univ-lille1.fr

samples varies. Indeed, CARiACT and SBA-15 are hexagonal silica, whereas TMPS is a tetragonal and KIT-6 a cubic silica.

To overcome this problem, SBA-15 with five different pore diameters of 5, 6, 8, 9 and finally 13 nm were prepared (cf. 3.1.2), impregnated with 20 wt.% of silicotungstic acid and tested under standard reaction conditions.

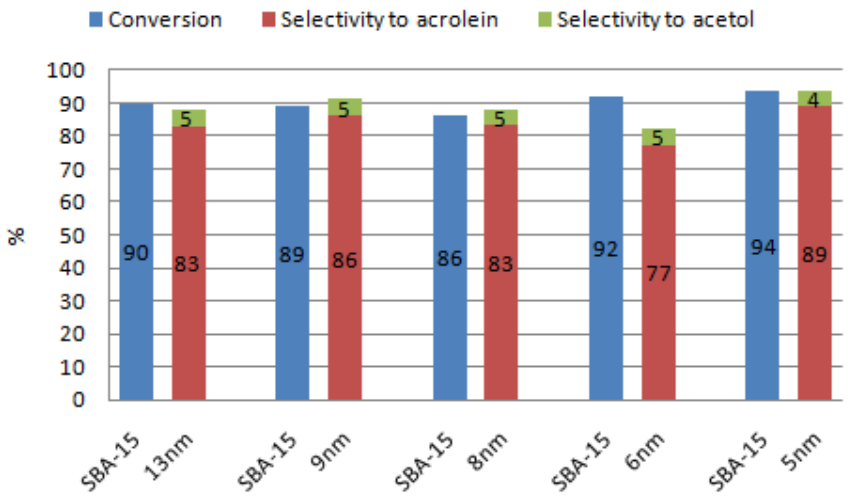

Figure 5-12: Catalytic performance for 20 wt.% silicotungstic acid over SBA-15 with different pore size during the first 5 h on stream.

The catalytic performances of the catalysts based on SBA-15 with different pore diameters are very similar (**Figure 5-12**). All the samples exhibit high conversion of about 90 % and the selectivity to acrolein varies around 85 % with an upper outlier for a pore size of 5 nm (89 %) and a lower one for 6 nm (77 %). As a conclusion, we find the same picture as in the previous case of the supports with different geometries, meaning that the influence of the pore size on the catalytic performance cannot be reliably quantified.

To study the impact of the pore size on the deactivation extent, the catalytic performances were once again measured after 24 h of reaction (**Figure 5-13**). From the results, one can see that the activity significantly decreased. The most important decrease was observed over SBA-15 with a pore size of 8 nm, which conserved only half of its initial conversion (41 % *vs.* 86 % initially), whereas the other samples still exhibited two-third of their initial conversion (50-60 % *vs.*90 % initially). Furthermore, the selectivity to acrolein decreased in all cases, whereby the highest remaining selectivity was observed over SBA-15 with a mean pore size of 6 nm (71 %). One

© 2011 Tous droits réservés.
http://doc.univ-lille1.fr

can conclude that, even though it was postulated with regard to internal diffusion,[6] larger pores do not show any positive impact on the catalytic performance over SBA-15 supported silicotungstic acid.

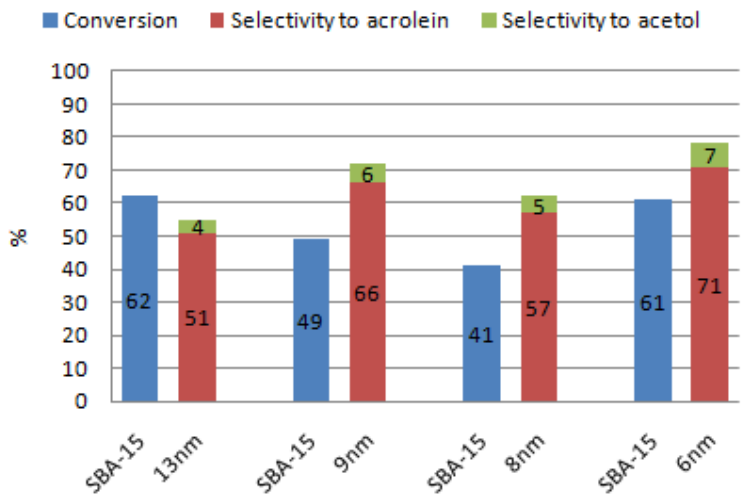

Figure 5-13: Catalytic performance for silicotungstic acid over SBA-15 with various pore sizes after 24 h on stream

5.3 Performance tests of zirconia-grafted catalysts

In the followings, the performances of the catalysts based silicotungstic acid supported on zirconia-grafted silica are presented. These studies were performed using silicotungstic acid as active phase, as it shows best catalytic long-term performance as demonstrated in chapter 5.2.1. On the other hand, SBA-15 of 8 nm poresize as used as host support, as it offers a poresize close to the optimal one postulated by Tsukuda *et al.*[3] In a first series, the amount of zirconia on the support was varied, then the influence of the calcination temperature was studied and, finally, the impact of the amount of the active phase was studied. Furthermore, like in the case of the non-grafted catalysts, the effect of the textural properties on the catalytic performances was investigated using various silica supports.

5.3.1 Influenceof the zirconia amount

The influence of the quantity of zirconia on the catalytic performances was studied for SBA-15 of 8 nm poresize. The silica was grafted following the afore described method (cf. 3.1.3) with 10 wt.%, 20 wt.% and 40 wt.% zirconia. After calcination at 650 °C, the support was impregnated with 20 wt.% of silicotungstic acid. The prepared catalysts were tested under standard conditions.

© 2011 Tous droits réservés.
http://doc.univ-lille1.fr

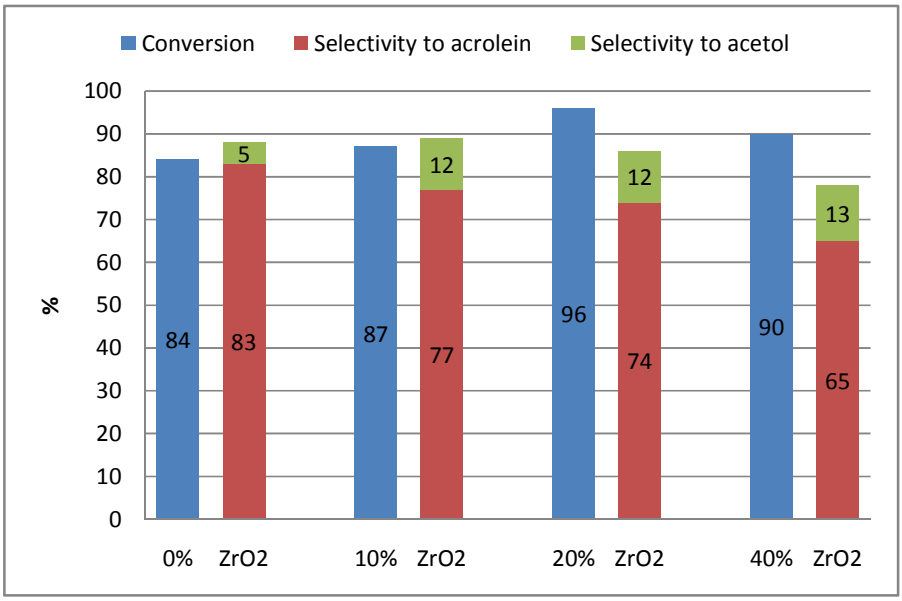

Figure 5-14: Catalytic performance during the first 5 h on stream for 20 wt.% silicotungstic acid over SBA-15 (8 nm poresize) grafted with 0-40 wt.% ZrO_2

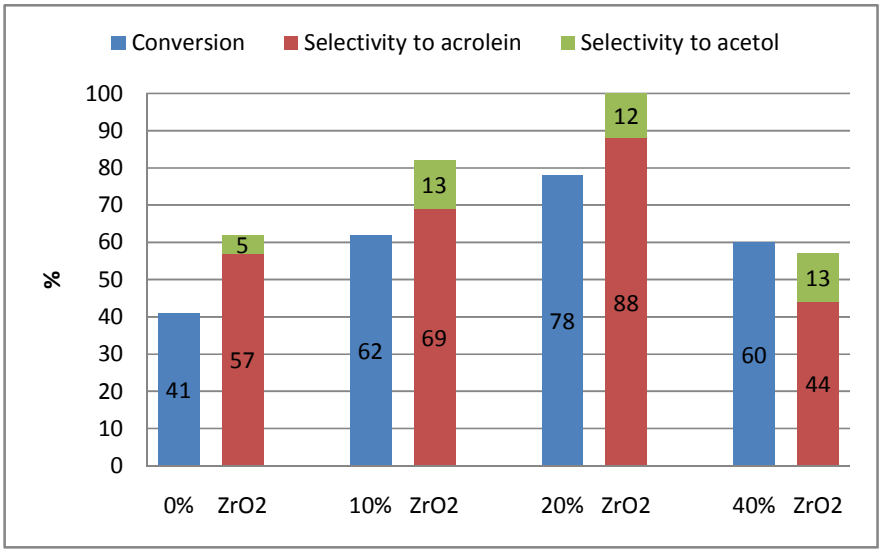

Figure 5-15: Catalytic performance after 24 h on stream for 20 wt.% silicotungstic acid over SBA-15 (8 nm poresize) grafted with 0-40 wt.% ZrO_2

The catalytic performances during the first 5 h under stream were similar for all the samples containing up to 20 wt.% zirconia, with a selectivity to acrolein between 77 and 83 % (Figure 5-14), whereas it was significantly lower (65 %) for the sample grafted with 40 wt.% zirconia. As second effect, one can state that the selectivity to acetol doubled by introducing ZrO_2, (12-13 % *vs.* 5 % without). After 24 h under stream, the beneficial effect of the zirconia grafting was clearly revealed (**Figure 5-15**): Whereas the conversion of the catalyst without zirconia was divided by a factor

© 2011 Tous droits réservés. http://doc.univ-lille1.fr

two (41 % after 24 h *vs.* 84 % during the first 5 h), all the zirconia-containing catalysts still exhibited rather high glycerol conversions of 60 % (40 wt.% ZrO_2), 62 % (10 wt.% ZrO_2) and even 78 % (20 wt.% ZrO_2). However, the selectivity to acrolein of the sample grafted with 40 wt.% zirconia remained still low (44 %).

The above results show the beneficial effect of zirconia for preventing catalytic deactivation. The best catalytic performance was obtained over the sample containing 20 wt.% zirconia, which showed a remarkably stable acrolein yield of 69 % after 24 h *vs.* 71 % during the first 5 h. To understand the effect of zirconia on the catalytic performances of supported silicotungstic acid, one has to correlate the acidity of the catalysts with and without ZrO_2. In section 4.3.4, the acidity of the catalysts containing 20 wt.% silicotungstic acid on ZrO_2-grafted SBA-15 (8 nm poresize) and on bare SBA-15 were compared, showing that the catalyst with zirconia had less strong acid sites than the catalyst based on non-grafted SBA-15 (Figure **4-19**). This slight decrease in the acid strength led to less formation of coke – thus less deactivation –, whereby the long-term performance increases.

The low selectivity to acrolein over the catalyst containing 40 wt.% zirconia can be correlated to the presence of the large zirconia domains detected by XRD and HRTEM (*cf.* 4.2.4, Figure **4-10**; Figure **4-11**). These agglomerates are formed due to ZrO_2 overloading, and confer a predominant Lewis acid character to the catalyst. These Lewis acid sites are known for favoring side-reactions (*cf.* 2.1.1, Scheme 2-1), whereby one can explain the observed decrease in acrolein selectivity. This effect was also observed over the other ZrO_2-containing catalysts, which all showed significantly increased selectivity to hydroxyacetone compared to the non-grafted samples. From **Figure 5-16**, one can see that higher amount of ZrO_2 leads to increased selectivity to acetol, whereby the reaction mechanism postulated by Alhanash *et al.* (Scheme 2-1) is confirmed.

© 2011 Tous droits réservés.
http://doc.univ-lille1.fr

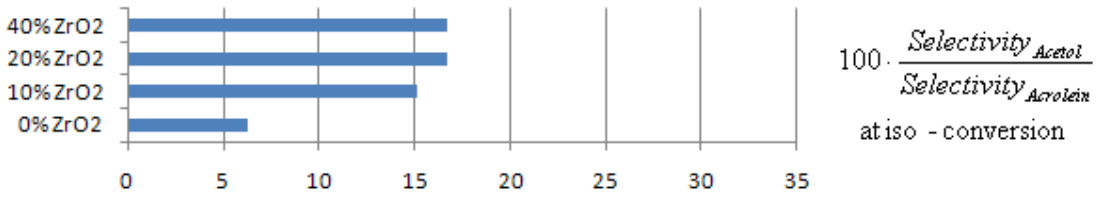

Figure 5-16: Selectivity ratio for catalysts containing 20 wt.% silicotungstic acid on SBA-15 (8nm poresize) grafted with 0-40 wt.% zirconia

5.3.2 Influence of the amount of active phase

The influence of the amount of silicotungstic acid on the catalytic performances was studied for a SBA-15 support of 8 nm poresize grafted with 20 wt.% of zirconia. The amount of zirconia (20 wt.%) was chosen with regard to the increased catalytic long-term performance shown in section 5.3.1. After calcination at 650 °C, the support was impregnated with 10 wt.%, 20 wt.% or 30 wt.% of silicotungstic acid. A comparative sample without silicotungstic acid was also prepared. The catalysts were tested under standard conditions.

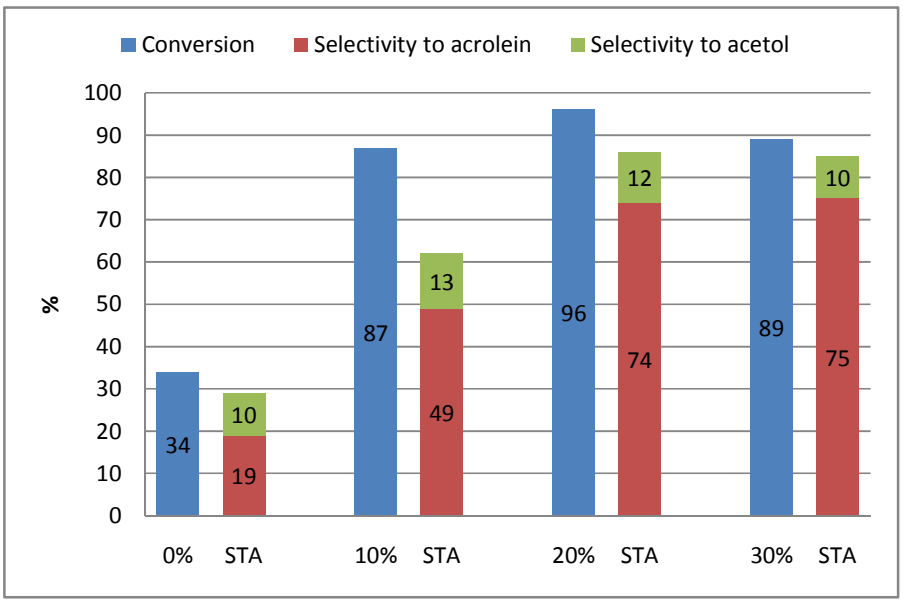

Figure 5-17: Catalytic performance during the first 5 h on stream for 20 wt.%ZrO_2/SBA-15 (8 nm poresize) with 0-30 wt.% silicotungstic acid (STA)

© 2011 Tous droits réservés.
http://doc.univ-lille1.fr

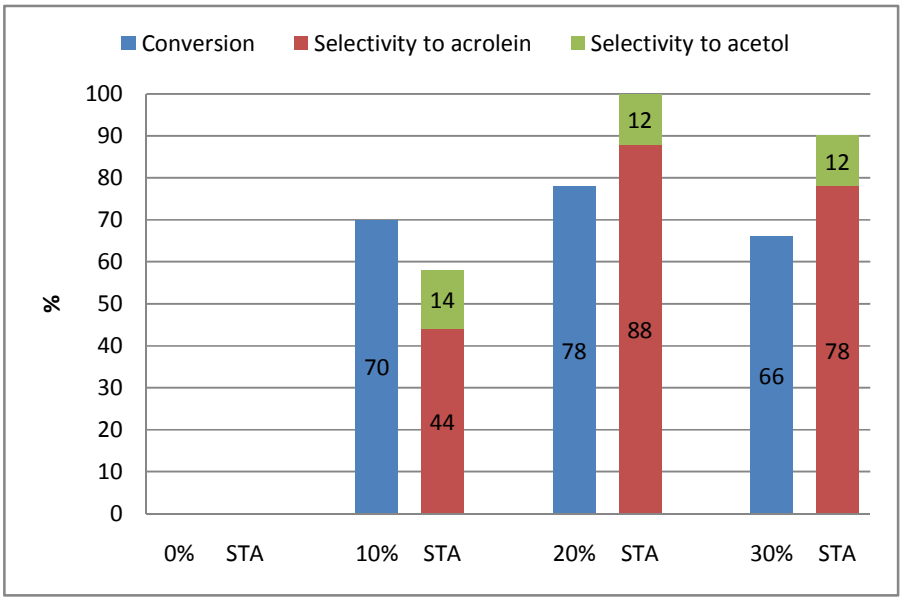

Figure 5-18: Catalytic performance after 24 h on stream for 20wt.%ZrO_2/SBA-15 (8 nm poresize) with 0-30 wt.% silicotungstic acid (STA)

The catalytic performances during the first 5 h on stream were rather similar for the samples containing 20 and 30 wt.% of silicotungstic acid, with a conversion of glycerol between 89 and 96 % and a selectivity to acrolein of 74-75 % (Figure 5-17). In contrast, the catalyst containing 10 wt.% of active phase exhibited a rather low selectivity to acrolein of 49 %. This effect was even more pronounced for the catalyst without silicotungstic acid, which showed both, low conversion (34 %) and very low selectivity to acrolein of only 19 %.

After 24 h, the catalyst containing 30 wt.% active phase showed a significantly lower conversion (66 %) than the one with 20 wt.% (78 %). Nevertheless the selectivity in both cases still achieved high values of 78% and 88% respectively. Meanwhile the performance of the 10 wt.% STA catalyst was still feeble due to its low selectivity to acrolein (44 %).

From this second series of experiments, two different factors that affect the catalytic performance were identified: *(i)* the surface density of acid sites and *(ii)* the nature of the acid sites. A low amount of silicotungstic acid (*i.e.*, 10 wt.%) resulted in an only partial coverage of the zirconia-grafted support (cf. 4.2.2). Accordingly, the Lewis acid character of the uncovered zirconia became dominant, which led to low selectivity to acrolein, as observed before for the high ZrO_2 loading of 40 wt.% (cf. 5.3.1). Furthermore, one can observe the same correlation as that found when

© 2011 Tous droits réservés.
http://doc.univ-lille1.fr

studying the influence of the zirconia amount, namely that for high loadings of heteropoly acid, the selectivity to acetol decreases (Figure 5-19). This gives evidence that the Brønsted character of the heteropoly acid masks the Lewis acid character of the support.

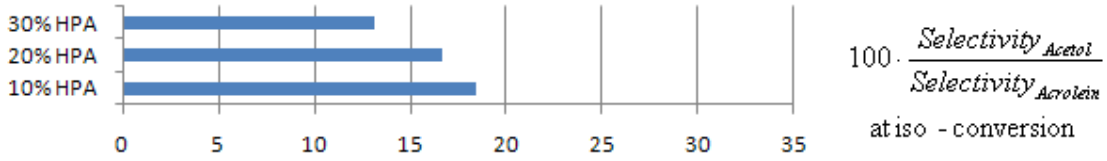

Figure 5-19: Selectivity ratio for catalyst based on 20 wt.% ZrO_2/SBA-15 (8 nm poresize) containing 10-30 wt.% silicotungstic acid

On the other hand, a high amount of STA (*i.e.*, 30 wt.%) led to the deposition of a larger quantity of active phase over bare silica, whereby the acid strength re-increased again. As a consequence, the coke formation became more important, as observed before for the non-grafted catalysts (cf. 5.2), which resulted in accelerated deactivation after 24 h on stream.

5.3.3 Influence of the calcination temperature of the support

The influence of the calcination temperature was studied for SBA-15 of 8 nm poresize grafted with 20 wt.% zirconia and calcined at 400 °C, 650 °C and 950 °C (**Figure 5-20**). The zirconia and STA amount (both 20 wt.%) were chosen with regard to the increased catalytic long-term performance of the catalyst shown in section 5.3.2. A non-calcined sample was also prepared. The supports were then impregnated with 20 wt.% of silicotungstic acid. The catalysts were tested under standard conditions.

© 2011 Tous droits réservés.
http://doc.univ-lille1.fr

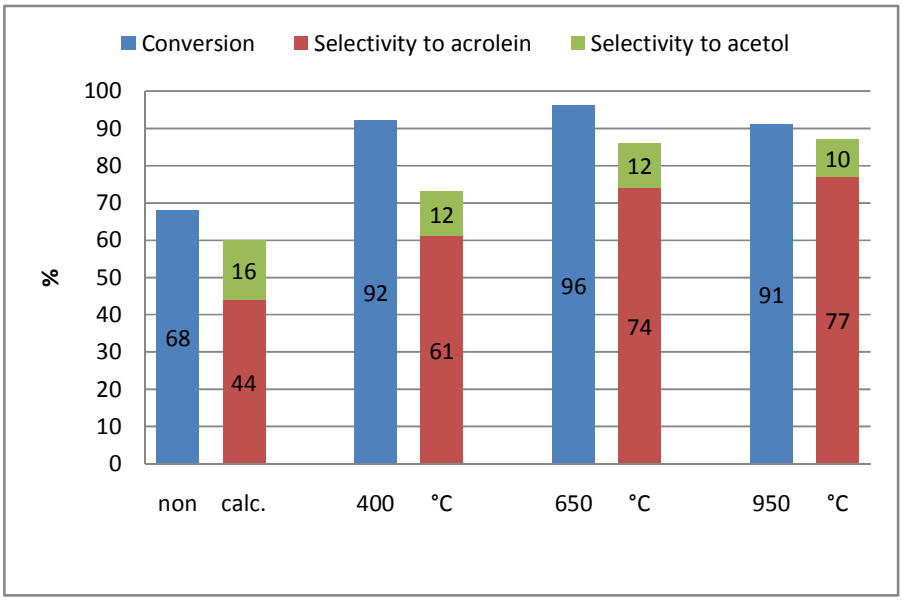

Figure 5-20: Catalytic performance during the first 5 h on stream for 20 wt.%ZrO_2/SBA-15 (8 nm poresize) calcined between 400-950°C and impregnated with 20wt.% silicotungstic acid

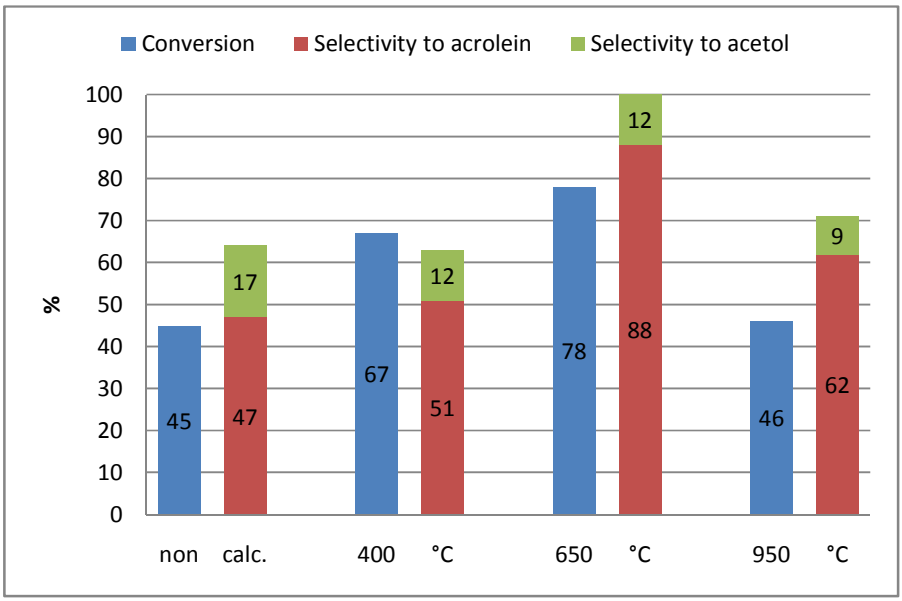

Figure 5-21: Catalytic performance after 24 h on stream for 20 wt.%ZrO_2/SBA-15 (8 nm poresize) calcined between 400-950°C and impregnated with 20wt.% silicotungstic acid

The catalytic performances during the first 5 h on stream were rather similar for the samples calcined at 650 °C and 950 °C, with a conversion of glycerol between 91

© 2011 Tous droits réservés.
http://doc.univ-lille1.fr

and 96 % and a selectivity to acrolein of 74-77 % (**Figure 5-20**). The non-calcined catalyst showed both rather low conversion (68 %) and low selectivity to acrolein (44 %).

After 24 h on stream, the catalyst calcined at 950 °C lost half of its conversion (46 % *vs.* 91 % initially) and showed also a decreased selectivity to acrolein of 62 % (**Figure 5-21**). On the other hand, the catalyst calcined at 650 °C is less affected giving still 78 % conversion after 24 h. The other samples calcined at 400 °C or non-calcined show once again only low selectivity to acrolein with 51 % and 47 % respectively.

The last mentioned results observed for the samples calcined below 650 °C are ascribed to the incomplete decomposition of the organic part of the zirconia-precursor [$Zr(n\text{-}PrO)_4$] as seen in section 4.2.3. This results in a support without any defined zirconia phase, whereby the interaction between the active phase and the support cannot be determined. On the other hand, the sample calcined at 950 °C exhibits comparable catalytic performance as that of the non-zirconia grafted catalyst (**Figure 5-14** and **Figure 5-15**). According to the XRD and HRTEM results (cf. 4.2.3, Figure **4-6**; Figure **4-7**), the highest calcination temperature of 950 °C results in a migration of the zirconia from the porous network to the entrance, leaving behind non-covered silica. This means that upon impregnation with silicotungstic acid, the active phase was in fact deposed on bare silica, whereby the acid strength increases again. As a consequence, the coke formation became more important, as observed before for the non-grafted catalysts (Chapter 3), which resulted in accelerated deactivation after 24 h on stream.

5.3.4 Influence of the silica support

The influence of the poresize on the catalytic performance was studied using different silica as support. Therefore CARiACT Q-10 (15 nm poresize), KIT-6 (5 nm poresize), SBA-15 (8 nm poresize), and HMS (3 nm poresize) were grafted with 20 wt.% of zirconia, calcined at 650 °C and finally impregnated with 20 wt.% silicotungstic acid as an active phase. The catalytic performances were determined under the standard reaction conditions.

© 2011 Tous droits réservés.
http://doc.univ-lille1.fr

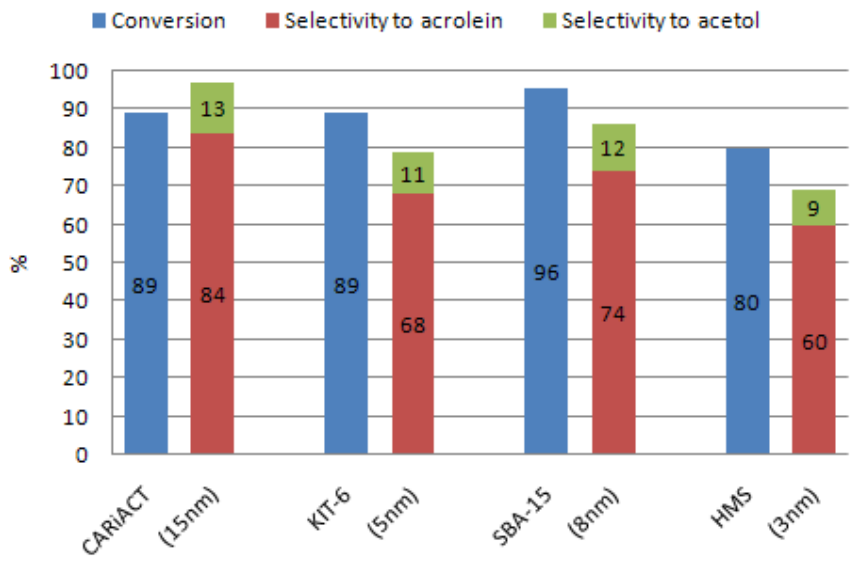

Figure 5-22: Catalytic performance during the first 5 h on stream for 20 wt.% of silicotungstic acid on various zirconia grafted silica supports (ZrO_2 content 20 wt.%, calcination temperature 650℃)

From the results, one can see that during the first 5 h on stream, the catalytic performances are quite similar among the various samples with conversions between 89 and 96 % (**Figure 5-22**). Only HMS showed lower conversion of only 80 %, which was already observed for the non-grafted HMS support (*cf.*5.2.3; **Figure 5-10**). On the other hand, the selectivity to acrolein was widely spread between 60 % (HMS) and 84 % (CARiACT). Furthermore, one can state an increase in the selectivity to acetol from 9 % (HMS) to 13 % (CARiACT) with increasing pore size. After 24 h of reaction (**Figure 5-23**), all the catalysts exhibit a lower conversion, but for all the samples, the decrease is less important than for the bare supports (*cf.*5.2.3; **Figure 5-11**). The catalyst based on HMS, for instance, lost two third of its conversion when non-grafted (26 % *vs.* 78 % initially), whereas the grafted one lost only one quarter of conversion (60 % *vs.* 80 %). Thereby, one can state that the positive effect of the zirconia grafting is not depending on the type of the used silica support. Concerning the selectivity after 24 h on stream, one can see that most of the catalysts exhibited a significant loss, except from the catalyst based on SBA-15-8nm, which still exhibited88 % of selectivity to acrolein. As already seen during the first five hours on stream, the selectivity to acetol is still very high over the zirconia-grafted CARiACTsupport.

© 2011 Tous droits réservés.
http://doc.univ-lille1.fr

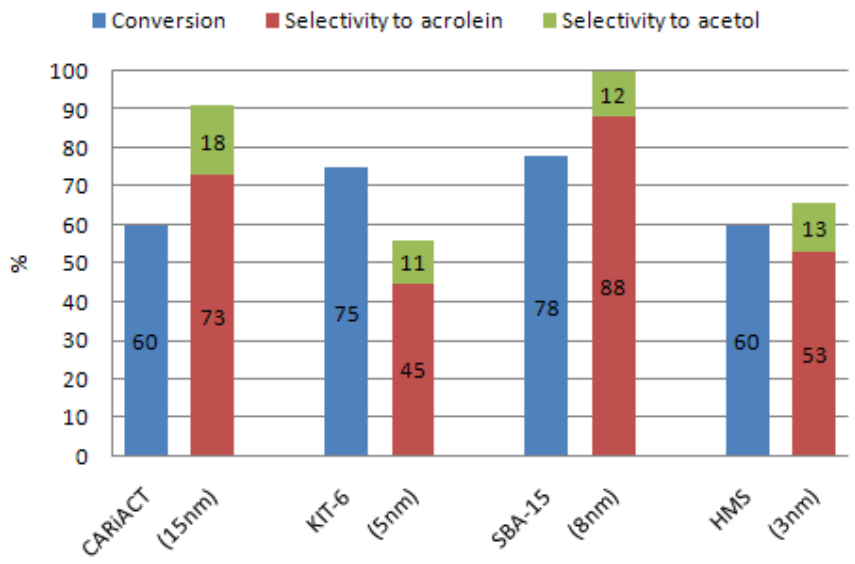

Figure 5-23: Catalytic performance after 24 h on stream for 20 wt.% silicotungstic acid on various zirconia grafted silica (ZrO_2 content 20 wt.%, calcination temperature 650 °C)

Like in the case of the non-grafted supports, one cannot state a direct relation between pore size and catalytic performances. Nevertheless, we have found that over supports with larger pore diameters the selectivity to acetol is increased (**Figure 5-24**).

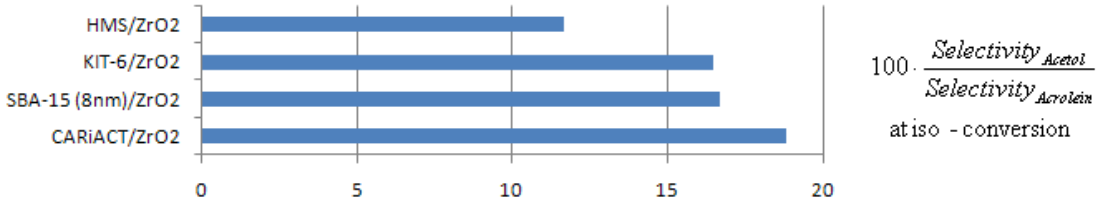

Figure 5-24: Selectivity ratio for 20 wt.% silicotungstic acid on various zirconia grafted silica (ZrO_2 content 20 wt.%, calcination temperature 650 °C)

Like for the non-grafted supports (cf. 5.2.3), a second study was performed for ruling out the influence of the geometry. Therefore, four SBA-15 supports with respective pore diameters of 4, 5, 6 and 8 nm were grafted with 20 wt.% zirconia and calcined at 650 °C. After impregnation with 20 wt.% of silicotungstic acid, the catalysts were tested under the standard reaction conditions.

© 2011 Tous droits réservés.
http://doc.univ-lille1.fr

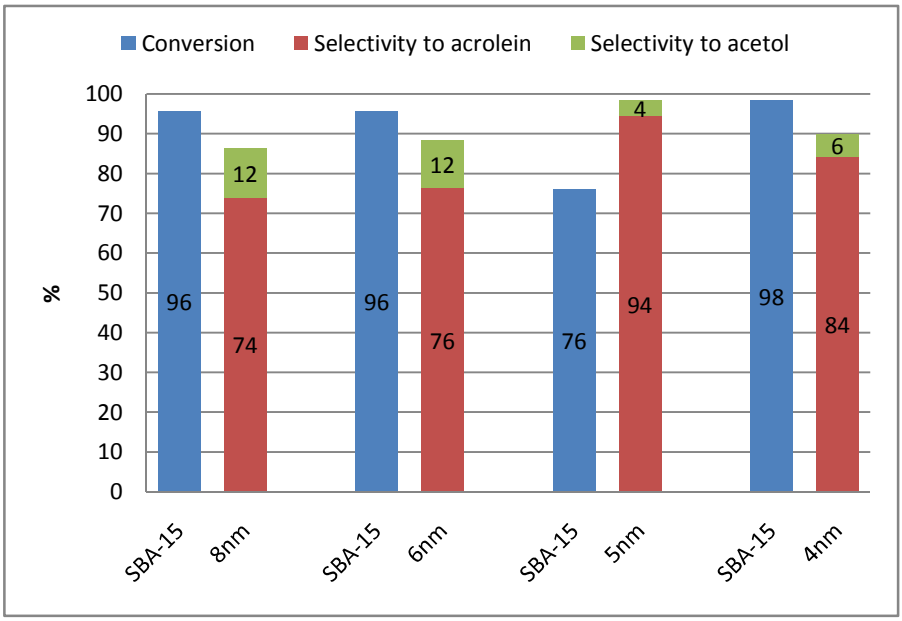

Figure 5-25: Catalytic performance during the first 5 h on stream for 20 wt.% silicotungstic acid on zirconia grafted SBA-15 with 4-8 nm poresize (ZrO_2 content 20 wt.%)

The early catalytic performances of the catalysts based on zirconia-grafted SBA-15 with different pore diameters are very similar (**Figure 5-25**). All the samples exhibit a high conversion of about 95 %, except the catalyst based on SBA-15-5nm. The selectivity to acrolein varies between 74 % (SBA-15-8nm) and 94 % (SBA-15-5nm). Here again, the selectivity to acetol seems to increase with the pore size (**Figure 5-27**), as already stated before for various zirconia-grafted supports. Nevertheless, one cannot find any clear picture of the influence of the pore size on the catalytic performances, at least for what is observed during the first 5 h of reaction.

After 24 h of reaction, one can see that the catalytic performances show a general trend of decreasing (**Figure 5-26**). Nevertheless, this decrease is more pronounced for the supports with small pore size (4-5 nm), where the conversion does not exceed half of the initial value (43 % *vs.*98 % initially), whereas the supports with larger pores (6-8 nm) still conserve three quarter of their initial activity after 24 h on stream (72-78 % *vs.* 96 % initially). Therefore, one can confirm this time that the pore size affects the deactivation rate, due to the absence of diffusion limitations for larger pores, which reduces the carbon deposit, as proposed by Erfle *et al.*[6] On the other hand, one cannot state a direct impact on the selectivity to acrolein, as the supports with 5

© 2011 Tous droits réservés.
http://doc.univ-lille1.fr

and 6 nm exhibit a selectivity of 72-75 %, whereas the support with large pores (8 nm) and small pores (4 nm) both exhibit a selectivity of 86-88 %. Only the selectivity to acetol seems once again increased over the supports with larger pores (12 % for 8 nm *vs.* 5 % for 4 nm).

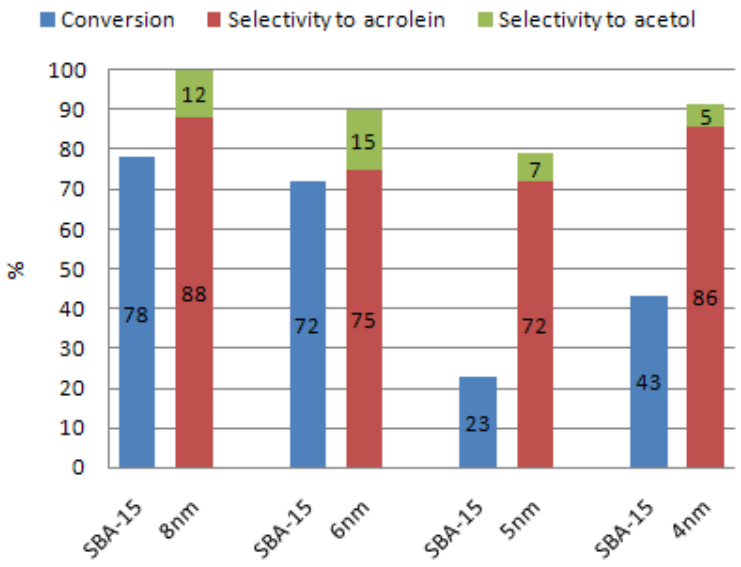

Figure 5-26: Catalytic performances after 24 h on stream for 20 wt.% silicotungstic acid on zirconia grafted SBA-15 with 4-8 nm poresize (ZrO_2 content 20 wt.%)

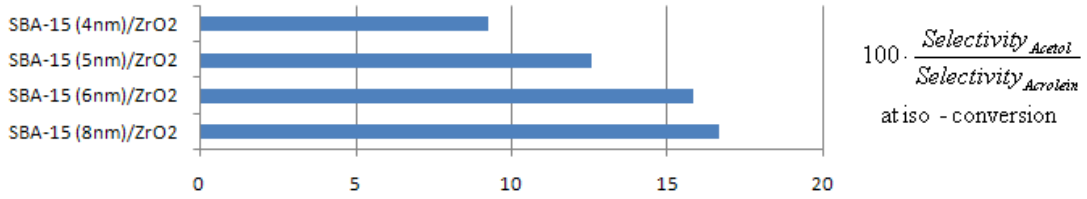

Figure 5-27: Selectivity ratio for 20 wt.% silicotungstic acid on zirconia grafted SBA-15 with 4-8 nm poresize (ZrO_2 content 20 wt.%)

As a conclusion, one can say that the zirconia grafting had in any case a positive impact on the long-term performances of the catalyst, without regard of the used silica. Even though no direct relation between the pore size and the selectivity to acrolein was found, we observed that the selectivity to acetol is increased with increasing pore diameter, independently of the used silica support. On the other hand, when SBA-15 with different pore sizes was used, the postulated relationship between the pore diameter and the catalytic activity was confirmed, as SBA-15 with

© 2011 Tous droits réservés.
http://doc.univ-lille1.fr

large pores (6-8 nm) exhibited superior conversions after 24 h on stream, which is explained by less carbon deposit due to reduced diffusion limitations that facilitate the mass transfer in the solid.

5.4 Regeneration of the catalysts

The catalyst based on zirconia grafted SBA-15 of 8 nm poresize and silicotungstic acid showed a significant increased long-term performance in comparison to the non-grafted catalyst. Nevertheless, a deactivation was stated, which is undesirable for industrial application. Therefore the possibility to regenerate the catalyst after reaction was studied for two catalysts, one based on zirconia (20 wt.%) grafted SBA-15 (8 nm poresize), the other based on non-grafted SBA-15. Both catalysts were impregnated with 20 wt.% of silicotungstic acid as an active phase and were initially placed under standard reaction conditions for 24 h, except that the catalyst (0.2g) was diluted in silicon carbide (0.99 µm, 0.8 g) to suppress hotspot formation during the regeneration. Afterwards, the catalysts were regenerated *in situ*, either with dry air or with humidified air (molar composition: 5 % water, 17 % oxygen, 78 % nitrogen). The flow of the regenerating gas was set at 20 mL/h and the temperature during regeneration was kept at 275 °C, like during the reaction. After 6 h of treatment, the catalytic performances were measured during 5 h to determine the impact of the regeneration conditions.

5.4.1 Regeneration of non-grafted catalyst

In the followings, the regeneration of a catalyst based on 20 wt.% silicotungstic acid on SBA-15 (8nm poresize) is shown.

© 2011 Tous droits réservés.
http://doc.univ-lille1.fr

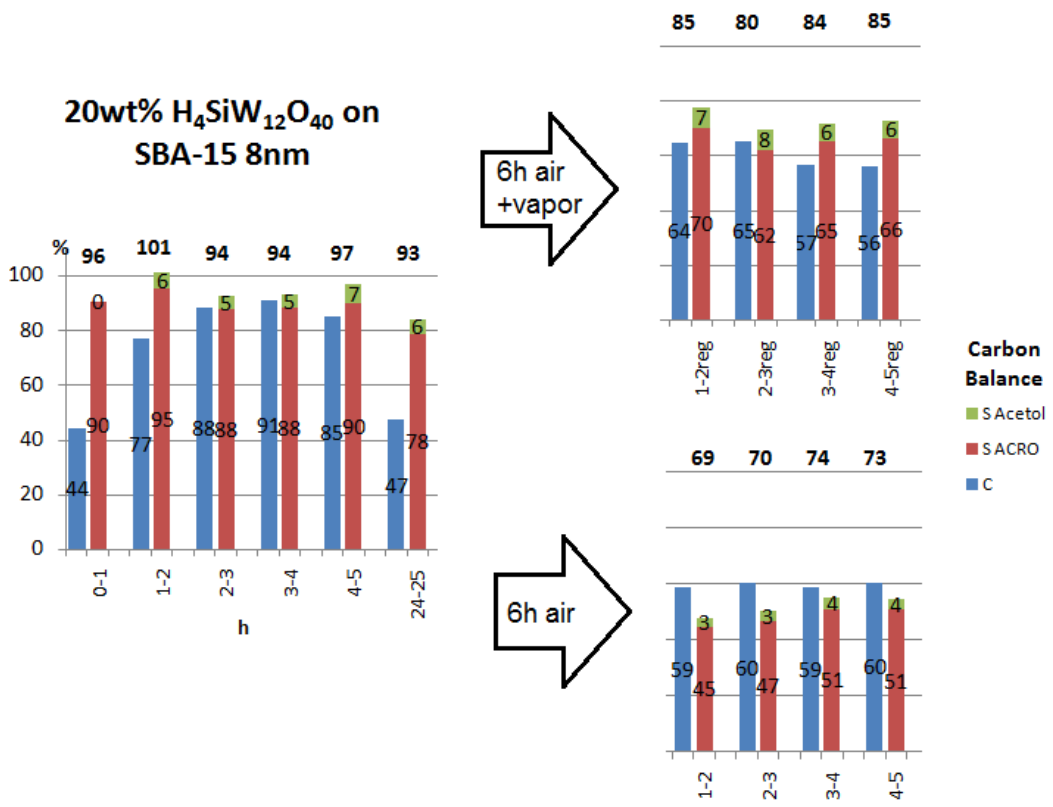

Figure 5-28: Regeneration of a non-grafted catalyst based on 20wt.% silicotungstic acid on SBA-15 (8 nm poresize) in dry and humid atmosphere

After 24 h of reaction, the catalyst lost half of its conversion (47 % *vs.*> 90 % initially; **Figure 5-28**). Therefore, the catalyst was regenerated either in dry or humidified air according to the aforementioned experimental conditions. From the catalytic performances after regeneration, one can see that the initial conversion in both cases is not completely recovered, but is higher than that observed before regeneration (59-64 % *vs.*47 %). Furthermore, the selectivity to acrolein is significantly decreased after regeneration (50 % in dry air and 65 % in humidified air *vs.* 78 % initially), whereby one can assume a partial decomposition of the silicotungstic acid. One can also state that the presence of vapor in the regeneration atmosphere has a positive impact on the selectivity and the carbon balance. This result is explained by the inhibition of the decomposition of the active phase. Actually, the regeneration in air will cause the burning of deposed carbon, which can result in local hotspots due to the exothermicity of this reaction. These hotspots may cause the decomposition of the active phase as the thermal stability of silica supported silicotungstic acid is limited to 350 °C (*cf.*4.3.5). The presence of vapor can act in two

© 2011 Tous droits réservés. http://doc.univ-lille1.fr

ways that limit the decomposition of the active phase: Either suppression of hotspots during the regeneration, due to the high heat capacity of steam, or shifting of the equilibrium reaction of the decomposition to the left side, due to the increased partial pressure of water:

$$H_4SiW_{12}O_{40} \Leftrightarrow SiO_2 + 12\ WO_3 + 2\ H_2O$$

Furthermore, the formed tungsten oxide from the decomposition products can explain the lower selectivity to acrolein, which is generally observed for Lewis acids (*cf.*2.1.1; Scheme 2-1).

5.4.2 Regeneration of zirconia-grafted catalyst

A catalyst based on zirconia grafted SBA-15 (8 nm) impregnated with 20 wt.% silicotungstic acid was reacted under standard conditions during 24 h. When the catalyst lost one third of its initial conversion (59 % *vs.* 90 % initially), it was regenerated for 6 h in dry or humidified air (Figure 5-29).

From the catalytic performances after regeneration, one can see that the conversion and the selectivity to acrolein are completely recovered for both types of regenerations. Nevertheless, the conversion after regeneration decreases rapidly in both cases to reach 63 % after the 5 h on stream.

© 2011 Tous droits réservés.
http://doc.univ-lille1.fr

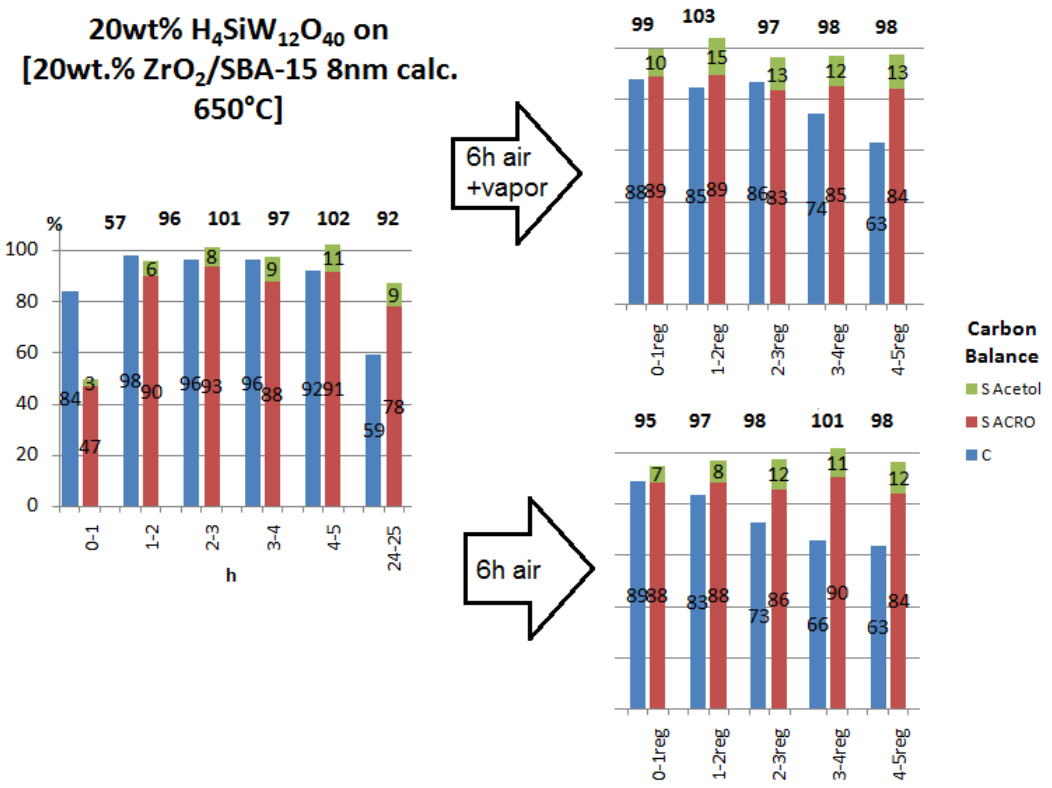

Figure 5-29: Regeneration of a catalyst based 20wt.% silicotungstic acid on zirconia-grafted (20 wt.%) SBA-15 (8 nm poresize) in dry and humid atmosphere

In comparison to the catalyst based on non-modified SBA-15 (*cf. 5.4.1*- Figure 5-28), the presence of vapor during the regeneration does not increase the catalytic performance of the zirconia-grafted catalyst after regeneration. In the case of the non-grafted support, we have explained the positive impact of vapor by the suppression of the decomposition of the silicotungstic acid in the hotspots formed during the regeneration. This effect is not observed over the zirconia-grafted catalysts, which can be explained by the increased thermal stability of silicotungstic acid over zirconia. As seen in Chapter 4.3.5 (Figure **4**-), the decomposition of silicotungstic acid over bare silica starts at 350 °C, whereas the zirconia supported one is stable up to 500 °C. Therefore, the hotspots formed during the regeneration will not lead to the decomposition of silicotungstic acid when supported on zirconia-grafted silica, which explains why the presence of water has no effect in this case.

[1] S-H. Chai, H-P. Wang, Y. Liang, B-Q. Xu, *Green Chem.* **2007**, 9, 1130-1136.
[2] M. Misono, T. Okuhara, N. Mizuno, *Catalysis by heteropoly compounds, Successful design of catalysis*, Amsterdam, Elsevier Science Publishers, **1988**, 267-278.
[3] E. Tsukuda, S. Sato, R. Takahashi, T. Sodesawa, *Catal. Comm.* **2007**, 8, 1349-1353.

© 2011 Tous droits réservés.
http://doc.univ-lille1.fr

[4] M.R. Nimlos, S.J. Blanksby, X. Qian, M.E. Himmel, D.K. Johnson, *J.Phys.Chem.A*. **2006**, 110, 6145-6156.
[5] A. Ulgen, W. Hoelderich. *Catal. Lett.* **2009**,131,122-128.
[6] S. Erfle, U. Armbruster, U. Bentrup, A. Martin, A. Brückner, *Appl. Catal. A Gen,* 2010, doi: 10.1016/j.apcata.2010.04.042 article in press

© 2011 Tous droits réservés.
http://doc.univ-lille1.fr

6 Synopsis

6.1 General discussion of the results

In the previous chapter, we have commented in details the results of the catalytic tests for various types of heteropoly acids selected as active phases. We could thus discuss the influence of the acidity and of the redox character of the active phase on the catalytic performances. In fact, a decrease in the acidity from phosphotungstic acid over silicotungstic acid to phosphomolybdic acid, results in a lower selectivity to acrolein, which is consistent with the literature. Nevertheless, one can also state that the increased acidity of phosphotungstic acid results in an accelerated deactivation due to coking. Furthermore, the well-known increased redoxpotential for molybdenum-containing heteropoly acids gives rise to allylic alcohol, a by-product issued from the reduction of acrolein. As a consequence of these findings, silicotungstic acid was chosen as the most adapted active phase.

In a second series of experiments, we studied the impact of the reaction temperature on the catalytic performances of the chosen silicotungstic acid supported on CARiACT. A reaction temperature lower than 275 °C leads to a decrease in the selectivity to both acrolein and acetol, which is ascribed to the formation of poly-glycerides from condensation. Actually, the activation energy of the dehydration reaction of glycerol is quite high (*cf.* 2.1.5). When the reaction temperature is insufficient promote the dehydration, other pathways, like the condensation reaction, are favored. The results also suggest that the activation energy for the acetol pathway is slightly higher than that of the acrolein pathway, as at low reaction temperatures the decrease in selectivity to acetol is more pronounced than that to acrolein. A reaction temperature of 275 °C seems therefore to be a good compromise.

In the third series of tests, the influence of the catalysts' porosity was studied, first for silica of various types and then for SBA-15 prepared with different pore sizes. According to the literature, larger pores should have positive impact on the catalytic performances, as internal pore diffusion is facilitated. Nevertheless, according to the catalytic results, no impact of the poresize on the performances was found in the case of non-zirconia grafted silica. On the other hand, when the support contained

© 2011 Tous droits réservés.
http://doc.univ-lille1.fr

zirconia, we have observed a higher catalytic conversion after 24 h for supports with larger pore diameters. This was ascribed to the aforementioned suppression of diffusion limitations, whereby the accumulation of coke is decreased. As a second matter of fact, we found a correlation between the selectivity to acetol, which increased with the poresize of the zirconia-grafted silica, irrespective of the support.

Concerning these catalysts based on zirconia-grafted supports, we obtained the following information: The grafting with zirconia decreases the Brønsted acid strength of the supported silicotungstic acid, which was ascribed to the distortion of the Keggin unit due to strong electronic interactions between zirconia and the heteropoly anion. This decrease in acid strength leads to less coke formation, whereby the long-term performances are increased. Furthermore, an increased selectivity to acetol for zirconia-containing catalysts was found for all the samples, which was in good agreement with the Lewis acid character of zirconia that is known to yield and increase in the selectivity to acetol.

These two effects were clearly observed in the next three series of experiments, where the impact of the amount of zirconia, of the amount of active phase and ofthe calcination temperature were successively studied. In fact, when catalysts with low zirconia loading or high amount of active phase were tested, the positive impact on the long-term performance was lower, as the decrease in the acid strength was not fully complete. This effect was also observed for an increased calcination temperature. This is explained by the migration of zirconia from the inside of the porous network to the outside, leaving behind bare silica. Then,the subsequently impregnated silicotungstic acid preserves its initial acid strength as it is mainly deposited on silica surface. On the other hand, when high zirconia amounts or low loadings of active phase were used, the aforementioned Lewis character of zirconia became predominant, whereby the selectivity to acrolein decreased and the selectivity to acetol increased.

In a last series of experiments, the regeneration of two types of catalysts, one based on zirconia-grafted SBA-15 and the other one based on the same bare SBA-15, was studied. The regeneration was performed either in dry or in humidified air atmosphere, whereby the catalyst based on zirconia-grafted SBA-15 recovered its initial performances. On the other hand, the catalyst based on bare SBA-15 showed

significantly lower catalytic performances after regeneration. Especially, the selectivity to acrolein remained low, which was ascribed to the partial thermal decomposition of the active phase in hotspots formed during the regeneration process. In fact, it was found that the thermal stability of silicotungstic acid was higher when supported on zirconia, than when supported on silica, which is – again – a consequence of the aforementioned strong electronic interaction between zirconia and the heteropoly anion. Thereby, the active phase was entirely preserved upon regeneration when supported on zirconia, but partially decomposed when supported on silica. Nevertheless, the presence of steam during the regeneration of the catalyst based on bare silica could slightly increase the selectivity to acrolein. This effect is explained by the fact that the vapor may either decrease the temperature in the hotspots due to its high heat capacity, or stabilize the Keggin structure by shifting the equilibrium of the decomposition reaction to the side of the intact species.

6.2 Conclusion

The feasibility of the use of supported heteropoly acids as catalysts for the dehydration of glycerol to acrolein has been successfully demonstrated. The combination of an adequate support and of these HPA active phases is highly interesting as their properties can be modified in various ways:

The acidity and the redoxcharacter of the heteropoly compounds can be adjusted with the choice of the hetero- and addenda atoms. Silicotungstic acid was found as the most adapted active phase for the dehydration reaction, as it provides well balanced acidity, which results in moderate deactivation extent, and complete absence of any redoxcharacter, whereby the formation of allylic alcohol is suppressed.

The choice of the support has a significant impact on the catalytic performances, which was demonstrated for zirconia grafted- and bare silica. In fact, the support influences the acidity and on the thermal stability of the supported heteropoly compound, due to specific electronic interactions. Actually, strong interactions, as observed over zirconia, result in a distortion of the Keggin structure, whereby the acidity decreases. On the other hand, the thermal stability of the supported heteropoly compound is increased as the stronger interaction has to be overcome before decomposition can take place, which means that additional energy is necessary.

Nevertheless, it is worth mentioning that the grafting with zirconia also introduces Lewis acid character to the catalyst, which generally results in a decreased selectivity to acrolein to the benefit of the formation of acetol. Therefore, it was deduced that the quantity of zirconia and active phase have to be properly balanced for finding the best compromise between the beneficial effect of the increased long-term activity and the negative side-effect of a decreased selectivity to acrolein.

Finally, the selection of a mesoporous silica as support was demonstrated as the last crucial parameter to get high catalytic performances, as the pore size of the zirconia-grafted silica support is also correlated to the long-term performances. As a matter of fact, larger pores result in decreased diffusion restrictions, whereby the mass transfer is facilitated and carbon deposit is largely suppressed, which entails better long-term performance.

The optimal balance of all these parameters was found for a catalyst containing 20 wt.% of silicotungstic acid over SBA-15 with a mean pore diameter of8 nm, which was previously grafted with 20 wt.% of zirconia. This combination enabled a remarkable increase in the long-term conversion by a factor 3, whilethe selectivity to acrolein remained stable.

6.3 Perspectives

The zirconia-grafting of silica followed by impregnation of heteropoly acids leads to increased catalytic performances in thelong-term and has a positive impact on the thermal stability of the Keggin unit. We have proposed a mechanistic explanation for this phenomenon based on the electronic interactions between the support and the heteropoly anion resulting in a slightly decreased acidity and therefore slowed down coke formation. These effects were also observed for alumina supported heteropoly acids, but should further be investigated using tungsten-oxide (WO_3), titania (TiO_2) or niobium-oxide (Nb_2O_5) or mixtures of them, following the idea of a fine-tuned acidity of the catalyst with increased long-term performances.

As observed for high loadings of zirconia, the selectivity to acrolein significantly decreases when the Lewis acid character becomes predominant. One possibility to by-pass this disadvantage is the increased loading with active phase, whereby the Lewis acid character is covered by the Brønsted character of the heteropoly acid. Another way is the selective blocking of the free Lewis-acid sites, which remain un-occupied after impregnation with the heteropoly acid. One way for the selective blocking might be the addition of small quantities amines or sulfites in the reaction feed. This concept is also of high importance for other kinds of catalysts dealing with the problem of undesired Lewis-acid sites.

The catalytic results obtained over non-zirconia containing catalysts indicate that the catalytic activity is very high in the beginning of the reaction. This results in an increased deactivation due to extensive formation of coke. Next to the possibility of tuning the catalytic activity by the aforementioned modification of the support, which as an effect on the acidity of the active phase, we have seen that the reaction conditions are another key-parameter for increasing long-term performances. In fact, decreased contact time may be a possibility to enhance the catalysts' lifetime. Therefore, further studies on this parameter should be done.

Next to the increase in the acid force, one can easily reduce the number of acid sites of the heteropoly acid by partial exchange of protons with counter-cations (caesium, potassium or sodium) by neutralization. Thereby, the activity of the catalyst in the startup phase could be decreased, resulting in the aforementioned higher long-term performance.

From the current point of view, there is no catalyst available, which maintains high catalytic performance over very long runtime. In fact, all the results published up to now reveal that the key-problem for the industrial application remains the deactivation of the catalysts. Nevertheless, we are crucially missing a fundamental approach for the deactivation mechanism and rate. For other catalytic systems, such as catalytic cracking using zeolites, this kind of study has already be done by Guisnet *et al.*[137] Indeed, the characterization of the carbon deposit by dissolving in organic solvents with further analyses by mass-spectroscopy or *Operando* techniques may enable the determination of the different organic molecules present at the surface of the catalysts after reaction. Taking into account the proposed reaction schemes, one might finally understand the pathway that leads to the coke formation and thereby to the deactivation of the catalyst which offers the possibility of specific countermeasures. This fundamental knowledge can also be applied to other catalytic systems.

[137] M. Guisnet, P. Magnoux, *Catal. Today*, **1997**, *36*, 477-483.

7 Annex

7.1 Introduction (French)

Des éléments de ce chapitre font l'objet de deux articles de revue :

B. Katryniok, S. Paul, M. Capron, F. Dumeignil *ChemSusChem* **2009**, *2*, 719-730.

B. Katryniok, S. Paul, V. Bellière-Baca, P. Rey, F. Dumeignil, *GreenChem.* **2010** ref. C0GC00194E soumis

L'épuisement progressif des ressources fossiles a conduit à des efforts de recherche intensive pour notamment produire des substituts de carburants, comme le bio-diesel, le bio-éthanol ou le bio-kérosène. Contrairement aux ressources fossiles, ces carburants offrent l'avantage d'un bilan carbone très favorable en raison de leur origine *ex*-biomasse renouvelable. Du point de vue économique, aucun des bio-carburants ne peut être produit compétitivement pour l'instant, mais dans le but d'atteindre les objectifs de réduction de CO_2 fixés dans le protocole de Kyoto, les décisions politiques ont poussé à la production de carburants à partir de ressources biologiques. Par exemple, l'Union Européenne a prévu d'augmenter progressivement la proportion de bio-éthanol dans l'essence à 10 % et du biodiesel comme additif dans le gazole à 7 %, d'ici à 2015. [1]

Les matières premières pour la production de biodiesel sont des huiles et graisses végétales – obtenues à partir de colza, soja, maïs, ... - et un mono-alcool (le plus souvent du méthanol), qui sert à cliver les acides gras de leur charpente de glycérol pour finalement produire les acides gras-esters désirés (**Scheme 1-1**). Ces esters peuvent être directement utilisés comme biodiesel, mais sont plus généralement mélangés avec le diesel « fossile ».

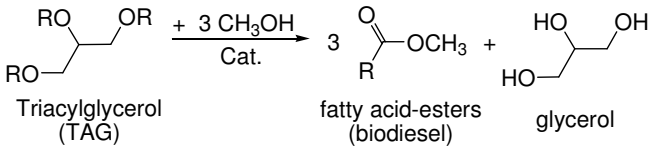

Schéma 7-1 : Réaction de transestérification des huiles végétales pour produire le biodiesel

© 2011 Tous droits réservés.
http://doc.univ-lille1.fr

La capacité de production de biodiesel est en expansion dans le monde entier. Par exemple, en 2008 les Etats-Unis en ont produit 2,1 millions de tonnes et l'UE 7,6 millions de tonnes (**Figure 1-1**), et ces quantités devraient par ailleurs doubler d'ici à 2012. [2,3] Cette croissance est accompagnée d'une augmentation significative de la production de glycérol, lequel est un co-produit de la filière biodiesel (**Scheme 1-1**) dans des proportions significatives (~ 10 pds.%). On prévoit ainsi que 1,54 millions de tonnes de glycérol seront produites dans le monde en 2015,[4] lesquelles devront être valorisées afin d'augmenter la compétitivité de la filière biodiesel, voire tout simplement d'en assurer la pérennité...

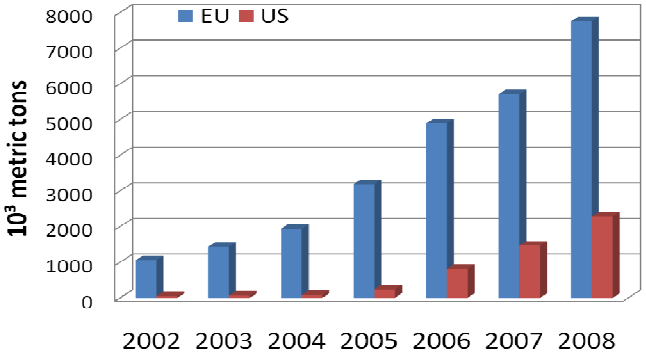

Figure 7-1 : Production de biodiesel dans l'Union Européenne (UE) et aux Etats-Unis (US) [2-3]

Selon la procédure appliquée pour le clivage des acides gras de leur squelette de glycérol (procédé de transestérification), la qualité du glycérol brut (souvent dénommé 'glycérine') peut varier considérablement au niveau de sa pureté. Le glycérol brut obtenu à partir de la plupart des procédés biodiesel est concentré à hauteur de 80 % en poids. Il comprend de l'eau, du méthanol, des traces d'acides gras, ainsi que divers composés organiques et inorganiques (rassemblés sous l'acronyme 'MONG', pour Matière Organique Non-Glycérol) dans des quantités variables (Table 1-1).

© 2011 Tous droits réservés.
http://doc.univ-lille1.fr

Table 7-1 : Exemples de qualités de glycérol provenant de divers procédés de production de biodiesel [5]

Entreprise/ Site de Production		Robbe/Diester Compiègne (France)	Saipol/Diester Rouen (France)	Diester/Bioenergy Marl (Allemagne)
concentration [% poids]	Glycérol	65	93	85
	Eau	31	4	10
	MONG	1	1	0,5
	Sels	3 (Na_2SO_4)	2,5 (NaCl)	4,5 (NaCl)
	Méthanol	0,3	0,2	< 0,01

En conséquence, dans la plupart des cas, le glycérol brut doit être purifié par une étape de distillation avant d'être utilisé. Dans les faits, la proportion de glycérol raffinée est en diminution constante en raison du coût élevé de l'étape de distillation nécessaire. En outre, la production de glycérol brut dépasse la demande, principalement en raison de l'absence de marché – *c-à-d*, de débouchés - (Figure 1-2). En revanche, un modèle basé sur la production et la vente de glycérol brut prédit une relation linéaire inverse entre le coût de production de biodiesel pur et le prix de la glycérine. [6] De nouvelles voies de valorisation du glycérol doivent donc être développées afin d'augmenter la demande et *de facto* le prix du glycérol brut, ce qui aura pour effet direct d'assurer *in fine* la pérennité de la filière biodiesel. [7]

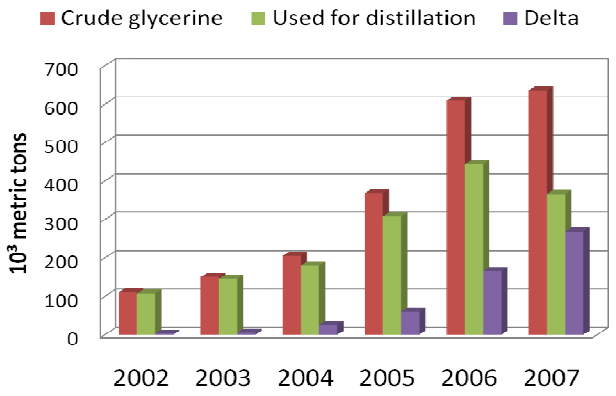

Figure 7-2: Production mondiale de glycérol brut et quantité distillée (la «différence» - delta - correspond à la quantité de glycérol qui n'est pas valorisée) [8]

On connaît plus de 1500 applications directes du glycérol, en particulier dans les cosmétiques, les produits pharmaceutiques et dans l'industrie alimentaire. [9]

© 2011 Tous droits réservés.
http://doc.univ-lille1.fr

L'utilisation versatile du glycérol (**Figure 1-3**) est basée sur ses propriétés chimiques et physiques particulières. En raison de la présence de trois groupes hydroxyles, le glycérol est complètement soluble dans l'eau ainsi que dans la plupart des alcools, et il est par ailleurs totalement insoluble dans les hydrocarbures. En raison de ses propriétés hydrophiles, le glycérol est utilisé dans des applications où la quantité d'eau doit être contrôlée - comme dans les colles ou autres adhésifs -. En outre, la présence de groupes hydroxyles conduit à la formation de réseaux intra- et inter-moléculaires au travers de liaisons hydrogène, ce qui explique un point d'ébullition élevé (290 °C à pression atmosphérique) et une viscosité importante. Cette dernière propriété rhéologique conduit à l'utilisation du glycérol comme un adoucisseur pour résines et plastiques, mais aussi comme lubrifiant, par exemple dans des applications pharmaceutiques. En outre, le glycérol est non toxique et a un goût sucré. Il peut ainsi être incorporé dans les aliments, médicaments et cosmétiques, mais, comme dit précédemment, le glycérol brut issu des procédés biodiesel contient des impuretés et n'est donc pas approprié pour de telles applications sans étapes de purifications préliminaires. En outre, comme mentionné plus haut, la taille du marché existant n'est pas suffisante pour absorber l'énorme quantité de glycérol actuellement produit, et, l'écart entre la capacité d'absorption du marché et la production effective de glycérol ne cessera d'augmenter dans un proche avenir.

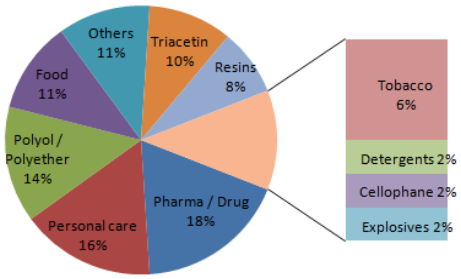

Figure 7-3 : Filières consommatrices de glycérol [7]

Aujourd'hui, le glycérol brut est généralement brûlé (Figure 1-2), ce qui constitue un gaspillage indéniable de cette ressource au potentiel applicatif important. En effet, le glycérol est une molécule hautement fonctionnalisée et qui offre donc de nombreuses possibilités de transformations chimiques ou biochimiques pour produire des produits chimiques à haute valeur ajoutée. Une sélection de ces possibilités est proposée dans le **Scheme 1-2**.

© 2011 Tous droits réservés. http://doc.univ-lille1.fr

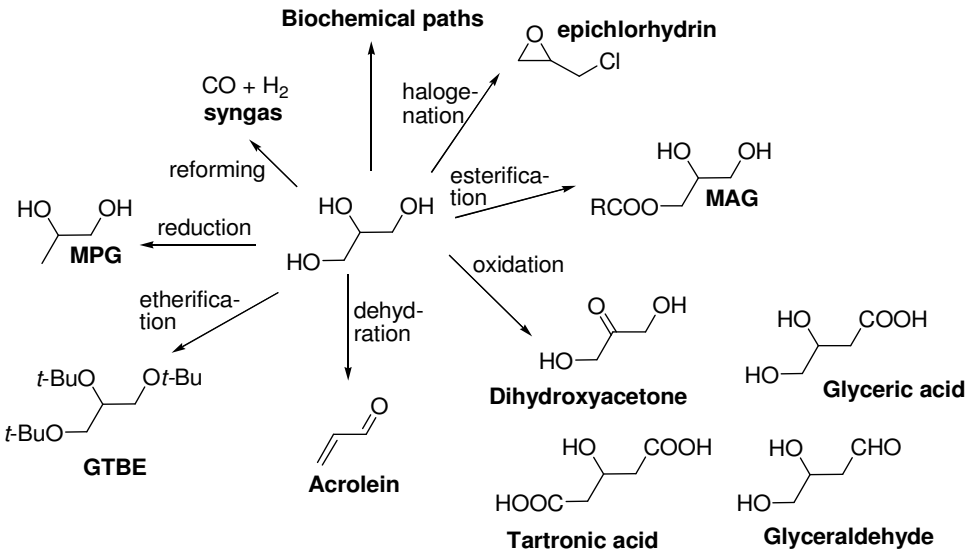

Schéma 7-2 : Sélection des voies de valorisation chimiques du glycérol

Récemment, le reformage du glycérol sur des catalyseurs Pt-Rh pour produire du gaz de synthèse utilisable dans le procédé Fischer-Tropsch pour produire des alcanes ou du méthanol, a été proposé. [10, 11] Une application qui pourrait découler de cette technologie est la production d'hydrogène par le procédé de Water-Gas-Shift. Une autre possibilité intéressante pour valoriser le glycérol est sa réduction sélective, qui conduit soit au propylène glycol (MPG) soit au 1,3-propanediol (PD) qui sont utilisés dans l'industrie des polymères. Il est également possible d'halogéner le glycérol à l'aide d'acide chlorhydrique en présence d'acides organiques (acide caprylique - Solvay - ou acide acétique - Dow -) pour produire l'épichlorhydrine, un intermédiaire important pour la synthèse des résines époxy.[12] Le procédé catalytique est effectué en phase gaz à 180-220 °C sous 1 ~ 5 bars de pression.[13] Cette technologie est maintenant assez mature, si bien que Solvay commercialise ce procédé depuis 2007 en France, en utilisant une installation de production existante où le glycérol était autrefois produit à partir de l'épichlorhydrine.

Une autre façon de valoriser le glycérol est l'éthérification pour produire du glycérol-tert-butylether (GTBE), qui est un excellent additif pour le diesel. L'estérification du glycérol en mono-acylglycérols (MAG) ou di-acylglycérols (DAG), utilisés comme agents émulsifiants, par exemple, dans les denrées alimentaires (margarines et les sauces), ou dans les cosmétiques, est également une option possible. Ce dernier procédé peut être catalysé par un catalyseur alcalin conventionnel ou par des enzymes (lipase-type).[14] L'oxydation partielle du glycérol

© 2011 Tous droits réservés.
http://doc.univ-lille1.fr

conduit, elle, à une chimie très riche avec de nombreux produits possibles, tels que l'acide glycérique, l'acide tartronique, l'acide cétomalonique (ou mésoxalique), le glycéraldéhyde ou le dihydroxyacétone (DHA). Le défi consiste à trouver des catalyseurs sélectifs. Par exemple, des catalyseurs à base de Bi/Pt se sont révélés efficaces pour la production de DHA avec un rendement de 37 % à 70 % de conversion.[15] L'oxydation peut également être effectuée en utilisant des bactéries modifiées.[16] Récemment, l'oxydation anodique du glycérol a permis un rendement de 25 % en DHA, ce qui est comparable à celui obtenu avec le processus biotechnologique susmentionné.[17]

Toutefois, l'un des moyens les plus prometteurs de valoriser le glycérol consiste en sa déshydratation catalytique pour donner de l'acroléine, laquelle est un intermédiaire important dans les industries chimiques et l'agro-industrie. La synthèse de l'acroléine est actuellement basée sur l'oxydation sélective du propène sur catalyseurs à base de BiMoOx (Scheme 1-3). La sélectivité obtenue dans ce procédé est proche de 85 % en acroléine à 95 % de conversion.[18] De nouvelles approches utilisant le propane comme matière première sont actuellement étudiées à l'échelle laboratoire, mais celles-ci souffrent encore de rendements largement insuffisants.[19] Eu égard l'épuisement progressif des ressources pétrolières, les ressources renouvelables deviendront de plus en plus concurrentielles, sans parler de l'effet positif en termes d'impact sur le climat. Dans ce contexte, la production d'acroléine à base des bio-ressources est un défi important. Une étude économique a montré que la production d'acroléine à partir du glycérol serait concurrentielle à condition que le prix de glycérol soit inférieur à 300 US$/t.[20] En janvier 2010, le glycérol raffiné coûtait environ 500 ~ 550 US$/t, mais le prix de la glycérine brute était en même temps d'environ 200 US$/t, ce qui fait d'ores et déjà de cette dernière une matière première très compétitive pour la production d'acroléine.[21]

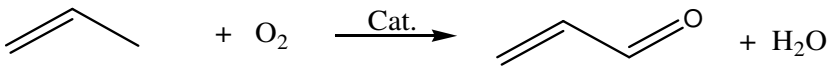

Schéma 7-3 : Oxydation sélective du propène

En raison de sa toxicité, l'acroléine est généralement directement convertie en dérivés tels que l'acide acrylique, par exemple. En effet, le débouché le plus important pour l'acroléine est la synthèse d'acide acrylique, lui-même utilisé comme matière première pour la synthèse du polyacrylate de sodium (Scheme 1-4). Grâce à

© 2011 Tous droits réservés.
http://doc.univ-lille1.fr

ses propriétés physiques, ce polymère est classé comme super absorbant, et est utilisé dans des produits d'hygiène, tels que les couches pour bébé. Le marché annuel mondial de ces polymères super absorbants (SAP) est estimé à 1,9 millions de tonnes en 2010. [22]

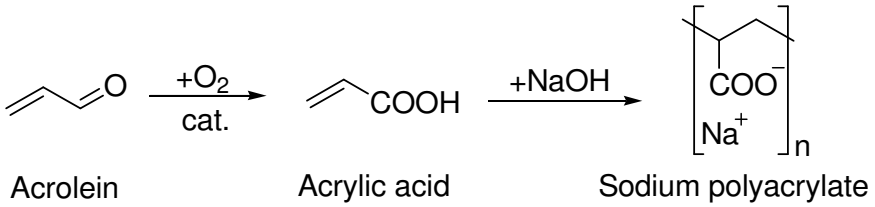

Schéma 7-4 : Synthèse de polyacrylate de sodium (polymère super absorbant)

Le deuxième débouché majeur de l'acroléine est représenté par la synthèse de la DL-méthionine *via* le 3-méthylthiopropionaldéhyde comme intermédiaire (Scheme 1-5).[23] La DL-méthionine est un acide aminé essentiel, qui ne peut pas être synthétisé par les organismes vivants. Elle est largement utilisée pour l'engraissement du bétail afin d'accélérer la croissance des tissus vivants. La capacité de production mondiale annuelle de la DL-méthionine est d'environ 500.000 tonnes. [24] On estime que la demande mondiale augmentera de 3 à 7 % dans un proche avenir selon les régions. [25]

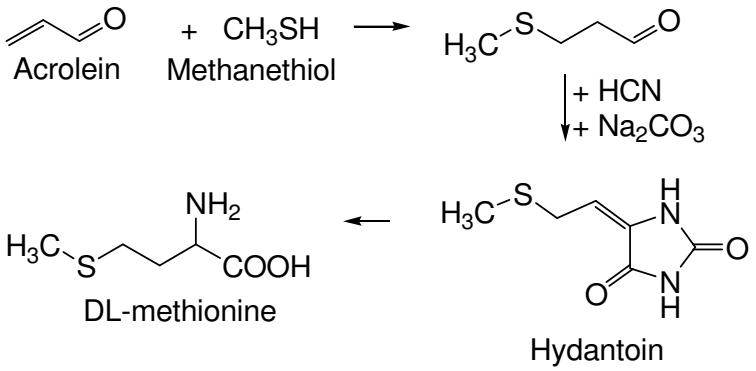

Schéma 7-5 : Voies chimiques pour la fabrication industrielle de la DL-méthionine

Dans le chapitre suivant, nous présenterons l'état de l'art concernant la synthèse de l'acroléine en phase gaz par déshydratation du glycérol. Les propriétés conduisant à de bonnes performances catalytiques ainsi que les trois systèmes catalytiques associés les plus courants seront répertoriés et discutés de manière détaillée. Les acides inorganiques supportés, lesquels présentent des performances catalytiques particulièrement intéressantes, feront l'objet d'une description plus approfondie. L'accent sera ensuite mis sur les phases actives à base

© 2011 Tous droits réservés. http://doc.univ-lille1.fr

d'hétéropolyacides supportées sur silices méso-structurées, à savoir le système catalytique choisi pour cette étude suite à l'examen de la littérature couplé au savoir-faire du laboratoire. Par ailleurs, une section consacrée au mécanisme réactionnel permettra d'appréhender le processus au niveau moléculaire et d'expliquer les tendances observées au niveau de la sélectivité, notamment suivant la nature des sites acides présents à la surface des solides.

[1] Directive 2003/30/EC of the European Parliament and of the council of 05/08/2003 on the promotion of the use of biofuels or other renewable fuels for transport.
[2] Eurostat European Commission, http://epp.eurostat.ec.europa.eu.
[3] U.S. National Biodiesel Board, http://www.biodiesel.org.
[4] Global Industry Analysts, http://www.strategyr.com/Glycerin_Market_Report.asp.
[5] J.L. Dubois, G.S. Patience (Arkema) WO2009044051, **2009**.
[6] M. J. Haas, A. J. Mc Aloon, W. C. Yee, T. A. Foglia, *Biores. Tech.*, **2006**, *97*, 671-678.
[7] M. Pagliaro, M. Rossi, in The Future of Glycerol: New Uses of a Versatile Raw Material, RSC Green Chemistry Book Series, **2008**.
[8] Data sources: European Biodiesel Board and HBI.
[9] C. S. Callam, S. J. Singer, T. L. Lowary, C. M. Hadad., *J. Am. Chem. Soc.* **2001**, *123*, 11743.
[10] D. A. Simonetti, J. Ross-Hansen, E. L. Kunkes, R. R. Soares, J. A. Dumesic, *Green Chem.* **2007**, *9*, 1073.
[11] R. R. Soares, D. A. Simonetti, J. A. Dumesic, *Angew. Chem. Int. Ed.* **2006**, *45*, 3982.
[12] D. Siano, E. Santacesaria, V. Fiandra, R. Tesser, G. Di Nuzzi, M. Di Serio, M. Nastasi (ASER), WO 2006111810, **2006**.
[13] D. Schreck, W. Kruper, F. Varjian, M. Jones, R. Campbell, K. Kearns, B. Hook, J. Briggs, J. Hippler (DOW Chemicals), WO 2006020234, **2006**.
[14] N. O. V. Sonntag, *J. Am. Oil. Chem. Soc.* **1992**, *75*, 795.
[15] H. Kimura, Appl. Catal. A: Gen., 1993, 105, 147-158; H. Kimura, K. Tsuto, T. Wakisaka, Y. Kazumi, Y. Inaya, *Appl. Catal. A: Gen.* **1993**, *96*, 217-228.
[16] K. Nabe, N. Izuo, S. Yamada, I. Chibata, *Appl. Environ. Microbiol.* **1979**, *38*, 1056.
[17] R. Ciriminna, G. Palmisano, C. Della Pina, M. Rossi, M. Pagliaro, *Tetrahedron Lett.* **2006**, *47*, 6993.
[18] G.W. Keulks, L.D. Krenzke, T.M. Notermann, *Adv. Catal.*, **1978**, *27*, 183.
[19] M.M. Lin, *Appl. Catal. A: Gen.*, **2001**, *207*, 1.
[20] A. Corma, G.W. Huber, L. Sauvanaud, P. O'Connor, *J. Catal.* **2008**, *257*, 163-171.
[21] ICIS Market-reporter – January 06 **2010** – www.icis.com.
[22] Global Industry Analysts, http://www.strategyr.com/Super_Absorbent_Polymers_Market_Report.asp.
[23] A. Yamamoto, Encyclopaedia of Chemical Technology, 3rd ed. **1978**, Vol. 2, 403.
[24] M. P. Malveda, H. Janshekar, K. Yokose, CEH Marketing Research Report – SRI Consulting, Major Amino Acids, June **2006**.
[25] M. P. Malveda, H. Janshekar, K. Yokose, Chemical Economics Handbook-SRI Consulting, June **2006**, 502.5000 B.

© 2011 Tous droits réservés.
http://doc.univ-lille1.fr

7.2 Conclusion (French)

La faisabilité de l'utilisation des hétéropoly acides comme catalyseurs pour la déshydratation du glycérol en acroléine a été démontrée avec succès. La combinaison d'un support adéquat et d'une phase active de type HPA est très intéressante parce que les propriétés de cette dernière peuvent être modifiées de diverses manières:

L'acidité et le caractère redox des hétéropoly composés peuvent être ajustés par le choix de l'hétéro- et addena-atome. L'acide silicotungstique a été observé comme étant la phase active la mieux adaptée pour la réaction de déshydratation de glycérol, car il fournit une acidité bien équilibrée - ce qui entraîne la désactivation à taux modérés - et l'absence complète de redox caractères - permettant la suppression d'une formation d'alcool allylique.

Le choix du support a un impact significatif sur les performances catalytiques, ce qui a été démontré pour le silice greffé par du zircone et des silices nus. En fait, le support a un impact significatif sur l'acidité et la stabilité thermique du hétéropoly composé, en raison des interactions électroniques. Des interactions fortes - comme observé pour le zircone - entraînent une distorsion de la structure de Keggin par laquelle l'acidité diminue. De plus, la stabilité thermique du hétéropoly composé augmente étant donné que l'interaction doit d'abord être clivée avant que la décomposition puisse avoir lieu, ce qui signifie qu'une énergie supplémentaire est nécessaire.

Néanmoins, il convient de mentionner que le greffage avec du zircone ajoute aussi un caractère d'acidité de Lewis au catalyseur, ce qui aboutit généralement à une diminution de la sélectivité en acroléine et à une formation accrue d'acétol. Par conséquent, il a été démontré que les quantités de zircone et de phase active doivent être équilibrées pour trouver un compromis entre l'effet bénéfique sur l'activité à long terme et l'effet secondaire négatif sur la sélectivité en acroléine.

Enfin, le choix d'un silice mésoporeux comme support a démontré que la taille de pore est un paramètre clé pour obtenir une haute performance catalytique. En fait, des grandes pores diminuent les restrictions de diffusion, d'où un transfert de matière facilité et une diminution du dépôt de carbone, ce qui entraîne de meilleures performances à long terme.

© 2011 Tous droits réservés.
http://doc.univ-lille1.fr

Un équilibre optimal de tous ces paramètres a été constaté en utilisant un catalyseur contenant 20wt.% d'acide silicotungstique sur SBA-15 avec des pores de 8 nm, greffé avec 20wt.% de zircone.

Il a donc été observé qu'une telle combinaison permet, à long terme, une augmentation de l'activité du catalyseur par un facteur 3, tout en conservant une sélectivité en acroléine assez stable.

© 2011 Tous droits réservés.
http://doc.univ-lille1.fr

7.3 Curriculum Vitae

Benjamin KATRYNIOK
365 Rue Faidherbe
62750 Loos-en-Gohelle
Landline +33 954040794
Cell phone +33 662594391
France

Born on April 22nd 1981 at Brilon (Germany – German nationality)

Actual position

Since 10/2007	PhD at the *Université des Sciences et Technologies de Lille* (France) in the laboratory *Unité de Catalyse et de Chimie du Solide* (UCCS) in cooperation with ADISSEO and RHODIA **Director of the thesis :** Prof. Franck Dumeignil **Subject:** New synthesis route for acrolein from biomass **Financing** : Scholarship from CNRS and ADISSEO **Date of defense:** November 9th 2010

Education

2006 – 2007	Master at the University of Aachen (RWTH Aachen) in *the Institute for Technical and Macromolecular Chemistry* (ITMC) in cooperation with SÜD-CHEMIE **Director of the Master-thesis :** Prof. Marcel Liauw **Subject:** Characterization of iron-molybdate catalysts by different techniques of spectroscopy and their application in the selective catalytic oxidation of methanol yielding formaldehyde
2003 – 2007	Master classes at the University of Aachen (Germany)
30/08/2004 - 07/10/2004	Research project with Mr. Sven Eichholz in the laboratory of Prof. Walter Leitner Spatial resolution of catalytic beds by UV-Vis fiberoptic spectroscopy
14/02/2005 – 30/03/2005	Research project with Mr. Julien Barbion in the laboratory of Prof. Dieter Enders Synthesis of (+)-Isoaltholactone
13/06/2005 – 17/07/2005	Research project with Miss Annika Bande in the laboratory of Prof. Arne Lüchow FN-DMC Calculations with soft-ECPs
30/06/2006 – 17/03/2006	Research project with Mr. Christian Severins in the laboratory of Prof. Albrecht Salzer New synthesis route of phospholane ligands for homogeneous catalysis
2001 – 2003	Bachelor classes at the University of Marburg (Germany)
2000 – 2001	Military Service
2000	A-Levels

© 2011 Tous droits réservés.
http://doc.univ-lille1.fr

Teaching and Supervision

2008 – 2010 **Teaching at Ecole Centrale de Lille**
(62 hours in 2008-2009, 64 hours in 2009-2010)
Supervision of master students during 3 months internship:
Andres Mino (2009) and Cyrille Guillon (2010)
Supervision of a technician student during 3 months internship:
Jimmy Decoster(2009)
Supervision of project students:
Sophie Mercier (2008), Alizée Chaban (2009) and Elodie Dekeister (2010)

Training workshops

21-25/09/2009 Summer school *Engineering of catalytic reactors* at Fréjus (France) organized by the CNRS and the Laboratory *Laboratoire de Génie des Procédés Catalytiques Lyon*

Language skills

- German
- English
- French

7.4 Publications

Articles (*articles without peer-review)

Glycerol Dehydration to Acrolein in the context of Glycerol new usages
B. Katryniok, S. Paul, V. Bellière-Baca, P. Rey, F. Dumeignil
GreenChem. (**2010**) Doi 10.1039/C0GC00194E accepted manuscript

Highly efficient catalyst for decarbonylation of lactic acid to acetaldehyde
B. Katryniok, S. Paul, F. Dumeignil
GreenChem. (**2010**), Doi 10.1039/C0GC00203H accepted manuscript

Long-Life Catalyst for Glycerol Dehydration to Acrolein
B. Katryniok, S. Paul, M. Capron, C. Lancelot, P. Rey, V. Bellière-Baca, F. Dumeignil
GreenChem. (**2010**), Doi 10.1039/C0GC00254B accepted manuscript

Towards the sustainable production of acrolein by glycerol dehydration
B. Katryniok, S. Paul, M. Capron, F. Dumeignil
ChemSusChem. 2 (**2009**), 719-730

Dehydration of Glycerol – A new pathway to Acrolein *
B. Katryniok, S. Paul, M. Capron, F. Dumeignil
Rapport final RDR 1 (**2009**), 28-32

© 2011 Tous droits réservés.
http://doc.univ-lille1.fr

Patents

Procédé de préparation d'acroléine à partir de glycérol ou de glycérine
B. Katryniok, S. Paul, M. Capron, F. Dumeignil, P. Rey, V. Belliere-Baca
Brevet déposé sous le N° 09 59276 (**2009**)

Procédé de production d'acétaldéhyde à partir d'acide lactique
B. Katryniok, S. Paul, F. Dumeignil
Brevet déposé sous le N° 10 534494 (**2010**)

Communications

Controlled synthesis of porous heteropolysalts used as catalysts supports
S. Paul, A. Mino, B. Katryniok, E. Bordes-Richard, F. Dumeignil
10th International Symposium "Scientific Bases for the Preparation of Heterogeneous Catalysts", Leuven (Belgique) 2010

Biomass valorization by dehydration of glycerol – a new pathway to acrolein
B. Katryniok, S. Paul, M. Capron, F. Dumeignil
ECSAW, Aussois (France) 2009

Glycerol Dehydration – Green Chemistry for Acrolein Production
B. Katryniok, S. Paul, M. Capron, F. Dumeignil
RDR1, Versailles (France) 2009

Liquid Phase Glycerol Catalytic Oxidation over Gold Based Catalysts: Activity and Dynamic Measurement of Dissolved Oxygen Concentration
R. Ducoulombier, P. Fongarland, M. Capron, B. Katryniok, M. Bonne, J. Girardon, N. Mimura, S. Paul, S. Royer, P. Marécot, F. Dumeignil
WCOC, Lille (France) 2009

Posters

Glycerol Dehydration to Acrolein over New Catalysts
B. Katryniok, S. Paul, M. Capron, P. Rey, F. Dumeignil
TOCAT6/APCAT5, Sapporo (Japan) 2010

Biomass valorization by dehydration of Glycerol – a sustainable pathway to acrolein
B. Katryniok, S. Paul, M. Capron, F. Dumeignil
TOCAT6/APCAT5, Sapporo (Japan) 2010

Long-Life Catalysts for Dehydration of Glycerol to Acrolein
B. Katryniok, S. Paul, M. Capron, P. Rey, F. Dumeignil
6th Flash Conference of ERA-Chemistry "Extreme Chemical Efficiency – Driving to the limits", Roscoff (France) 2010

Synthesis of heteropolyanionic porous supports and catalysts for the selective oxidation of isobutane into methacrylic acid
C. Wei, M. Sultan, B. Katryniok, S. Paul

© 2011 Tous droits réservés.
http://doc.univ-lille1.fr

WCOC, Lille (France) 2009

Influence of the preparative conditions on the textural properties of porous heteropolycompounds
S. Paul, A.M. Ron, B. Katryniok, E. Bordes-Richard, F. Dumeignil, 3rd Int. Symp. on Advanced micro- and mesoporous materials, Albena (Bulgarie) 2009

© 2011 Tous droits réservés.
http://doc.univ-lille1.fr